Air–Surface exchange of elemental mercury in uncontaminated grasslands

Determination of fluxes and identification of forcing factors with micrometeorological methods and controlled laboratory studies

Inauguraldissertation

zur
Erlangung der Würde eines Doktors der Philosophie
vorgelegt der
Philosophisch-Naturwissenschaftlichen Fakultät
der Universität Basel

von

Johannes Fritsche

aus Ludesch (Österreich)

Basel, 2008

Genehmigt von der Philosophisch-Naturwissenschaftlichen Fakultät
auf Antrag von

Prof.Dr. Nikolaus Kuhn
Prüfungsvorsitzender

Prof. Dr. Christine Alewell
Fakultätsverantwortliche / Dissertationsleiterin

Prof. Dr. Harald Biester
Korreferent

Basel, den 19.2.2008

Prof. Dr. Hans-Peter Hauri
Dekan

Abstract

The burning of fossil fuels, incineration of waste, smelting of metals and other industrial processes and applications have been adding considerable amounts of mercury to the atmosphere. Of the total atmospheric mercury, Hg^0 (elemental mercury) represents more than 95%, a species which is highly volatile and dispersed globally. Eventually Hg^0 is transformed and deposited to land and sea where various processes may produce organic mercury species that have the power to bioaccumulate to levels that are toxic for humans.

In Europe and North America mission controls are in place for more than two decades and have reduced mercury emissions substantially. However, due to large uncertainties in global emission estimates and uncertainties regarding the potential of different ecosystems to act as sources or sinks for atmospheric mercury, it is yet not known if deposited Hg^0 is stored permanently in soils and if the atmospheric pool is actually reduced. Attempts to estimate the magnitude of the air-surface mercury exchange have focused on polluted sites, boreal regions and arid zones of North America. In contrast, uncontaminated, continental regions of the temperate climate belt haven't received much attention and respective studies have been mostly limited to spot measurements with flux chambers.

The first objective of our study was to describe and evaluate the influence of microbiological activity on the emission of Hg^0 from terrestrial background soils. It has been discussed that apart from physically and chemically mediated Hg^0 emission, microbial activity might contribute to the emission flux. The importance of this contribution in uncontaminated terrestrial soils is still unclear. Under controlled laboratory conditions it was tested how stimulation and inhibition of microbial activity would affect Hg^0 emissions. This was done by comparing sterilised with intact soil samples in an incubation chamber and investigating the response of Hg^0 emissions to environmental variables such as temperature and soil moisture.

The results of these experiments showed consistent changes of Hg^0 emissions with stimulation and inhibition of microbiological activity. Stimulatory effects were observed after addition of glucose, after inoculation of sterilised soil as well as upon temperature shifts and re-moistening of dried samples. We conclude that Hg^0 emissions from uncontaminated, terrestrial soils are partly controlled by microbiological activity. Microorganisms might reduce Hg^{2+} either directly in order to detoxify their immediate environment, or they might indirectly induce Hg^0 evasion by producing reductive soil compounds such as humic and fulvic acids.

To obtain a comprehensive picture of elemental mercury exchange of background areas we performed measurements on an ecosystem scale at three temperate lowland and subalpine grassland sites. A subalpine meadow at Fruebuel in central Switzerland was chosen to record the seasonal cycle of the Hg^0 exchange and with two additional sites in Oensingen/Switzerland and Neustift/Austria the spacial variability was addressed. By measuring concentration gradients, fluxes of elemental mercury and CO_2 were estimated by application of two micrometeorological methods – the flux gradient method and the modified Bowen ratio method. Due to the low atmospheric concentrations (between 1.2 and 1.7 ng m^{-3}), it proofed to be extremely challenging to extract acceptable Hg^0-gradients. Although the measurement configuration entailed substantial variability, the applied methods agreed well with respect to the direction of the flux and seem appropriate to estimate the magnitude of background Hg^0 exchange rates. With the applied methods mean deposition rates in the range of 4 ng $m^{-2}h^{-1}$ were calculated throughout the vegetation period, which indicates that temperate grasslands are a small net sink for atmospheric mercury.

It was also investigated whether changes in environmental conditions affect the exchange of Hg^0 and it could be shown that atmospheric Hg^0 is depleted during the night, probably by co-deposition with condensing water. Mercury deposited in such a way is likely to be volatilised again in the morning with increasing temperature. However, it might be oxidised in the aqueous phase and immobilised – temporarily or permanently – by adsorption to soil particles. Also, ozone correlated significantly with atmospheric Hg^0 concentration, but the resolution of the applied micrometeorological methods was insufficient to quantify the associated mercury fluxes. Biological stimulation and enhanced Hg^0 emission as they were observed in the initial incubation experiments could not be detected in the field measurements. Finally, it could be shown, that during the springtime snow melt Hg^0 is emitted from the snow surface and that solar radiation and temperature are the key factors that drive emission.

The present study was completed with further flux measurements in the laboratory with the aim to clarify the role of the vegetation cover on the Hg^0 exchange. Preliminary results of these experiments indicate, that Hg^0 deposition is enhanced in the presence of a vegetation cover, but it could not be clarified if this enhancement is due to the much bigger surface area, or the result of increased humidity, that affects the deposition rate.

Contents

List of Figures

List of Tables

Nomenclature

$\Phi_h(z/L)$	Universal temperature profile
ψ_z	Integrated similarity functions
A	Surface Area
c_x	Concentration of a trace gas
EC	Eddy covariance
F_x	Vertical turbulent flux of trace gas c
GEM	Gaseous elemental mercury
k	von Karman constant
K_x	Turbulent exchange coefficient (eddy diffusivity)
L	Monin-Obukhov length
MBR	Modified Bowen ratio
Q	Air flow-rate
u_*	Fritction velocity
z	Measurement height above ground
Hg^0	Elemental mercury
Hg_p	Particulate mercury
Hg_{tot}	Total mercury
p	p-value
QA/QC	Quality assurance and quality control
RGM	Reactive gaseous mercury

Introduction

Due to its unique properties, mercury has fascinated mankind for more than three millennia. About 200 years ago mercury was introduced in dental amalgams and shortly after first concerns about mercury poisoning emerged. Mercury has also been used intensively in other, large scale industries such as chlorine production, power generation and gold mining, but consciousness about health risks associated with these industries manifested themselves only in the last few decades. It was realised, that mercury's unique properties not only made it precious for a variety of applications, but that these properties were also the basis for its significance as a serious health risk. Mercury emitted to the atmosphere circulates between air, water, soil and biota in various ways and due to global dispersion it even affects regions with no considerable mercury releases (IOMC, 2002). This re-circulation in the environment is one major feature that distinguishes mercury from other heavy metals.

Once deposited, mercury can be transformed to even more toxic methylmercury by anaerobic microorganisms, which in turn biomagnifies more than a million-fold along the aquatic food chain (Schroeder et al., 1998; Wolfe et al., 1998). Therefore, communities that rely on fish as their primary diet are at high risk from methylmercury intoxication (Mergler et al., 2007). It is well documented that methylmercury compounds not only impair the developing brain and the cardiovascular system, but they are also considered possible carcinogens to humans (IOMC, 2002).

Continued exposure to elevated mercury levels can also have negative consequences on vulnerable ecosystems (wetlands, polar and tropical regions) and soil microbial communities. Mercury exposure not only adversely affects reproduction of wildlife populations, recent evidence also suggests that it is responsible for reduced microbiological activity vital to the terrestrial food chain in soils (IOMC, 2002).

Mercury is released into the biosphere by natural sources (volcanic activity, weathering of rocks), anthropogenic emissions and re-mobilisation of previously deposited, anthropogenic discharges. Currently, anthropogenic emissions to the atmosphere are estimated to be in the range of 2000 to 2400 t y^{-1} (Gustin & Lindberg, 2005) and are primarily attributed to the combustion of fossil fuels, chlor-alkali and metal production as well as small scale gold mining operations (Fitzgerald & Lamborg, 2004; IOMC, 2002). While in Asia and Africa the atmospheric burden is still increasing, emissions in Europe and North America have started to decline again in the 1980's (Lindberg et al., 2007a; Pacyna et al., 2005). It has been estimated that since the Industrial Revolution the overall mercury deposition has multiplied by a factor of three

(Lindberg et al., 2007a). It is argued, that this increase is not only the result of direct anthropogenic emissions, but also the consequence of mounting atmospheric ozone concentrations (which in turn are generated by the rising release of primary pollutants and which promote mercury deposition; Lindberg et al., 2007a).

Mercury emitted to the atmosphere primarily consists of elemental mercury (Hg^0), which is transported over very long distances and eventually leads to elevated levels in remote areas. On the other hand, reactive gaseous mercury (Hg^{2+} compounds) and particulate mercury (Hg_p), which constitute less than 10% of the total gaseous mercury (Hg_{tot}) in the atmosphere, have a much shorter lifetime and are deposited closer to their emission source (Schroeder et al., 1998).

Atmospheric mercury in all three forms can undergo various physical and chemical transformations before being deposited to the ground by dry or wet deposition. Besides interactions with ozone, water vapour, hydroxyl and nitrate radicals, photooxidation and -reduction seem the most important transformation pathways (Lindberg et al., 2007a; Lin & Pehkonen, 1999). Once the oxidised species of mercury are deposited on water, soil or vegetation surfaces they will tend to remain non-volatile and hence relatively immobile unless chemical, photolytic or biological reduction to the elemental form occurs (Schroeder et al., 1998). It follows, that the atmospheric load will only be reduced permanently if mercury is sequestered by soils and sediments.

Modelled estimates of global mercury emissions and depositions show a large discrepancy, which accounts to some 3000 t y^{-1} (Gustin & Lindberg, 2005). It has been suggested, that besides the oceans and polar regions, terrestrial ecosystems could constitute an unrecognised sink (Schlueter, 2000). The significance of the latter remains uncertain, especially as the role of vegetation in the mercury exchange between soil and atmosphere, the importance of re-emission of previously deposited mercury and the extent of dry deposition are still unclear (Gustin et al., 2004; Gustin & Lindberg, 2005; Fitzgerald & Lamborg, 2004). The importance of background ecosystems in the global mercury cycle has been recognised (Lindberg et al., 2007b) and numerous studies have addressed various aspects of inter-media transfer processes (e.g. the exchange of Hg^0 between air and forest canopies [Graydon et al., 2006; Lindberg et al., 1998] or so-called "mercury depletion events" in Arctic regions [Lindberg et al., 2002; Schroeder & Munthe, 1998]). Also, much effort has been devoted to describe and quantify mercury emissions from contaminated and naturally enriched areas (Gustin et al., 2003, 2000; Wallschlager et al., 2000; Lindberg et al., 1995), but terrestrial background ecosystems have received little attention. However, the role of these systems is of special interest for several reasons:

- Mercury emissions to the atmosphere have increased continuously since the onset of industrialisation (Fitzgerald et al., 1998). Although emissions of the European and North American economies have decreased substantially during the last two decades, atmospheric background concentrations have not followed this trend as increasing emissions of developing Asian countries seem to offset the reduction (Wangberg et al., 2007). However, the atmospheric load will only be reduced if deposition exceeds emission – and soils of background ecosystems may act as

the required sink.

- Recent studies indicate that background soils can accumulate atmospheric mercury, as shown for example by Obrist et al. (2006), but in other climates soils might as well represent a significant source (e.g. Obrist et al., 2005). Therefore, the question whether background soils are a source or sink of mercury remains unresolved.

- Toxic methylmercury is biomagnified over many orders of magnitude across the aquatic food chain (Fitzgerald & Lamborg, 2004; IOMC, 2002). Mercury deposited on land may be washed off to surface waters, thus increasing the aquatic mercury pool available for methylation and uptake by fish (IOMC, 2002).

- Microbiological activity in topsoils appears to be very sensitive to increasing mercury levels (Johansson et al., 2001; Pirrone et al., 2001). An increasing mercury burden may therefore affect the bottom of the terrestrial food chain.

- In order to understand the biogeochemical cycle of mercury it is important to determine the spatial and temporal variability of the mercury exchange and its response to different environmental factors.

- Accurate flux data from diverse ecosystems are essential for the modelling of the global biogeochemical mercury cycle. Such models are a valuable tool to quantify mercury deposition and to identify risk areas.

With this PhD thesis it is intended to shed light on the role of uncontaminated grasslands in the global mercury cycle. Grasslands are a typical biome of Europe and may constitute a significant sink or source for atmospheric mercury. The aim of this study is to clarify the actual direction of the Hg^0 flux and to assess the source/sink strength of temperate grasslands by estimating air-surface exchange rates. Also, biotic and abiotic factors that may influence this exchange are investigated with additional laboratory experiments.

After a brief illustration of the mercury cycle in the first section of this work, Chapter 2 describes controlled laboratory studies of background soils. These were performed to determine whether biotic processes are relevant in the formation and release of Hg^0 to the atmosphere and whether changing physical and chemical soil conditions stimulate or inhibit microbiologically mediated Hg^0 emission. In Chapters 3 and 4 the application of two classical micrometeorological methods to estimate net Hg^0 exchange rates of selected background grasslands along the Alps is illustrated. Micrometeorological methods are desirable, since they allow independent and continuous monitoring, and provide spatially averaged values, while sampling conditions remain – contrary to flux chamber methods – unaltered. While Chapter 3 describes temporal variations of the Hg^0 flux recorded during a one-year measurement campaign, Chapter 4 focuses on the variability of the Hg^0 flux between three grassland sites and discusses the response of the Hg^0 flux to rapid changes in environmental conditions. In Chapter 5 an investigation of the mercury dynamic in an alpine

snow cover and the exchange of Hg^0 between the snow surface and the atmosphere is illustrated (in this study, which was led by Xavier Fain of Laboratoire de Glaciologie et Geóphysique de l'Evrionnement, Université Joseph Fourier, France, we contributed Hg^0 flux measurements in the field). Finally, Chapter 6 describes some preliminary results of a second set of laboratory studies that are intended to clarify the role of the vegetation cover on the Hg^0 exchange.

Chapter 1

Mercury in the Environment

Mercury is an element with distinctive physical properties: it is liquid at room temperature, amalgamates with noble metals and has a high saturation vapour pressure (0.18 Pa at 20°C, Lin & Pehkonen, 1999). Especially the latter renders mercury extremely mobile and as a result it is found in all environmental compartments around the globe (IOMC, 2002). Mercury's biogeochemical cycle is complex and involves both abiotic and biotic processes in the gaseous, aqueous and solid phases (Lin & Pehkonen, 1999; Gabriel & Williamson, 2004; Morel et al., 1998). Figure 1.1 illustrates the mercury cycle with the main transformation pathways.

Mercury exists in various inorganic and organic forms at concentrations ranging from 1.2 ng m^{-3} in the air of remote areas to several $\mu g\ g^{-1}$ in certain fish species (IOMC, 2002). Under ambient conditions mercury occurs in three oxidation states with very different reactivity: Hg^0, mercurous ion Hg_2^{2+} and mercuric ion Hg^{2+}. While Hg^{2+} can form stable complexes with OH^-, Cl^-, Br^-, I^-, SO_3^{2-} and CN^-, Hg_2^{2+} is not stable and is readily transformed to Hg^0 or Hg^{2+} (Lin & Pehkonen, 1999). The most important reactions of mercury known to date are listed in Tab. 1.1.

Elemental mercury has low solubility in water, thus volatilisation results in a flux of Hg^0 to the atmosphere, where it constitutes more than 95% of Hg_{tot} (Morel et al., 1998). Furthermore, as Hg^0 has a low reactivity its residence time in the atmosphere is rather long and it is distributed homogenously over wide areas (Lin & Pehkonen, 1999). Eventually it is removed from the atmosphere through oxidation of Hg^0 to Hg^{2+}. Most of this oxidation occurs at the solid-liquid interface of fog and cloud droplets where reaction is accelerated (Lin & Pehkonen, 1999). The predominant oxidant for Hg^0 in the atmosphere is ozone, but HOCl and $OH^\cdot$ may also be significant (Lin & Pehkonen, 1999; Schroeder et al., 1998). Gas-phase oxidation reactions of Hg^0 by O_2, H_2O_2 as well as Cl_2 may be important as well, but large uncertainties exist regarding their rates (Lin & Pehkonen, 1999; Zhang & Lindberg, 1999). Ozone, H_2O_2, $OH^\cdot$ and $HO_2^\cdot$ are daytime oxidants that are produced by photochemical reactions of NO_x and VOC, while Cl_2 is an important oxidant in the marine atmosphere (Lin & Pehkonen, 1999). At typical pH values of atmospheric droplets the primary oxidation products are either $HgCl_2$ or $Hg(SO_3)_2^{2-}$, depending on the relative concentrations of Cl^- and S(IV) (Lin & Pehkonen, 1999). Some of the Hg(II) produced in the at-

mosphere is reduced again by SO_3^- or by photoreduction of $Hg(OH)_2$ (Morel et al., 1998). However, most Hg(II) will return to the Earth's surface by wet and dry deposition either dissolved in precipitation or adsorbed to aerosols (a significant fraction of dissolved Hg(II) may be associated with soot particles; Morel et al., 1998).

In surface waters mercury is present at concentrations of ~1 ng l^{-1} in various chemical forms such as ionic mercury bound to Cl^-, S^{2-} and organic acids, methyl-, dimethyl- and ethylmercury and Hg^0 (Morel et al., 1998). The transformation reactions in water are complex and involve redox, photochemical and biological processes, all of which are highly dependent on the prevailing pH value and redox potential (Gabriel & Williamson, 2004; Fitzgerald & Lamborg, 2004). After transformation mercury may eventually be reduced again to Hg^0, re-emitted to the atmosphere or exported to the sediments by formation of stable HgS (Morel et al., 1998). Yet, some mercury will be transformed by different strands of bacteria and fungi – and to a lesser extent by abiotic processes – to methylmercury (Gabriel & Williamson, 2004). Methylmercury is of particular concern since its toxicity is much higher than that of Hg^0 and because it can bioaccumulate and biomagnify in many edible fish and mammals to levels that are several orders of magnitude higher than in their habitat (IOMC, 2002). The amount of methylmercury available for uptake depends primarily on the concentration of mercury in the water and the rate of methylation and demethylation. The latter is accomplished by aerobic organisms or photolytical decomposition at the water surface (IOMC, 2002; Schlueter, 2000).

Especially in the mid and high latitudes some atmospheric mercury is deposited with snow, where it is present as hydroxo- and chlorocomplexes (Ferrari et al., 2002). Recent research has documented, that mercury in the snow might not be accumulated, but rather re-emitted within a short time after deposition (Lalonde et al., 2002). It is suggested that, again, photodissociation is the primary reaction responsible for reduction of mercury in and volatilisation from the snow cover. This process seems to be enhanced during snow melt through the presence of liquid water around the snow crystals (Lalonde et al., 2002).

In terrestrial soils, mercury principally occurs in the form of inorganic salts ($HgCl_2$, HgO, HgS, $HgSO_4$) and organic compounds (Gabriel & Williamson, 2004). The behaviour of mercury and its distribution are mainly controlled by adsorption and desorption processes, in which organic constituents and mineral surfaces (e.g. clay minerals, amorphous oxides and hydroxides of Fe and Al) play an important role (Gabriel & Williamson, 2004; Schuster, 1991). Mercury has a distinct affinity to sulphur that results in a high binding capacity of soil organic matter, which in turn may lead to its accumulation in soils (Schuster, 1991). It is suggested, that this characteristic could also promote methylation, as organic matter generally harbours bacteria capable of methylating mercury (Gabriel & Williamson, 2004).

Generally less than 2% of Hg_{tot} in soils is present as methylmercury (Gabriel & Williamson, 2004). It is believed that a large fraction of mono-methylmercury (CH_3Hg^+) is bound to the organic soil matrix, while dimethylmercury – $(CH_3)_2Hg$, a highly volatile mercury species – is released to the atmosphere, where it is rapidly de-

Oxidation	Reduction
Reactions in the aqueous phase of the atmosphere[a]	
$Hg^0_{(aq)} + O_{3(aq)} \longrightarrow Hg^{2+}_{(aq)} + OH^-_{(aq)} + O_{2(aq)}$	$HgSO_{3(aq)} \longrightarrow Hg^0_{(aq)} + \text{Products}$
$Hg^0_{(aq)} + 2\ {}^{\cdot}OH \longrightarrow Hg^{2+}_{(aq)} + 2OH^{-(aq)}$	$Hg(OH)_{2(aq)} \xrightarrow{h\nu} Hg^0_{(aq)} + \text{Products}$
$Hg^0_{(aq)} + HOCl_{(aq)} \longrightarrow Hg^{2+}_{(aq)} + Cl^-_{(aq)} + OH^-_{(aq)}$	$Hg(II)_{(aq)} + 2HO^{\cdot}_{2(aq)} \longrightarrow Hg^0_{(aq)} + 2O_{2(aq)} + 2H^+_{(aq)}$
$Hg^0_{(aq)} + OCl^-_{(aq)} \longrightarrow Hg^{2+}_{(aq)} + Cl^-_{(aq)} + OH^-_{(aq)}$	
Reactions in the gaseous phase of the atmosphere[a]	
$Hg^0 + O_3 \longrightarrow HgO + O_2$	
$Hg^0 + NO_3^- \longrightarrow HgO + NO_2$	
$Hg^0 + H_2O_2 \longrightarrow Hg(OH)_2$	
Reactions in the aqueous phase of soils[b]	
	$Hg^{2+}_{(aq)} + DOC \xrightarrow{h\nu} Hg^0 + DOC^+$
	$Hg^{2+}_{(aq)} \xrightarrow{\text{Microorganisms}} Hg^0$
	$Hg^{2+}_{(aq)} + H_2O_2 + 2OH^- \longrightarrow Hg^0_{(aq)} + O_2 + 2H_2O$
	$Hg(OH)_{2(aq)} \xrightarrow{h\nu} Hg^0 + 2\ {}^{\cdot}OH$
	$> \text{organic acid complex} - Hg^{2+} \xrightarrow{h\nu} Hg^0$

[a]Lin & Pehkonen (1999), [b]Gabriel & Williamson (2004); Schlueter (2000)

Table 1.1: Transformations of mercury in the environment

composed photolytically to Hg^0 and methyl-radicals (Schlueter, 2000). Organic mercury compounds are not stable in natural environments, but physico-chemical and biological transformation processes of some methylmercury species are slow enough to yield concentration levels that are of environmental concern and which might pose a serious bioaccumulation problem (Schlueter, 2000; Gabriel & Williamson, 2004).

A multitude of redox reactions occurs in the aqueous phase of soils, which either leads to volatilisation or permanent sequestration of mercury (Gabriel & Williamson, 2004). Under reducing conditions sulphur is normally present as S^- and HgS is formed, which is precipitated (Schuster, 1991). However, with the help of electron donors such as Fe^{2+} and humic and fulvic compounds, conditions with higher redox potentials (above which sulfate reduction occurs) are also favourable for reduction of Hg^{2+} and volatilisation of Hg^0 (Gabriel & Williamson, 2004). Besides, it is also known that various strands of bacteria mediate the reduction of Hg^{2+} in similar ways as in aquatic environments (Schroeder et al., 1998). At the soil surface reduction is further enhanced in the presence of sunlight (Gabriel & Williamson, 2004; Schroeder et al., 1998). The underlying mechanisms of this transformation pathway are still unclear, but seem to involve direct reduction of $Hg(OH)_2$ or soil-bound mercury, photochemically reduced metals (Fe[II], Mn[II]) that reduce mercury when re-oxidised and light-induced formation of microbiological metabolites and radicals capable of mercury reduction (Morel et al., 1998; Schlueter, 2000). The efficiency of photoreduc-

tion depends on the level of reducible Hg(II)-complexes, wave length and radiation intensity (Morel et al., 1998).

All biotic and abiotic reduction processes are strongly dependent on factors like soil and air temperature, soil pH, soil moisture content and solar radiation, and the constellation of these factors determines the fate of mercury in the environment (Gabriel & Williamson, 2004; Schlueter, 2000).

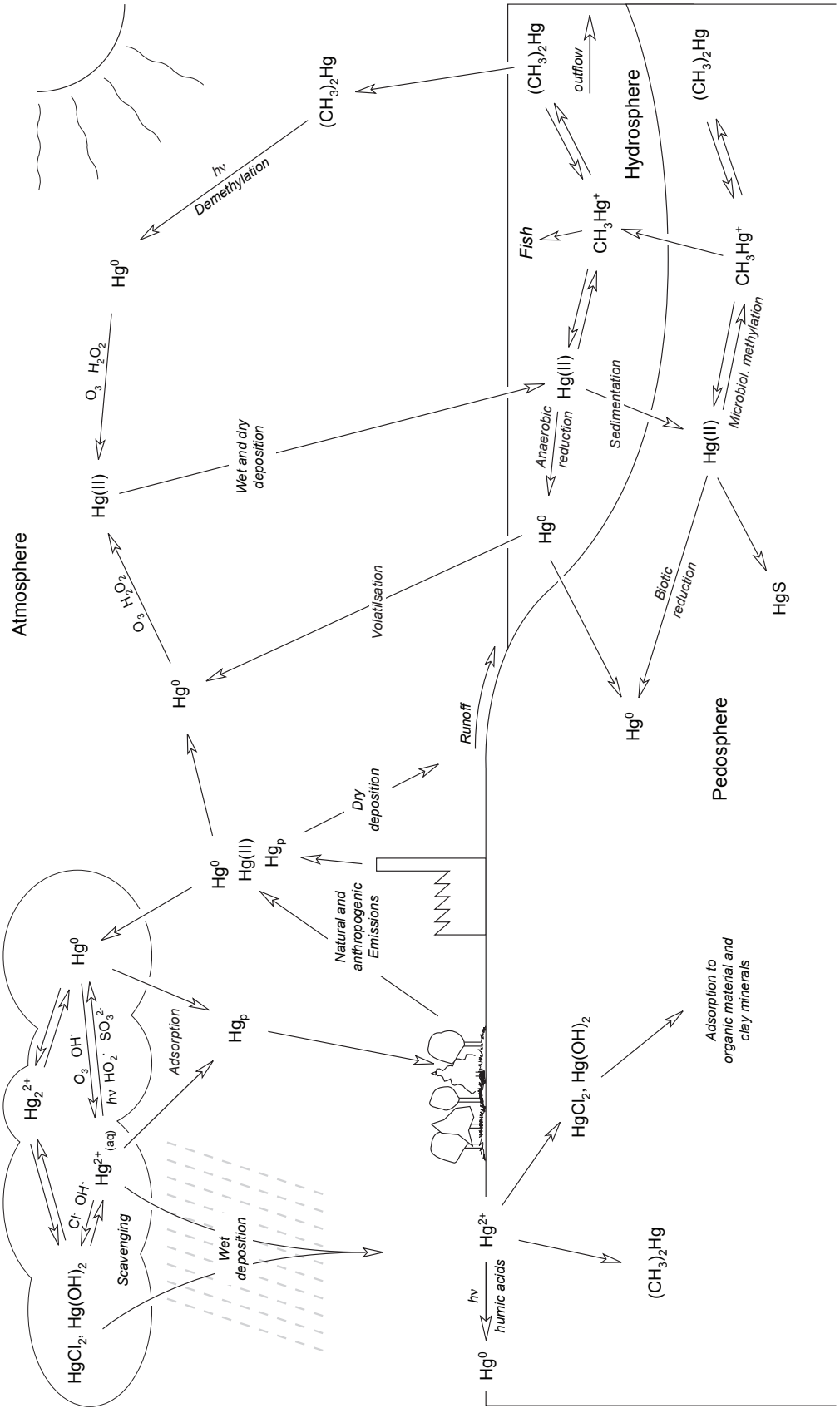

Figure 1.1: Biogeochemical mercury cycle (adapted from Dommergue, 2003)

Chapter 2

Hg^0 emissions from soils mediated by microbiological activity

This chapter will be published in the Journal of Plant Nutrition and Soil Science as:
Fritsche, J., Obrist, D., Alewell, C., 2008: Evidence of microbial control of Hg^0 emissions from uncontaminated terrestrial soils. Journal of Plant Nutrition and Soil Science, accepted 18 February 2007.

2.1 Abstract

It is known that direct biotic reduction of Hg^{2+} to Hg^0 in wetland soils and soils contaminated with mercury leads to Hg^0 emissions to the atmosphere. In terrestrial soils numerous factors have been reported that control Hg^0 emissions, but it is still unclear if biotic processes are also important. In this study microbiological activity of cambisol monoliths from a sub-alpine grass land with mercury concentrations of $\sim$100 ng g^{-1} was manipulated in laboratory incubation experiments. Elemental mercury emissions were recorded together with CO_2 emission rates as proxy for microbiological respiration. Emissions of Hg^0 increased from $\sim$5 ng m^{-2} h^{-1} up to 130 ng m^{-2} h^{-1} with stimulated biological activity (glucose addition, increase in temperature) and decreased with inhibited activity (chloroform fumigation, autoclaving, drying). Similar patterns with evasion rates of more than 90 ng m^{-2} h^{-1} were observed after dried soils were remoistened again. Our results indicated that processes leading to Hg^0 emissions from uncontaminated terrestrial soils are at least partly controlled by biotic processes. However, it is still uncertain if Hg^0 emission is caused directly by biotic reduction of Hg^{2+} or indirectly by abiotic reduction, induced by products of microbiological degradation, e.g. humic acids.

2.2 Introduction

Mercury is ubiquitous in the environment and poses a threat to the fauna and to humans, mainly by the processes of bioaccumulation and biomagnification (Morel

et al., 1998; Summers & Silver, 1978; Wood, 1974). Besides volatilization from natural sources emissions of mercury are dominated by combustion of coal and waste (Fitzgerald & Lamborg, 2004). Especially in its elemental form (Hg^0) mercury can spread via atmospheric transport to even remote areas and is therefore considered a global pollutant (Fitzgerald, 1995). Increased awareness and substitution of mercury-containing products have reduced the past, unheeding use of mercury in industrialized countries and have led to decreases in atmospheric concentrations and subsequent deposition to terrestrial ecosystems (Iverfeldt et al., 1995; Schuster et al., 2002). However, anthropogenic emissions are still significant in the emerging economies of Asia. In addition, the release from natural sources and re-emission of previous depositions add continuously to the atmospheric mercury load (IOMC, 2002).

Wet deposition of soluble Hg(II) species is the primary input of mercury to soils, but dry deposition, throughfall, wash-off, and litterfall add significant amounts to terrestrial ecosystems (Grigal, 2003); wet deposition rates to open fields have been shown to be between 4 to 28 $\mu g\ m^{-2}yr^{-1}$ (Fitzgerald & Lamborg, 2004). Soils are considered resilient reservoirs for deposited mercury due to the strong adsorption capacity of clays and organic material (Gabriel & Williamson, 2004). Losses of mercury from soils and watersheds by runoff are generally small (Grigal, 2003; Lee et al., 1998), and discharge via leaching to groundwater is almost negligible (Johnson and Lindberg, 1995). In contrast, evaporation of Hg^0 from the soil's surface constitutes a potentially important factor for the release of soil-bound mercury (Grigal, 2003). The main mercury forms that evaporate from terrestrial surfaces to the atmosphere are the two volatile species Hg^0 and dimethylmercury, although the release of the latter is probably quantitatively less important (Schlueter, 2000).

The rate at which Hg^0 is emitted to the atmosphere is dependent on the pool size of mercury in the soil, the supply rate of mercury from the underlying bedrock, the soil characteristics such as porosity, soil moisture and its associated redox-conditions, and soil temperature (Gabriel & Williamson, 2004; Lindberg et al., 1995; Schlueter, 2000; Siciliano et al., 2002; Zhang & Lindberg, 1999). As most of the mercury in terrestrial soils under natural pH/Eh conditions and Cl^- concentrations is present as Hg^{2+} compounds (e.g. $Hg(OH)_2$, $HgCl_2$, and HgS (Schlueter, 2000)) reduction processes are important for the formation and emission of Hg^0 to the atmosphere. The factors responsible for the reduction of Hg^{2+} to Hg^0 are believed to be mainly of physical and chemical nature, such as photoreduction (Bahlmann & Ebinghaus, 2003; Carpi & Lindberg, 1997; Gustin et al., 2002; Zhang & Lindberg, 1999) or reduction in the presence of humic and fulvic substances (Alberts et al., 1974; Ravichandran, 2004; Schlueter, 2000) or reactive Fe^{2+} adsorbed to mineral surfaces, which acts as a reductant (Charlet et al., 2002). Nevertheless, it has also been discussed that apart from physically and chemically mediated Hg^0 emission, microbial activity might contribute to mercury evaporation (e.g. Schlueter (2000)). This notion is based on the ability of a wide range of bacteria to detoxify inorganic and organic mercury compounds by reduction of Hg^{2+} to Hg^0, which is then lost to the vapor phase (Summers & Silver, 1978; Wood, 1974). Schlueter (2000) concluded that the induction of biotic mercury

reduction seems to require high concentrations of bioavailable mercury, probably in the range of several parts per million. However, the importance of biotic processes on Hg^0 evaporation in terrestrial soils with background mercury content (<0.1 μg g^{-1}) is still unclear as only few studies have addressed microbial influence. For example, Rogers & Mc Farlane (1979) amended soils with mercury and Mason et al. (1995) incubated natural water. Both studies demonstrated substantial mercury reduction by microorganisms. Autoclaved sandy soils amended to 1 μg g^{-1} lost 31% of mercury within 10 days after inoculation (Rogers & Mc Farlane, 1979). Schlueter (2000) concludes that in many soils mercury evaporation might even be dominated by biological processes.

The aim of this study was to estimate the influence of microbiological activity on the emission of Hg^0 from terrestrial soils with background mercury concentrations. Under controlled laboratory conditions the effect of stimulation and inhibition of microbial activity on Hg^0 emissions was tested using chemical and physical treatments. We hypothesize that the emission of Hg^0 from soils is affected by inhibition or stimulation of microbial activity.

2.3 Incubation experiments

2.3.1 Soil samples

All soil samples investigated in this study were collected from the A horizon of a subalpine meadow situated in central Switzerland about 30 km south of Zurich (Zuger Berg; 47°6'47" N, 8°32'16" E). The area at an elevation of about 1'000 m a.s.l. has a mean annual temperature of 7°C and receives an average of 1'200 mm of precipitation per year. The bedrock consists of alpine conglomerate and is covered primarily by cambisols and stagnic cambisols.

A total of 16 soil samples in the size of 30×12×6 cm (approx. 3 kg) were cut with a knife from a depth of 10 to 20 cm. This soil layer had few plant roots that could have influenced Hg^0 exchange. To minimize disturbance, the soil samples were directly put into polystyrene containers which later constituted the bottom part of the flux chambers (see below). A first set of samples was taken in December 2004, a second set in March 2005. Samples were stored in plastic bags at 2°C until the start of each incubation run (up to 10 weeks after sample collection).

2.3.2 Experimental setup and data acquisition

Dynamic flux chambers as illustrated in Fig. 2.1 were used to determine elemental mercury and CO_2 fluxes. Carbon dioxide served as a proxy for the activity of the soil microbial population (Harris, 1988; note that all soil samples were free of calcium carbonate). Concentrations of Hg^0 and CO_2 were measured alternately at the chamber in- and outlets and fluxes were calculated as

$$F = \frac{\Delta c_x \cdot Q}{A} \tag{2.1}$$

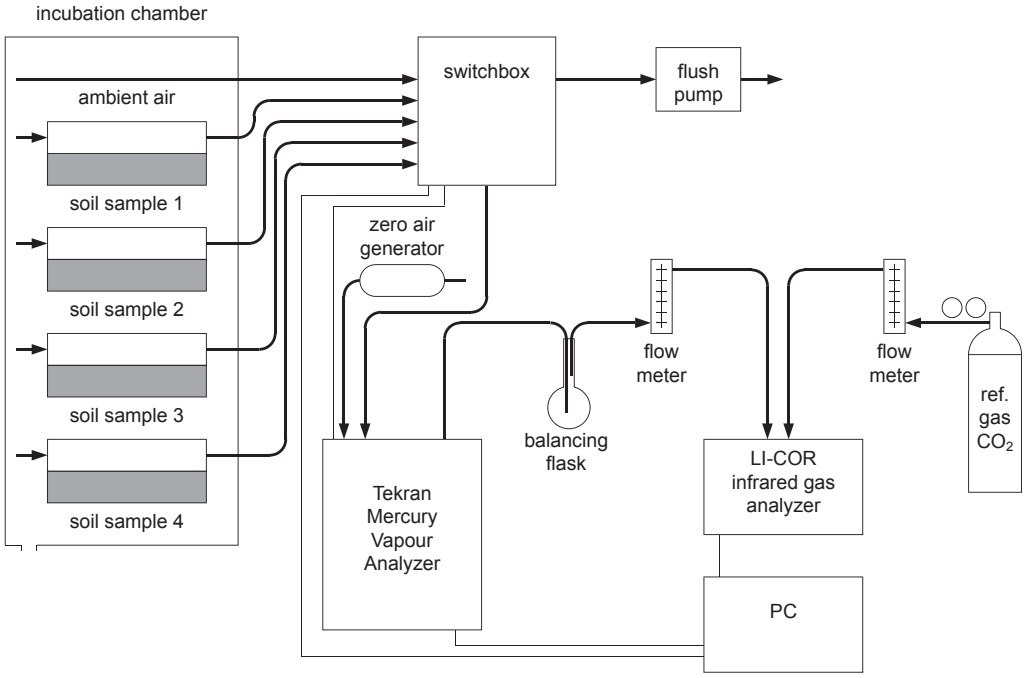

Figure 2.1: Experimental setup for the determination of CO_2 and Hg^0 fluxes of background soil samples. Bold lines represent the air flow.

where Δc_x is the concentration difference between in- and outlet lines, Q the air flow-rate and A the soil surface area. The soil samples in the polystyrene containers were covered with lids fitting the containers. Holes on the inlet side and a 1/4" connector at the outlet side of the lids allowed a steady air-flow over the sample (Fig. 2.1). Lid and bottom part of the flux chambers were sealed together with silicontubing. The chambers were then placed in a temperature controlled, dark incubator. Elemental mercury concentrations in the incubation chamber ranged from 3.5 to 7.8 ng m^{-3}; background concentrations outside the building were 2.6 ng m^{-3} [Obrist et al. 2006]. Outlet lines were connected with Teflon tubing to a 5-port Teflon solenoid switching unit, an elemental mercury analyzer and an infrared CO_2-gas analyzer. To avoid any particles entering the analytical system, 0.2 μm Teflon® particulate filters were mounted to the sampling lines. For reasons of convenience and simplicity ambient air was used.

The 5-port switching unit allowed the simultaneous measurement of four samples by switching in a cyclic mode between the inlet line – placed in the centre of the incubator to sample ambient air entering all flux chambers – and four outlet lines; inlet measurements always preceded outlet measurements. The lines that were not measured were flushed continuously by drawing air through them with a small pump.

Every 3 to 5 days the soil moisture of the samples was adjusted to the levels measured at the beginning of the incubation runs.

Each incubation run was carried out with two samples undergoing treatment as described below and two samples functioning as reference. Sets of samples taken on different days were also studied in different runs. Treatment effects on CO_2 and Hg^0 fluxes were examined through t-tests with Matlab® at the 0.05 significance level. Measurements within 12 to 24 hours before and after the treatments were chosen as data basis for these tests.

Elemental mercury and CO_2 fluxes are presented on an area basis (ng m^{-2} h^{-1}, mmol m^{-2} h^{-1}). To allow comparison with other studies data within the text are also shown on a dry mass basis (pg kg^{-1} h^{-1}, μmol kg^{-1} h^{-1}).

2.3.3 Analytical instruments

Elemental gaseous mercury concentrations were determined with a Tekran 2537A Mercury Vapour Analyzer (Tekran Inc., Toronto, Canada), which is designed to predominantly measure Hg^0 within a concentration range of 0.1 to 2000 ng m^{-3} (see Lindberg & Meyers, 2001 for more details). The instrument was operated with a flow rate of 1.5 l min^{-1} with a sampling interval of 5 minutes.

A LI-6262 infrared gas analyzer (LI-COR Inc., Lincoln, USA) was used to measure CO_2 concentrations. The air for CO_2 analysis was split from the sampling line right before the mercury analyzer and drawn to the instrument at a flow-rate of 0.5 l min^{-1}. The CO_2 concentrations, recorded at a frequency of 1 Hz, were averaged over 5-minute intervals to match the measurement cycle of the mercury analyzer.

For the determination of soil characteristics (clay and silt fractions, C_{org} content, soil pH, Hg content) the soil samples were dried and sieved at the end of the experiments to obtain the 2 mm fraction. Soil texture was determined with a Sedigraph 5100 (Micromeritics, Moenchengladbach, Germany) and C_{org} with a Leco RC-412 carbon analyzer (Leco, St. Joseph, USA). The soil pH was measured with a glass electrode after 5 min stirring of the soil-water suspensions (soil-water ratio of 1:2).

Total soil mercury concentrations were determined with four replicates using a Milestone DMA-80 Direct Mercury Analyzer (Milestone Inc., Bergamo, Italy) in the laboratory of Dr Gustin at the University of Nevada, Reno, USA.

2.3.4 Treatments of soil samples

Before any samples were treated, their CO_2 and Hg^0 emissions were measured in the incubator at 15°C until fluxes stabilized (for at least 3 days). For inhibition of microbiological activity in the soil samples two different treatment methods were applied: chloroform fumigation and pressure boiling in an autoclave. For the first method the soil samples were placed in a desiccator together with 50 ml liquid chloroform, analytical grade, for 24 hours. To ensure efficient evaporation of chloroform and effective fumigation of the soil samples the desiccator was evacuated several times (Horwath & Paul, 1994). Samples treated by pressure boiling were put in an autoclave and heated

to 120°C for two successive 30-minute intervals. Autoclaving is a widely used and efficient method to sterilize soil (Wolf & Skipper, 1994).

To stimulate microbiological activity the soil samples were treated with glucose. A solution of 7.5 g in 50 ml of water was added to each soil sample. For stimulation after sterilization, samples were inoculated with fresh soil (∼50 g) 5 to 7 days after sterilization to induce microbial recuperation.

To simulate dry and wet conditions in sterilized and non-sterilized soil, autoclaved and untreated samples were dried for two days at 40°C, placed in the incubator for several days and finally rewetted to their initial moisture levels. Effects of temperature changes were observed with untreated and autoclaved samples by shifting the soil temperature from 5 to 20°C and 15 to 5°C, respectively. Water used in the experiments was of ultra-pure grade (Milli-Q® Academic, Millipore Corporation), but not sterile.

2.3.5 QA/QC

All sampling lines and Teflon parts were cleaned with chelating soap (Micro-90, Fisher Bioblock Scientific, France) and hot 10% HNO_3 before use. Prior to each run the lines were checked for any Hg^0 contamination using a Tekran 1100 zero-air-generator (Tekran Inc., Toronto, Canada). Blanks of the cleaned and empty flux chambers were determined between each run and averaged 0.83 $\pm$0.51 ng m^{-2} h^{-1} Hg^0. Concentration differences between in- and outlet lines were corrected accordingly.

Apart from the daily internal calibrations, using an internal mercury permeation source, the accuracy of the Tekran Hg^0 analyzer was validated by manual injections of predefined volumes of Hg^0 vapor from the temperature controlled Tekran 2505 injection source (Tekran Inc., Toronto, Canada). The CO_2 gas analyzer was operated in a differential measurement mode with compressed, ambient air as a reference gas. Calibrations were performed regularly by measuring a CO_2-free gas (N_2 or Ar) to set the zero-point and a three-component span gas (N_2, O_2 and 451 ppm CO_2) to set the reference.

2.4 Results and discussion

2.4.1 Characteristics of soil samples

Mercury concentrations, soil composition as well as soil pH of the investigated samples are listed in Table 2.1. The soils used in this incubation study were characterized as loamy soils with a soil texture ranging from clayey to silty loam. The samples were relatively rich in organic carbon (2.2 to 7.6% C_{org}, which translates to approximately 4 to 13% soil organic matter) and were neutral to moderately acidic with a pH between 4.6 and 7.1. Treatment with HCl solution proved the samples to be free of carbonate. Average bulk density was 1.1 $\pm$0.1 g cm^{-3}. Mercury concentrations were between 82 and 142 ng g^{-1}, values common for uncontaminated background soils (Salminen, 2006). There was a good correlation of the mercury concentration with the silt fraction (r^2=0.67, p=0.002), but none with the clay fraction nor the soil C_{org} content. The lack

ID	Run	Treatment of sample	Clay[n] [%]	Silt[n] [%]	Sand[n] [%]	C_{org}[n] [%]	pH[k]	Hg conc.[m,n] [ng g^{-1}]	
1b	2	autoclaved, T-shift	22.5	44.5	33.0	3.4	5.2	90.3	± 1.6
4b	2	autoclaved, T-shift	21.3	53.5	25.2	5.3	5.9	142	± 7
3b	2	untreated reference, T-shift	26.0	46.6	27.4	2.6	4.6	103	± 5
2b	2	untreated reference, T-shift	19.4	53.4	27.2	6.6	7.0	101	± 7
1e	4	fumigated with chloroform	25.1	37.5	37.4	2.3	5.2	81.9	± 7.5
4f	4	fumigated with chloroform	21.5	50.0	28.5	2.9	5.4	109	± 6
1f	4	untreated reference	26.3	37.5	36.2	2.7	5.0	84.3	± 3.4
4e	4	untreated reference	26.2	47.6	26.2	3.2	5.6	109	± 3
1a	1	addition of glucose	24.1	41.8	34.1	3.0	4.9	90.3	± 5.5
2a	1	addition of glucose	15.9	53.7	30.4	7.6	7.0	97.3	± 2.6
3a	1	addition of glucose	27.5	46.0	26.5	3.9	5.0	105	± 4
4a	1	addition of glucose	17.4	64.0	18.6	6.0	6.1	142	± 7
1j	6	autoclaved, dried, rewetted	-[p]	-[p]	-[p]	3.4	5.4	89.3	± 6.5
4i	6	autoclaved, dried, rewetted	-[p]	-[p]	-[p]	5.3	6.7	120	± 3
1i	6	dried, rewetted	-[p]	-[p]	-[p]	2.2	4.9	91.7	± 5.6
4j	6	dried, rewetted	-[p]	-[p]	-[p]	4.5	6.8	117	± 6

[k] measured in H_2O-extract
[m] total Hg concentration; mean and standard deviation of 4 replicates
[n] based on soil mineral fraction ≤2 mm
[p] not determined

Table 2.1: Composition and Hg concentrations of studied soil samples.

of a correlation with the latter two was surprising since soil mercury is known to have a high affinity to both, clay particles and soil organic matter (Schlueter, 2000).

2.4.2 Effects of manipulation of microbiological activity on Hg^0 emissions

Effects of autoclaving and inoculation of sterilized soil samples

In the incubation run presented in Fig. 2.2 microbial activity of two samples was reduced by pressure boiling in an autoclave, while two samples were left untreated to serve as references. The CO_2 fluxes of the autoclaved samples dropped significantly ($p<0.001$) from their initial levels of 0.8 and 2.0 mmol m^{-2} h^{-1} (20 and 30 μmol kg^{-1} h^{-1}) to zero which indicates that complete sterilization of the soil samples was achieved (Fig. 2.2, day 5). In contrast, the CO_2 fluxes of the reference samples remained at the levels observed before the treatment. The Hg^0 fluxes switched from emissions of 4.0 and 0.5 ng m^{-2} h^{-1} (90 and 10 pg kg^{-1} h^{-1}) to depositions of 1.2 and 0.5 ng m^{-2} h^{-1} (30 and 10 pg kg^{-1} h^{-1}; significant with $p<0.001$), i.e. the sterilized samples turned from a net source of mercury to a net sink. While one of the reference samples emitted Hg^0 at steady levels throughout the measurement period, another showed gradually increasing emissions during the first 9 days. We ascribed this difference to natural variability of the soil properties, because both reference samples were exposed to exactly the same experimental conditions. The described effects of

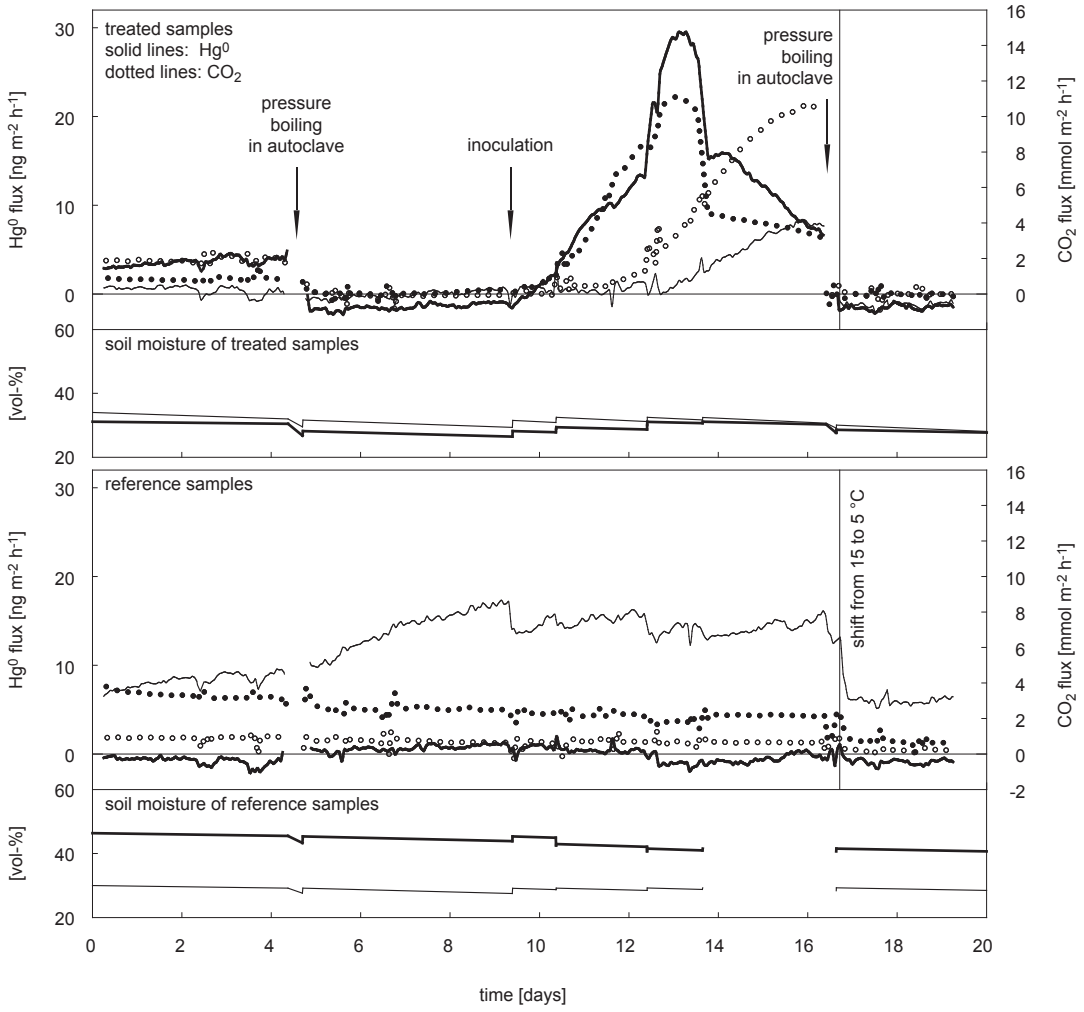

Figure 2.2: Inhibition and stimulation of microbiological activity. CO_2 and Hg^0 fluxes of autoclaved samples (sample-ID: 1b, 4b). Lower plots represent reference samples, which were not autoclaved but handled in the same way as the treated samples (sample-ID: 2b, 3b).

inhibition could be reproduced with a subsequent autoclave treatment (Fig. 2.2, day 16).

The cessation of the Hg^0 emissions could have various reasons: The collapse of microbial activity caused by autoclaving could have directly stopped mercury emissions from the soil, the severe heat and pressure conditions could have completely depleted the mercury available for volatilization, or the treatment could have altered the soil's physical or chemical properties in such a way that no further mercury evaporation was possible. However, after the sterilized soil samples were inoculated with a few grams of untreated soil a distinct Hg^0 emission flush could be recorded (Fig. 2.2, days 10 to 16), indicating that autoclaving did not completely deplete the available mercury pool. The Hg^0 fluxes increased significantly ($p<0.001$) from slightly negative values to 30 ng m^{-2} h^{-1} (670 pg kg^{-1} h^{-1}). Interestingly, these Hg^0 flushes were syn-

chronized with the CO_2 fluxes (i.e. the intensifying microbial activity). For example, microbial recuperation of one sample was delayed by two days, but was accompanied by an equally delayed Hg^0 signal. We therefore propose that the parallel de- and increases of mercury emissions and microbial respiration are due to a direct effect of microbial activity on Hg^0 mobilization and not artefacts induced by the autoclave treatment. This proposition is also supported by the second sterilization experiment where similar emission patterns were observed, although the treatment was not based on physical destruction of microbes but on a chemical chloroform treatment (see next section). However, it can not be excluded that the effects of autoclaving strongly affect the potential of the soil to emit Hg^0. A more than five times higher Hg^0 emission after chloroform fumigation (see below) indicates that in fact significant amounts of mercury were lost during autoclaving.

These results are in good agreement with the findings of a study by Rogers & Mc Farlane (1979) who applied autoclaving to sterilize soil samples amended to elevated levels of Hg^{2+}. High rates of Hg^0 volatilization were observed after inoculation, but Rogers & Mc Farlane (1979) presented no measure of microbial activity.

Effects of chloroform fumigation

Chloroform is highly toxic and has been used to fumigate soils for sterilization and the estimation of microbial biomass (Dickens & Anderson, 1999; Horwath & Paul, 1994; Toyota et al., 1996). Fumigation with chloroform was applied, like autoclaving, to inhibit the soil's microbiological activity and to observe the effects on the associated Hg^0 fluxes after sterilization as well as during the period when the microbial population recovered. Figure 2.3 shows the fluxes of the fumigated and the reference samples before and after chloroform fumigation. Right after the soil was transferred from the chloroform treatment to the flux chambers CO_2 fluxes around 1.4 mmol m^{-2} h^{-1} (20 μmol kg^{-1} h^{-1}) were recorded, which were not significantly lower than the pre-treatment levels, indicating that the chloroform fumigation inhibited microbial activity only partially. A significant ($p<0.001$) but temporally limited (1-2 days) reduction of the Hg^0 fluxes from the soil was observed in the fumigated samples (from 5-10 ng m^{-2} h^{-1} to 2-3 ng m^{-2} h^{-1} [80-160 to 30-50 pg kg^{-1} h^{-1}]). The fact that Hg^0 emissions were significantly lower than those observed before the chloroform treatment and lower than those of the reference samples shows that inhibition of microbial activity affected Hg^0 volatilization. However, the response of the CO_2 and Hg^0 fluxes to chloroform fumigation was not as pronounced as observed after autoclaving. Previous studies have shown that chloroform fumigation rarely results in total death of microbial populations, and might thus be only used as a partial sterilization technique for soils. Approximately 10% of bacterial and 0.5% of fungal colony forming units, but all spores of the investigated bacteria survived chloroform fumigation (Toyota et al., 1996).

Within one day after the fumigation treatment both, microbial respiration (i.e. CO_2 fluxes) and Hg^0 emissions started to increase progressively (Fig. 2.3). The CO_2 fluxes increased within two days from levels below 1 mmol m^{-2} h^{-1} to 10-13 mmol m^{-2} h^{-1}

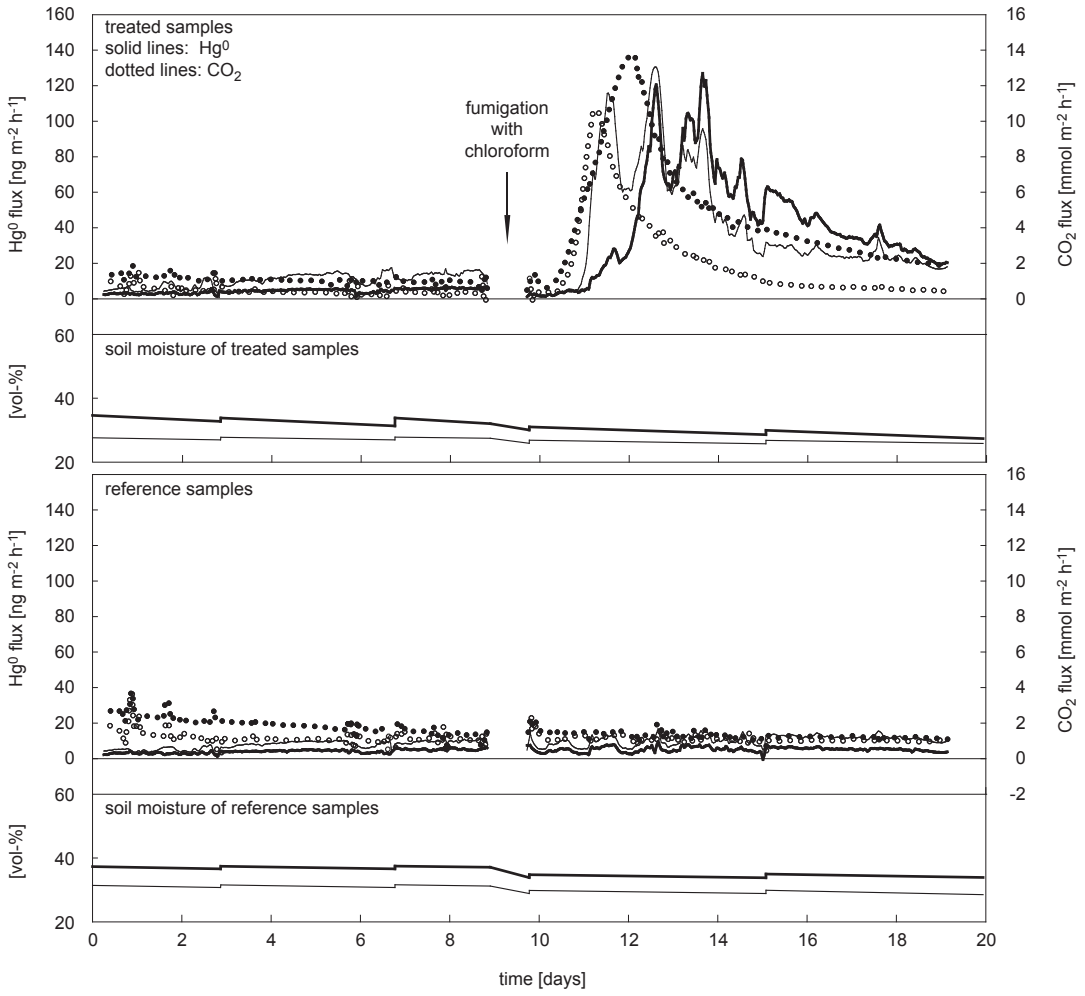

Figure 2.3: Inhibition and stimulation of microbiological activity. CO_2 and Hg^0 fluxes of samples treated by chloroform fumigation (sample-ID: 1e, 4f). Lower plots show fluxes of reference samples, which were not fumigated, but handled in the same way as the treated samples (sample-ID: 1f, 4e).

(20 to 160-210 μmol kg^{-1} h^{-1}). This boost was most likely due to cell lysis during chloroform treatment and subsequent, enhanced respiration of labile carbon compounds. Similarly, Hg^0 fluxes increased equally fast and peaked at values of 130 and 125 ng m^{-2} h^{-1} (2'120 and 2'010 pg kg^{-1} h^{-1}), which is a more than 80-fold increase compared to the levels observed immediately after sterilization. In comparison, the fluxes of CO_2 and Hg^0 of the reference samples remained constant at the low levels observed before the treatment (Fig. 2.3). However, the pronounced flushes of CO_2 and Hg^0 were not permanent; after one week the fluxes were still significantly ($p<0.001$) higher, but approached pre-treatment levels. Thus, similar to the pattern observed after autoclaving, inhibition of microbial activity led to reduced Hg^0 emissions, while increasing microbial activity strongly promoted Hg^0 evasion.

Two important differences between the autoclaving and chloroform treatments

were observed. First, the increase of Hg^0 emissions during microbial recuperation was much more pronounced after the chloroform treatment (up to 125-130 ng m^{-2} h^{-1} [2'010-2'120 pg kg^{-1} h^{-1}]) than after autoclaving (up to 22-30 ng m^{-2} h^{-1} [360-670 pg kg^{-1} h^{-1}]). As discussed above, the reason for this difference could be a significant Hg^0 loss due to the heat exposure during autoclaving. In addition, the large flush of CO_2 after chloroform fumigation might be associated with the decomposition of carbon compounds of lysed microorganisms (Dickens & Anderson, 1999; Horwath & Paul, 1994; Wolf & Skipper, 1994), which are easily oxidized by the surviving and recuperating microbial population. Thus, we speculate that the observed Hg^0 flush might be associated with this process; lysed cells constituted a readily available carbon source for the surviving microbial population, which might have triggered increased Hg^{2+} reduction and release of Hg^0.

The second difference between the effects of the two sterilization methods was a temporal offset of the Hg^0 flush, observed after chloroform fumigation; the Hg^0 flush lagged behind the CO_2 flush by about one day (Fig. 2.3). The presence of such a lag-phase, which was not observed with the autoclaved samples, might indicate that different mechanisms are associated with microbially stimulated Hg^0 emission. These mechanisms could be (a) direct microbial reduction of Hg^{2+} (Summers & Silver, 1978; Wood, 1974), (b) reduction of Hg^{2+} via reductive byproducts of microbial decomposition (humic and fulvic substances) and reactive Fe^{2+} species (Charlet et al., 2002) or (c) release of Hg^0 when organic substances, which are strong binding agents for mercury (Gabriel & Williamson, 2004), are mineralized. Direct microbial reduction might cause immediate Hg^0 emissions while indirect processes may result in a time lag. Yet, with this study we are not able to characterize the mechanisms responsible for enhanced Hg^0 emission as a result of increased microbial activity. If, however, direct microbial reduction was in fact involved in Hg^0 release as hypothesized to occur in soils amended to high levels of mercury (Rogers & Mc Farlane, 1979), it would challenge the view that it would only occur at mercury concentrations of several hundred parts per million as proposed by Van Faassen (1973).

Apart from these findings it has to be mentioned that the strongly fluctuating Hg^0 signal recorded during days 12 to 16 (Fig. 2.3) was the result of variations in atmospheric ozone levels. A pronounced relationship was detected between ozone concentrations and the Hg^0 emission flux. The experiment was performed during hot summer days when ambient ozone concentrations during the day increased significantly in the urban air shed (up to 50-65 ppm), while night time concentrations were much lower (6-11 ppm). Ozone is known to readily oxidise Hg^0 to Hg^{2+}, which is then deposited on the soil surface (Engle et al., 2005).

Stimulation of microbial activity by glucose addition

We added glucose and water to supplement the soil's nutritional requirements and to test if enhanced microbial activity would result in increased Hg^0 emissions. After applying it to four soil samples the CO_2 fluxes responded immediately to the substrate with a two-phased increase: they first rose within one day from 1.2 to a near plateau of

8.0 mmol m^{-2} h^{-1} (from 30 to 200 μmol kg^{-1} h^{-1}) and then increased within another day to an average peak flux of 19 mmol m^{-2} h^{-1} (480 μmol kg^{-1} h^{-1}; Fig. 2.4). This two-step pattern of increasing CO_2 emissions is well known; while the first step is attributed to an increasing respiration rate due to additional substrate available, the second is recognized as the result of a growing microbial population (e.g. Tsai et al. (1997)). A similar, significant increase ($p<0.001$) was observed for the Hg^0 emissions, although in a more linear fashion. The Hg^0 emissions increased within the same period from 2.2 to 6.7 ng m^{-2} h^{-1} (60 to 170 pg kg^{-1} h^{-1}). These results are in good agreement with a study performed by Landa (1978), even though measurement techniques were less sensitive and soils were amended with $Hg(NO_3)_2$.

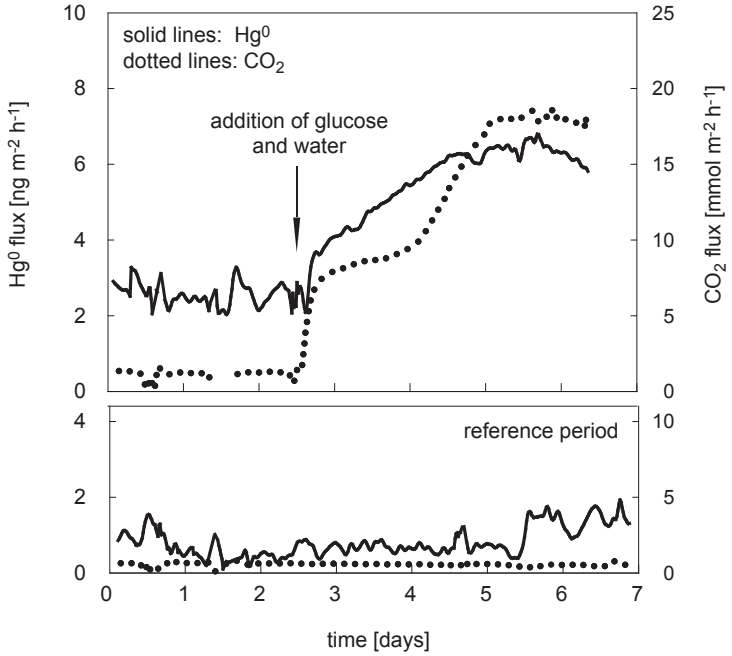

Figure 2.4: Stimulation of microbiological activity. Top: CO_2 and Hg^0 fluxes of samples treated with glucose to stimulate microbiological activity. Bottom: CO_2 and Hg^0 fluxes of the reference period, i.e. before glucose was added (plots represent means of four replicates; sample-ID: 1a, 2a, 3a, 4a). Soil moisture of all samples was kept constant throughout the experiment (30 vol%).

Temperature and drying effects on sterilized and non-sterilized samples

It is known that both temperature and soil moisture are important factors that affect Hg^0 emission from soils (Schlueter, 2000), although the underlying mechanisms are not yet fully understood. Bahlmann et al. (2006) found a strong exponential correlation between soil surface temperature and mercury emission flux and hypothesized that thermally controlled emission of mercury from soils is governed by the interfacial equilibrium of Hg^0 between soil and soil gas. In order to test if biotic processes are involved in temperature and soil moisture effects, the responses of the CO_2 and

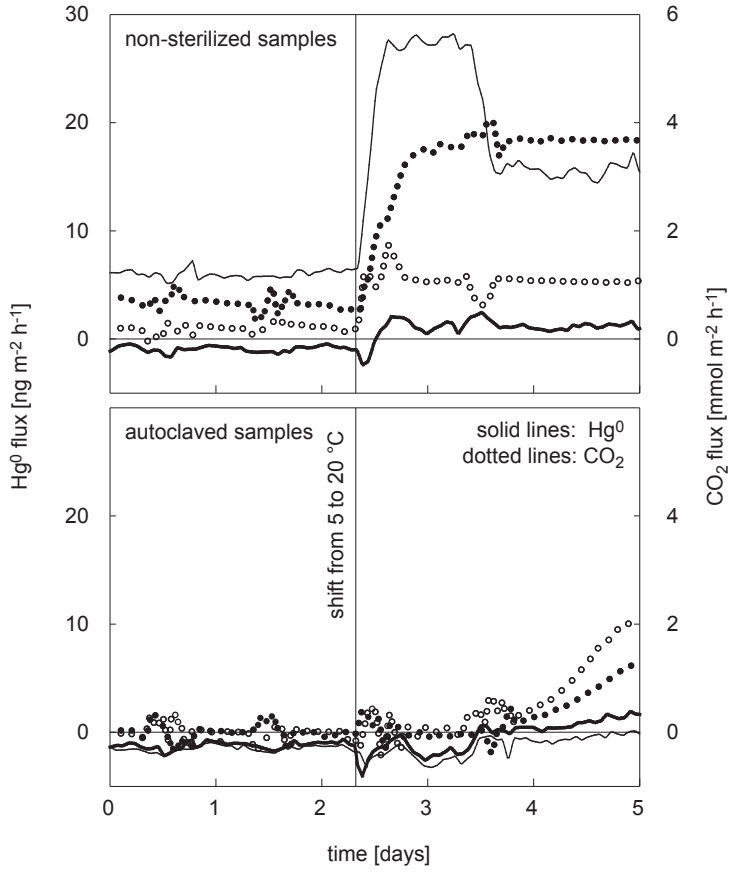

Figure 2.5: Effects of a temperature shift from 5 to 20°C. Upper plots show CO_2 and Hg^0 fluxes of non-sterilized (sample-ID: 2b, 3b), lower plots fluxes of sterilized samples (sample-ID: 1b, 4b). Soil moisture of all samples was kept constant throughout the experiment (30 vol %).

Hg^0 emission fluxes of sterilized and untreated soil samples were compared. Autoclaving was used for sterilization since this method was more effective than chloroform fumigation. Upon a temperature increase from 5 to 20°C the untreated soil samples displayed an immediate, significant shift ($p<0.001$) of the CO_2 and Hg^0 emissions by 0.8-3.2 mmol m^{-2} h^{-1} (10-70 μmol kg^{-1} h^{-1}) and 3.0-20 ng m^{-2} h^{-1} (50-450 μmol kg^{-1} h^{-1}), respectively (Fig. 2.5). It is important to note that the relationship between the CO_2 stimulation and the Hg^0 emissions is not linear and a strong increase in microbial respiration does not necessarily lead to an equally strong increase in Hg^0 evaporation. In contrast, the Hg^0 flux of the autoclaved soil samples did not show any immediate response to the temperature shift. An increase of Hg^0 emissions was recorded after 2 days, most likely due to microbial recovery or autoinoculation under non-sterile conditions. It might be argued that the absence of a temperature induced signal may be due to a loss of volatile mercury by autoclaving, but considering the impressive flush of Hg^0 emissions of the autoclaved and re-inoculated samples described above (see Fig. 2.2) this is not likely to be the case. Other than that, the shape

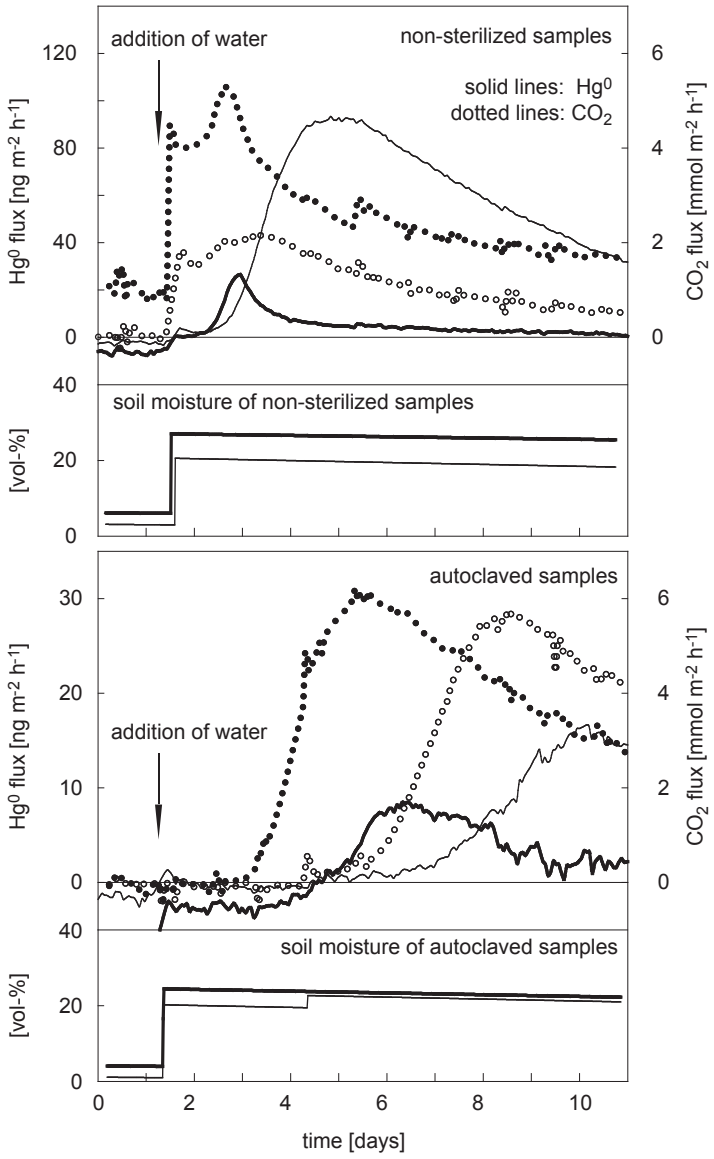

Figure 2.6: Effects of drying and remoistening. CO_2 and Hg^0 fluxes of samples dried at 40°C for two days and then rewetted to initial soil moisture levels; samples represented in lower plots were autoclaved prior to drying (sample-ID: 1i, 4j and 1j, 4i). Note that the Hg^0 flux axis of the lower plot is stretched.

of the plots of the non-sterilized samples indicates that the higher Hg^0 emission is not primarily the result of physical effects like enhanced gas diffusion or air expansion due to warming. Purely physically induced effects would produce a distinct peak in the Hg^0 emission fluxes immediately after a temperature increase. We conclude that temperature effects in our experiments were mainly mediated microbially. The small increase of microbial respiration and the associated slight increase of the Hg^0 fluxes of the autoclaved samples (day 3-5) is indicative of a close relationship between microbial activity and Hg^0 volatilization.

To investigate if the effects of changing soil moisture on Hg^0 evaporation rates are driven by microbial activity, untreated and autoclaved soil samples were dried and rewetted and the emission patterns of CO_2 and Hg^0 compared (Fig. 2.6). Upon addition of water (to ∼30%-vol, the level of the fresh soil samples) the untreated samples exhibited an immediate boost of CO_2, which was followed – with a delay of two days – by a similar increase in Hg^0 emissions. The CO_2 fluxes peaked at 2.2 and 5.6 mmol m^{-2} h^{-1} (50 and 230 μmol kg^{-1} h^{-1}) and the Hg^0 fluxes at 93 and 23 ng m^{-2} h^{-1} (2'300 and 950 pg kg^{-1} h^{-1}). The CO_2 fluxes of the autoclaved and dried soil samples started to increase 1-2 days after rewetting, which indicates incomplete sterilization or inoculation by the added water. Again, with a time-lag of two days relative to the CO_2 fluxes (i.e. four days after rewetting of the samples), the Hg^0 fluxes increased progressively to reach their maximum at 8 and 17 ng m^{-2} h^{-1} (270 and 440 pg kg^{-1} h^{-1}). This time-lag is similar to the one observed with the fumigated samples as discussed above. In a recent study on the effects of soil moisture Gustin and Stamenkovic (2005) suggested, that the addition of water in amounts less than necessary to saturate the soil resulted in an immediate release of elemental mercury from the soil because the more polar water molecules replace elemental mercury from binding sites. Our results suggest that the enhanced Hg^0 emissions observed during rewetting may not be of purely abiotic origin, but partially controlled by microbial activity. It might be possible that Hg^{2+} reducing bacteria were severely stressed during drying, but recovered rapidly upon addition of water, which is evident in the delayed Hg^0 flushes.

2.5 Conclusions

The results of our experiments have clearly shown concurrent increases and reductions of Hg^0 emissions with stimulated and inhibited microbiological activity. This characteristic did not only appear after glucose addition and inoculation of sterilized soils but became also visible after temperature shifts and rewetting of dried soils. It can therefore be concluded that Hg^0 emissions from uncontaminated, terrestrial soils are at least partly controlled by microbiological activity. Microorganisms might reduce Hg^{2+} either directly – in order to detoxify their immediate environment – or indirectly by either decomposing organic matter – a strong binding agent for mercury – or by converting their substrate into compounds capable of Hg^{2+} reduction, e.g. humic and fulvic acids. Besides, co-metabolism would be another possible mechanism

of Hg^{2+} reduction. The consistent lag-effect of Hg^0 with respect to CO_2 in the sterilization and drying treatments might indicate that indirect effects were pronounced.

Dried soil that was previously sterilized did not respond to rewetting with Hg^0 emissions as intense as untreated soils did. Likewise, Hg^0 evaporation after a temperature increase was retarded in sterilized samples. This suggests that specific microbes capable of Hg^{2+} reduction did not fully recover from the severe conditions of sterilizing and drying.

These results may have implications for the cycling of mercury in terrestrial environments. Viewed in a wider context, extreme environmental conditions such as intense droughts, incidents of heavy rain or forest clear cuts resulting in soil warming and nutritional boosts affect the soil's microbial activity substantially. A microbial population that would recover from such an incident might generate extreme Hg^0 boosts which would only last a few days or weeks, but which could affect the long-term emission budget considerably. Measurements of Hg^0 emission rates might therefore be underestimated if such events are missed.

2.6 Acknowledgements

We thank the Swiss National Science Foundation (project number: 200021-105308 to D. Obrist and C. Alewell) for financing this project and would like to express our appreciation to Werner Eugster of ETH Zurich for access to their field site. We are grateful to Dr M. S. Gustin and her laboratory staff for soil Hg analyses and to H. Hürlimann, H. Strohm, M. Caroni for their help with soil characterization.

Chapter 3

Longterm Hg^0 fluxes between air and grassland determined with micrometeorological methods

This chapter will be published in Atmospheric Environment as:
Fritsche, J., Obrist, D., Zeeman, M., Conen, F., Eugster, W., and Alewell, C., 2008: Elemental mercury fluxes over a sub-alpine grassland determined with two micrometeorological methods. Atmospheric Environment, accepted 21 December 2007.

3.1 Abstract

The exchange of gaseous elemental mercury (GEM) over a sub-alpine grassland in central Switzerland was measured over a full year. Seasonal and diurnal variability were measured with two micrometeorological techniques: the aerodynamic method and the modified Bowen ratio method. With these two methods mean deposition rates of 4.3 ng m^{-2} h^{-1} and 1.7 ng m^{-2} h^{-1} were calculated throughout the vegetation period. As no significant GEM exchange occurred under snow covered conditions the mean annual deposition fluxes reached 2.9 ng m^{-2} h^{-1} and 1.1 ng m^{-2} h^{-1}, respectively. A fair weather period in October 2005 was selected to specifically study diurnal patterns of GEM exchange. During this time vertical day-time GEM gradients averaged 0.01 ng m^{-4} and night-time gradients 0.07 ng m^{-4}, but no clear diurnal pattern of the GEM fluxes was observed. The measured gradients were very small, which entailed considerable uncertainties in the calculated GEM fluxes. However, the observed exchange pattern is verified by the agreement of the applied methods regarding the direction of the flux and the pronounced seasonal trends. Complementary measurements of total mercury in precipitation during three rain events revealed that dry deposition of GEM would account for 67% of a total annual input of 0.26 g ha^{-1} and would therefore constitute a major deposition pathway.

3.2 Introduction

The 2006 conference on Mercury as a Global Pollutant has highlighted again the relevance of mercury as an environmental hazard (see Lindberg et al., 2007b, for the conference declaration). Many research projects have described in detail the long-range transport of elemental mercury and the processes leading to the formation of methylmercury. The latter not only affects the health of humans, wild birds, mammals and fish (IOMC, 2002; Pirrone & Mahaffey, 2005) but might also disturb soil microbial processes at the very bottom of the food chain (Johansson et al., 2001).

In background ecosystems the exchange of elemental mercury is primarily controlled by physicochemical properties of the soil, biological processes in the soil, atmospheric chemistry and meteorological conditions. Depending on these variables mercury might be cycled fairly rapidly between terrestrial surfaces and the atmosphere (Gustin & Lindberg, 2005). However, it remains unclear whether deposited mercury is retained in background soils or whether terrestrial ecosystems are even a source of mercury (Pirrone & Mahaffey, 2005). Moreover, mercury might be taken up by plant leaves or removed through the plant from the soil to the atmosphere (Du & Fang, 1982; Gustin & Lindberg, 2005; Landis et al., 2005; Millhollen et al., 2006a).

To address these processes air-surface exchange fluxes of gaseous elemental mercury (GEM) have been measured with various techniques (Edwards et al., 2005; Gustin et al., 2006; Obrist et al., 2006). One of these widely used techniques are dynamic flux chambers. These are easy to handle and provide results instantly, but affect atmospheric turbulence, temperature and humidity considerably and therefore their application is restricted to short-term measurements (Cobos et al., 2002). On the other hand, micrometeorological techniques allow spatially averaged measurements without disturbing ambient conditions, but require detailed knowledge of the prevailing micrometeorological situation and the footprint area.

A variety of micrometeorological methods for trace gas flux measurements have been developed (for details see Baldocchi, 2006; Dabberdt et al., 1993; Foken, 2006; Lenschow, 1995). With today's sensitive analytical instrumentation that allows accurate measurement of background GEM levels of 1.2 to 1.8 ng m^{-3} (Landis et al., 2005; Pirrone & Mahaffey, 2005) most micrometeorological methods are apt to be applied to mercury flux measurements. The eddy covariance (EC) method – the state of the art in turbulent energy, momentum, CO_2 and H_2O flux measurements – would be straightforward but is not yet practicable for GEM flux measurements as it requires fast response, field deployable sensors that are currently not available for GEM at reasonable costs (laser based systems are being developed and seem promising; Bauer et al., 2002). Alternatively, flux-gradient methods only require a relatively simple setup, which is advantageous for long-term GEM flux measurements. Generally, these methods are based on the theory that the gradient of a scalar quantity is the driving force of the mass or energy flux. Translated to the flux of a trace gas this relationship can be expressed as

$$F_x = -K_x \frac{\partial c_x}{\partial z} \tag{3.1}$$

where F_x is the vertical trace gas flux, K_x the turbulent exchange coefficient (or eddy diffusivity) and $\partial c_x / \partial z$ the concentration gradient of the trace gas in question (Baldocchi, 2006; Dabberdt et al., 1993; Lenschow, 1995). Using the flux-gradient relationship of the Monin-Obukhov similarity theory, fluxes can be estimated by the so-called aerodynamic method and the modified Bowen ratio (MBR). The MBR technique is widely used to estimate air-surface exchange rates of GEM and has the advantage of being independent of empirically derived stability corrections. On the other hand, the aerodynamic method does not require the knowledge of gradients and fluxes of a surrogate scalar.

In this work we describe the first year-long measurement of GEM fluxes above uncontaminated, sub-alpine grassland. With these measurements we intend to compare the aerodynamic and MBR methods and evaluate their suitability for GEM flux measurements. Additionally we attempt to record the seasonal and diurnal variability of the GEM exchange and to capture any events that would eventually enhance or reduce GEM fluxes, e.g. during or after intensive rain, upon snow fall and during snow melt or after grass cuts.

3.3 Experimental

3.3.1 Methodology

The similarity theory by Monin & Obukhov (1954) relates vertical gradients and fluxes in a way that also allows to compute GEM fluxes from GEM gradient measurements. Accordingly, if K_x is substituted in Equ. 3.1 the turbulent GEM flux calculated by the aerodynamic method becomes

$$F_{GEM} = -\frac{k \cdot u_* \cdot z}{\Phi_h(z/L)} \cdot \frac{\partial c_{GEM}}{\partial z} \tag{3.2}$$

where k denotes the von Karman constant (0.4), u_* the friction velocity, $\Phi_h(z/L)$ the universal temperature profile, L the Monin-Obukhov length and $\partial c_{GEM}/\partial z$ the vertical GEM gradient. The dimensionless Monin-Obukhov stability parameter z/L is used to characterise atmospheric stratification. Dyer (1974) parametrised the universal function Φ_h as $(1 - 16 \cdot z/L)^{-0.5}$ for unstable, $(1 + 5 \cdot z/L)$ for stable and 1 for neutral conditions. Using this parametrisation in Equ. 3.2, F_{GEM} is obtained as a function of the measured GEM concentration gradient and atmospheric stability. More details about this technique and its underlying assumptions are described in Edwards et al. (2005).

For determination of the turbulent GEM flux by the MBR method the measurement of a surrogate scalar, i.e. sensible heat or a second trace gas, is required. In our application we used CO_2 as a surrogate, since its concentration can be easily determined and as its flux is less constrained by solar radiation than the flux of sensible

heat (Meyers et al., 1996). By measuring gradients of GEM and CO_2 the GEM flux is calculated as

$$F_{GEM} = F_{CO_2} \cdot \frac{\Delta c_{GEM}}{\Delta c_{CO_2}} \tag{3.3}$$

where the F_{CO_2} flux is obtained directly by eddy covariance (Baldocchi, 2006; Dabberdt et al., 1993; Meyers et al., 1996). An elaboration of the method is given by Lindberg & Meyers (2001) and Meyers et al. (1996).

Both flux-gradient techniques are limited in their application. First, the determined fluxes are the result of a spatially averaged signal that require an adequate footprint. This footprint depends on the prevailing atmospheric conditions, site heterogeneity and the measurement height (Foken, 2006; Lenschow, 1995). A brief description of the fetch at our field site is given in the following section. Second, the assumptions of the applied micrometeorological methods necessitate gradient measurements above the canopy, although fetch requirements are greater and gradients are smaller (Lenschow, 1995). The latter issue poses an additional challenge in our study, as atmospheric GEM concentrations are already extremely low. Third, the methods assume fully developed turbulent conditions, which is adequate for day-time and less so for night-time conditions. Finally, regarding the MBR method, it is assumed that the transport processes as well as the sinks and sources of the investigated trace gas and the surrogate scalar are equal (Dabberdt et al., 1993).

3.3.2 Site description

We chose the sub-alpine grassland at Fruebuel in central Switzerland at an elevation of 1000 m a.s.l. as location for our GEM flux measurements (47°6'47"N, 8°32'16"E). This undulating plateau, which is a research site of ETH Zurich (Eugster & Zeeman, 2006), is used for hey production with 2 to 3 cuts per year and cattle grazing. The temperate continental climate yields an average annual temperature of 7°C with a mean precipitation of 1200 mm per year (Dipner-Gerber et al., 2004). In the centre of the 9 ha large field ETH Zurich operates a micrometeorological tower that was also used for our flux measurements. The site which is bordered by a birch alley in the south-west and a raised-bog in the north-east, consists of Cambisols in different water influenced varieties. In the proximity to the micrometeorological tower the soil is 1.3 m deep with a bulk density of 1.28 g cm^{-3} (A horizon). The top soil layer has an organic carbon content of 18.4 mg g^{-1} and a pH of 4.5 (Roth, 2006). A total mercury concentration (Hg_{tot}) of 100.8 $\pm$14.5 ng g^{-1} was measured in the A horizon. Soil solution was sampled three times during the measurement campaign and Hg_{tot} concentrations of 3.5 $\pm$0.75 ng l^{-1} were determined at the Swedish Environmental Research Institute IVL, Gothenburg. The dominant species of the pasture include Alopecurus pratensis, Lolium perenne, Lolium multiflorum, Dactylis glomerata, Heracleum sphondylium, Rumex acetosa, and Rumex alpinus.

The predominant wind direction is south-west to south-south-west, showing a distinct channelled flow as a result of the local, undulating, sub-alpine topography. The

largest contributions to the footprint are within approximately 60 m of the eddy covariance setup.

3.3.3 Experimental setup and data analysis

In order to determine the GEM fluxes by the micrometeorological methods described above, the GEM concentrations and CO_2 mixing ratios were measured at 5 heights above ground. A dual-amalgamation mercury vapour analyser (Tekran 2537A, Tekran, Toronto, Canada) with 5 minute accumulation intervals per cartridge was used to measure atmospheric GEM concentrations; features of this instrument are described in e.g. Lindberg et al. (2000). The CO_2 concentrations were analysed with a closed path infrared gas analyser (LI 6262, LI COR Inc., Lincoln, Nebraska, USA) at a frequency of 1 Hz. At a distance of about 5 m from the micrometeorological tower the sampling lines were mounted to a separate pole at heights of 0.20, 0.27, 0.94, 1.58 and 1.70 m above ground. The 1/4"-Teflon® sampling lines of 7 m length were run to a 5-port solenoid switch unit to enable sequential sampling of all heights. Downstream of the switch unit the Tekran instrument and the CO_2 analyser were connected in series. The internal air pump of the Tekran instrument was operated at a flow rate of 1.5 l min^{-1}. To maintain steady flow conditions an auxiliary pump with a flow rate of 6 l min^{-1} was connected to a second port of the switch unit. In this configuration the four lines that were currently not sampled were flushed continuously. Teflon® cartridges with 0.45 μm filters were mounted to the inlet of each line to avoid any particles entering the system. The sampled air was not dried, which necessitated a correction of the calculated fluxes (see below).

With this setup one vertical 5-point concentration profile could be measured every 50 minutes. Sampling was switched every 10 minutes in such a way that a measurement of a line at a lower level was followed by one at a higher level and vice versa. Higher frequencies were not feasible, due to the required analytical pre-concentration of the sampled air.

A suite of ancillary meteorological data (air temperature, net radiation, PAR, humidity, etc.) were recorded by the micrometeorological tower. Carbon dioxide and water vapour fluxes were determined by eddy covariance using a three-dimensional sonic anemometer (Solent R3, Gill Ltd., Lymington, UK) and a LI 7500 open path infrared gas analyser (LI COR Inc., Lincoln, Nebraska, USA).

After the measurement campaign the logged data were analysed with an algorithm written in Matlab®. As one of the first data processing steps the GEM and CO_2 gradients were extracted by subtracting the atmospheric concentration trend measured at the top sampling line. This step was considered essential as atmospheric concentrations changed during the course of a measurement cycle of 50 minutes (i.e. 20 minutes for one height pair). GEM exchange rates were then determined according to Equ. 3.2 and 3.3. This was done by calculating the gradients and fluxes of 5 sequential height pairs within the 50 minute intervals (i.e. pairs 0.20/1.58 m, 0.27/1.58 m, 0.27/1.70 m, 0.94/1.70 m and 0.20/0.94 m). The median of these 5 values was then calculated to obtain the raw flux. Uncertainty could thus be reduced noticeably. Fluxes determined

with the aerodynamic method were then corrected for density fluctuations caused by differences in water vapour content of the air stream (the Tekran instrument measures the GEM concentration relative to moist air). The correction terms of Webb et al. (1980), which are also described in more detail by Lee (2000) were applied. As the Tekran GEM analyser monitors the sampling volume with a mass flow controller, i.e. measures the concentration relative to the sampled air mass, no correction for the sensible heat flux was necessary. Finally the flux data were screened for outliers and values outside the range of the monthly mean ± 3 standard deviations were rejected. All GEM flux data presented in this paper are reported on a mass basis in ng m^{-2} h^{-1}. Fluxes have to be divided by 4.985 to obtain values in pmol m^{-2} s^{-1}.

As a means to evaluate the quality of the GEM fluxes we also calculated the CO_2 fluxes by the aerodynamic method (equation 3.2) and compared the results with the CO_2 fluxes gained by eddy covariance. Keeping in mind that the sinks and sources of GEM and CO_2 might not be identical, equal CO_2 fluxes would nonetheless imply that the measured GEM fluxes are reliable (assuming the CO_2 fluxes determined by EC to be accurate).

3.3.4 QA/QC

The mercury vapour analyser was calibrated every 24 hours by means of the internal mercury permeation source of the Tekran instrument. Additionally, external calibrations were performed at regular intervals by manually injecting pre-defined volumes of mercury saturated air from a mercury vapour generation unit (Model 2505, Tekran, Toronto, Canada). Likewise, the LI 6262 CO_2 analyser was calibrated every 2 to 4 weeks by measuring a zero and span gas. Argon was used as zero gas (relative zero-offset to a N_2/O_2 gas mixture was 0.4 ppm) and pressurised air with 451 ppm CO_2 as span gas. GEM and CO_2 concentrations were corrected accordingly. In order to exclude any line bias we replaced the particle filters every 2 to 4 weeks and exchanged the sampling lines for cleaned ones 3 times during the campaign. Additionally the system was checked for leaks either by measuring mercury-free air generated by a zero air generator (Model 1100, Tekran, Toronto, Ontario) or constricting the sampling lines temporarily to generate low pressure within the lines. Teflon® parts and tubing were cleaned with ultra pure HNO_3 and deionised water according to an internal standard operating procedure (adapted from Keeler & Landis, 1994).

3.4 Results

3.4.1 Detection limit and data coverage

To obtain the detection limit of our system we measured GEM and CO_2 concentrations with all sampling lines at 1 m above ground over three days and determined the minimum resolvable gradient (MRG). We defined the MRG as the mean plus 3 standard deviations of the concentration differences measured between the 5 sampling lines (determined according to the calculation of the gradients described in section 3.3.3).

For GEM the MRG was calculated as 0.05 ng m^{-3} and for CO_2 7.6 ppm. As a large proportion of the measured gradients were around the MRG we set a more relaxed threshold for acceptable values at the mean plus one standard deviation, which translates to 0.02 ng m^{-3} for GEM and 2.5 ppm for CO_2, keeping the reduced confidence in mind. Please note that the mean flux values reported in the following sections include data below the MRG (average exchange rates would otherwise be overestimated).

Concentration measurements of GEM and CO_2 covered 56% of the period between September 2005 and August 2006. Besides using the instruments at other sites data gaps resulted from maintenance work, failure of instrumentation and invalid measurements within the vegetation or below the snow surface. With the MRG criterion mentioned above an overall data coverage of 28% for the GEM fluxes and of 32% for the CO_2 fluxes was achieved.

3.4.2 Seasonal air-surface exchange of GEM

During the measurement campaign the air temperature averaged 6°C and 1'150 mm of precipitation were recorded. Between 24.11.2005 and 26.03.2006 the site had a closed snow cover. Figure 3.2 illustrates the seasonal variation of air temperature and measured atmospheric GEM concentrations. The latter averaged 1.42 ng m^{-3} and ranged from 0.69 ng m^{-3} to 2.42 ng m^{-3} throughout the study period. Lowest concentrations were measured in August 2006 with an average of 1.21 $\pm$0.08 ng m^{-3} and highest in March 2006 with 1.64 $\pm$0.18 ng m^{-3}. No association with wind direction could be observed (see Fig. 3.1).

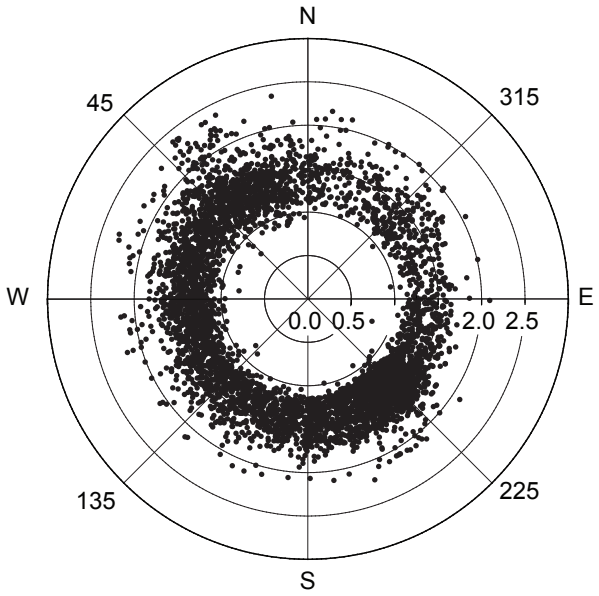

Figure 3.1: GEM concentration in ng m^{-3} vs. wind direction. Shown are all data points from September 2005 to August 2006 of the sampling line at 1.7 m above ground.

A summary of the CO_2 and GEM fluxes is shown in Tab. 3.1. During the vegetation period (between 26.09. and 23.11.2005 and between 27.03. and 30.08.2006) a mean CO_2 uptake of 4.2 $\pm$10.7 μmol m^{-2} s^{-1} was observed with the EC technique and of 6.3 $\pm$19.0 μmol m^{-2} s^{-1} with the aerodynamic method. On the other hand, CO_2 emissions of 1.0 μmol m^{-2} s^{-1} were recorded during the snow covered season (see Fig. 3.2).

Mean GEM deposition rates of 4.3 ng m^{-2} h^{-1} and 1.7 ng m^{-2} h^{-1} were measured during the vegetation period with the aerodynamic and the MBR method, respectively. Fluxes determined by both approaches ranged from $-$42 to 20 ng m^{-2} h^{-1} and from $-$35 to 34 ng m^{-2} h^{-1} respectively. During the snow covered period GEM fluxes were reversed and mean emissions of 0.3 ng m^{-2} h^{-1} (range $-$34 to 29 ng m^{-2} h^{-1}) and 0.4 ng m^{-2} h^{-1} (range $-$68 to 82 ng m^{-2} h^{-1}) were recorded (see Fig. 3.1). Average deposition velocities ($v_d = F_{GEM}/c_{GEM}$) for the two methods were calculated to be 0.09 cm s^{-1} and 0.03 cm s^{-1} for the vegetation period.

In Fig. 3.1 one distinct period in May 2006 can be noticed: from the second half of April the aerodynamically determined GEM deposition rate increases progressively from 1 ng m^{-2} h^{-1} to 19 ng m^{-2} h^{-1} at the end of May and then drops again to 7 ng m^{-2} h^{-1}. A similar, although less pronounced increase with a maximum of 10 ng m^{-2} h^{-1} was identified with the MBR method.

In addition to dry deposition we also measured the total mercury content (Hg_{tot}) of rain water during three precipitation events between June and September 2006. The mean Hg_{tot} concentrations of the samples collected over 48 hours each were between 6.1 and 14.0 ng l^{-1} (N=6).

3.4.3 Diurnal air-surface exchange of GEM

The fair weather period between 6.10.2005 and 16.10.2005 was selected to evaluate the diurnal variability of the measured GEM fluxes. As Fig. 3.3 shows the diurnal cycle of air temperature, net radiation and turbulence were steady throughout this time.

Table 3.2 lists the average fluxes of CO_2 and GEM separated by method and time

Mean CO_2 flux [µmol m^{-2} s^{-1}]	Aerodynamic method	N	EC method	N
Entire period[c]	−2.5 (−86 to 66)[a]	5111	−2.5 (−55 to 43)[a]	5345
Vegetation period[d]	−4.7 (−86 to 66)[a]	3209	−4.2 (−55 to 43)[a]	3513
Snow covered period[e]	1.1 (−26 to 27)[a]	1387	1.0[b] (−27 to 30)	1334
Mean GEM flux [ng m^{-2} h^{-1}]	Aerodynamic method	N	MBR method	N
Entire period[c]	−2.9 (−42 to 29)[a]	5214	−1.1[b] (−68 to 82)[a]	4039
Vegetation period[d]	−4.3 (−42 to 20)[a]	3338	−1.7 (−35 to 34)[a]	2670
Snow covered period[e]	0.3[b] (−34 to 29)[a]	1357	0.4[b] (−68 to 82)[a]	957

[a] range
[b] not significantly different from zero
[c] from 26.09.2005 to 30.08.2006
[d] from 26.09.2005 to 23.11.2005 and from 27.03.2006 to 30.08.2006
[e] from 24.11.2005 to 26.03.2006

Table 3.1: Summary of seasonal CO_2 and GEM flux data (entire measurement period).

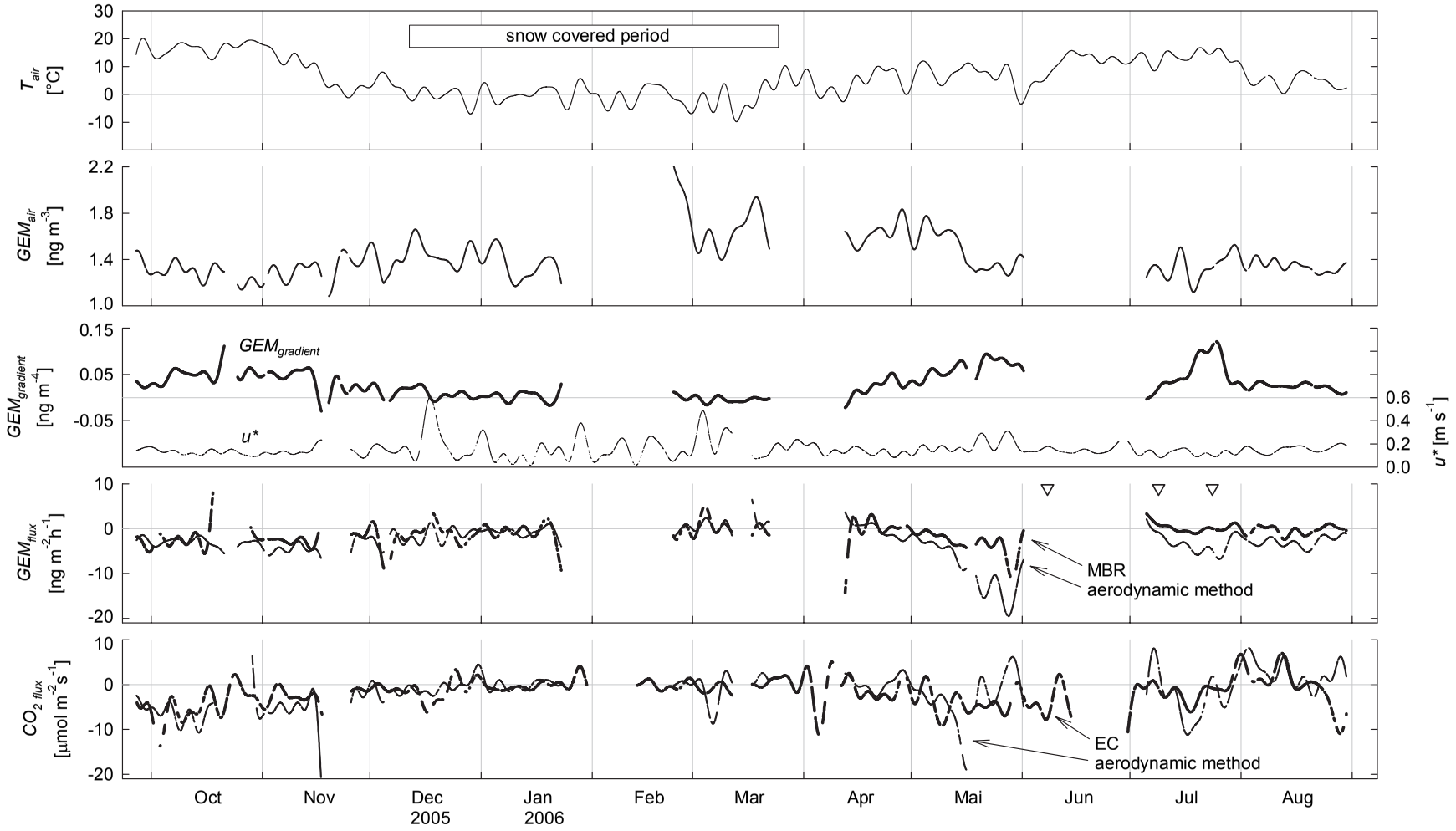

Figure 3.2: Seasonal trends of air temperature (T_{air}), atmospheric GEM concentration at 1.7 m above ground (GEM_{air}), GEM gradients, friction velocity (u_*) as well as the turbulent fluxes of GEM (determined by the aerodynamic and MBR methods) and CO_2 (determined by the aerodynamic method and the eddy covariance technique). Time series are low-pass filtered (rectangular filter with fast fourier transform) with a cut-off period of 8 days. Positive GEM and CO_2 fluxes indicate emission, negative deposition. White triangles in the GEM flux plot indicate grass cuts.

of day, where day-time was defined to last from 9–15 hours and night-time from 23–5 hours. A mean day-time CO_2 deposition rate of 16.8 μmol m^{-2} s^{-1} and a mean night-time emission flux of 3.8 μmol m^{-2} s^{-1} was measured with the aerodynamic method; the corresponding rates for the EC method were 14.4 μmol m^{-2} s^{-1} and 2.7 μmol m^{-2} s^{-1}.

During this fair weather period average day-time GEM gradients of 0.01 $\pm$0.03 ng m^{-4} and night-time gradients of 0.07 $\pm$0.05 ng m^{-4} were measured. Figure 3.4 illustrates the gradients of GEM and CO_2. Although the nocturnal profile was pronounced, no stationary diurnal pattern of the GEM fluxes could be observed. The mean exchange rates determined by the aerodynamic and MBR methods were similar with day-time values of -0.8 ng m^{-2} h^{-1} and -0.7 ng m^{-2} h^{-1} respectively, and night-time values of -1.0 ng m^{-2} h^{-1} and -0.9 ng m^{-2} h^{-1} respectively. No correlation of the GEM fluxes with any meteorological variable could be detected.

3.5 Discussion and Conclusions

3.5.1 Evaluation of aerodynamic and MBR method

Despite the extremely low GEM fluxes and the low temporal resolution of the measurements the aerodynamic and MBR methods produced comparable results. Our measurements during the fair weather period show that the fluxes agree well, although on few occasions the MBR values are considerably smaller or reversed with respect to the aerodynamic fluxes. The smaller MBR fluxes are primarily the result of very small GEM gradients which diminish the GEM flux. Reversed fluxes on the other hand seem to be due to inconsistent GEM gradients caused by non-stationary turbulence regimes. Over the seasons it has to be noted that during spring and summer 2006 the aerodynamic fluxes were consistently higher than the fluxes determined by the MBR method. During this period when the grass grew rapidly, one or two lines sampled close above or even within the top of the vegetation, which resulted in enhanced CO_2 gradients and diminished GEM fluxes (compare with Equ. 3.3).

In general, the MBR technique has the advantage that no stability corrections are

Mean CO_2 flux [µmol m^{-2} s^{-1}]	Aerodynamic method	N	EC method	N
day-time[c]	−16.8 (−46.3 to −3.6)[a]	66	−14.4 (−27.8 to 14.7)[a]	71
night-time[d]	3.8 (−0.5 to 23.3)[a]	40	2.7 (−6.5 to 8.8)[a]	23
Mean GEM flux [ng m^{-2} h^{-1}]	Aerodynamic method	N	MBR method	N
day-time[c]	−0.8[b] (−12.8 to 9.5)[a]	67	−0.7[b] (−10.5 to 10.0)[a]	69
night-time[d]	−1.0 (−10.3 to 1.4)[a]	40	−0.9 (−4.0 to 1.9)[a]	32

[a] range
[b] not significantly different from zero
[c] from 9 – 15 hours
[d] from 23 – 5 hours

Table 3.2: Summary of diurnal CO_2 and GEM flux data (fair weather period of October 2005).

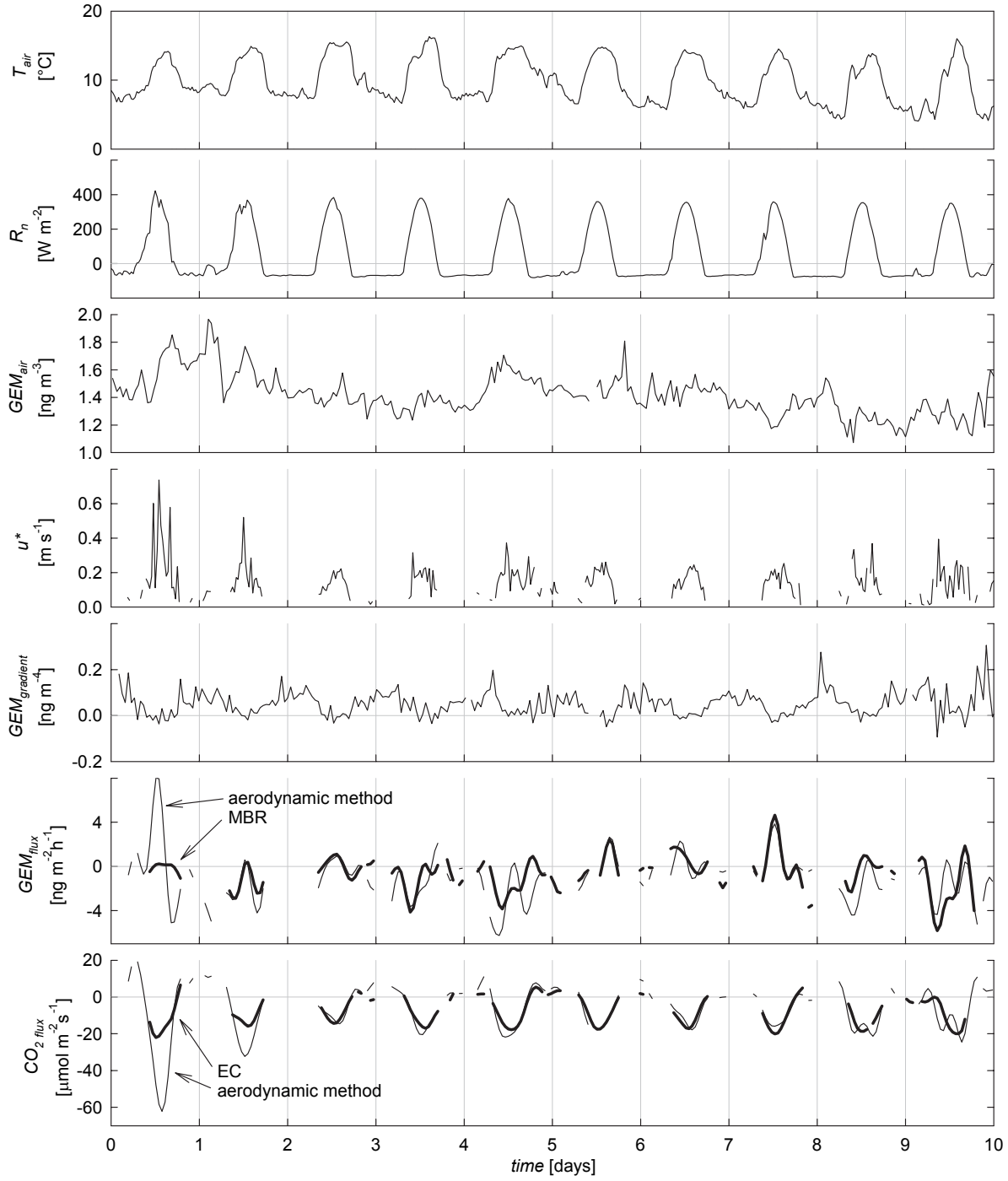

Figure 3.3: Diurnal variation for the fair weather period in October 2005. Shown are the time series for air temperature (T_{air}), net radiation (R_n), atmospheric GEM concentration at 1.7 m above ground (GEM_{air}), friction velocity (u_*), GEM gradients as well as the turbulent fluxes of GEM (determined by the aerodynamic and MBR methods) and CO2 (determined by the aerodynamic method and the eddy covariance technique). Flux data are low-pass filtered (rectangular filter with fast fourier transform) with a cut-off period of 5 hours. Positive GEM and CO_2 fluxes indicate emission, negative deposition.

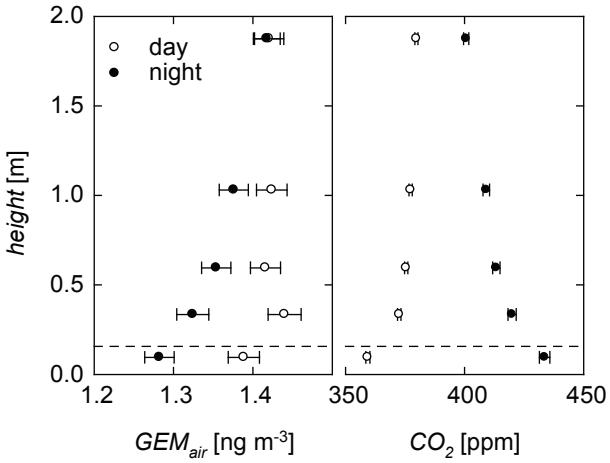

Figure 3.4: GEM and CO_2 concentration profiles of the fair weather period in October 2005 separated by day (9–15 hours) and night (23–5 hours). Dots and error bars represent means and standard errors of the 10 day period. The dashed line shows the approximate height of the vegetation.

required (Lenschow, 1995). The technique therefore seems more robust compared to the aerodynamic method. However, our measurements showed similar variability (see ranges in Tab. 1 and 2) and suggest that both methods seem appropriate to estimate the magnitude of background GEM fluxes. Applying the aerodynamic approach also to CO_2 and considering its good agreement with the fluxes determined by eddy covariance has given us additional confidence in our GEM flux estimates.

3.5.2 Sources of uncertainty

Our results show that determination of small GEM exchange fluxes over uncontaminated areas is difficult and subject to uncertainties. According to Equ. 3.2 and 3.3 the components of these uncertainties are errors associated with the gradient measurements of GEM and CO_2 and the determination of either the atmospheric turbulence or the CO_2 flux by eddy covariance. Generally, the variables that describe atmospheric turbulence, u_* and z/L, are determined with a random error of approx. 30%RSD and eddy covariance fluxes of CO_2 with $\sim$10%RSD (for 30-minute intervals).

The gradients were determined with one instrument, by measuring air concentrations in a sequential mode. Therefore, the random errors of the gradients consist of a temporal component, that results from the time lag between the measurements, and an instrumental component. For GEM the latter was determined with 5%RSD, derived from calibration data; the uncertainty for the CO_2 concentrations was estimated to be $<$5%RSD. The temporal component could not be quantified and was excluded from the following error estimation, keeping in mind that it might add considerably to the overall uncertainty.

The computation of the GEM fluxes with the aerodynamic and the MBR methods

yielded random errors in the order of 43% and 14%, respectively. The clear seasonal pattern confirms that the variability in the measured fluxes is not random and that in fact significant uptake occurs during the emerging vegetation period in April and May, while during other times fluxes seem in fact to be close to zero.

3.5.3 Atmospheric GEM concentrations

The average GEM concentration of 1.42 ng m^{-3} measured at our grassland site fits well into the global estimated mean of 1.2 to 1.8 ng m^{-3} (Pirrone, 2001). There is no monitoring station in the Alps that measures atmospheric GEM on a continuous basis. However, comparison with concentrations measured at Mace Head in Ireland of 1.55 ng m^{-3} (Kim et al., 2005) and at Pallas, Finnland with 1.34 ng m^{-3} (Kim et al., 2005) implies, that atmospheric GEM is not elevated in the sub-alpine region of Switzerland, which is dominated by north-westerly winds from France (contrary to Mace Head and Pallas we would expect to measure increased anthropogenic emissions).

3.5.4 GEM gradients

In order to determine the GEM fluxes of uncontaminated sites with flux-gradient techniques it is of main importance to measure the required concentration profiles accurately. This proved to be very challenging as the measured concentration differences were around the minimum resolvable gradient. However, the concentration profiles in Fig. 3.3 and the gradient plot of Fig. 3.2 indicate that the applied approach is still feasible, at least under fair weather conditions. Figure 3.3 illustrates the logarithmic decrease of the CO_2 and GEM concentrations with height, with a clear inversion of the CO_2 profile during the night. The very small day-time GEM gradients suggest that any superficial GEM accumulation from the previous nights was quickly disappearing with increasing turbulence during the day. This is also evident in the diurnal cycle of the GEM gradient shown in Fig. 3.2.

Our results agree with other studies performed at uncontaminated sites. For example, Edwards et al. (2005) applied the aerodynamic approach to measure GEM fluxes above various mercuriferous substrates and reached a gradient resolution of 0.01 ng m^{-3} with a similar setup. Kim et al. (1995) measured GEM gradients of -0.16 to 0.32 ng m^{-3} above forest soils and Lindberg & Meyers (2001) measured GEM over wetland vegetation and determined mean gradients of 0.03 ng m^{-3} with a standard deviation of 0.03 ng m^{-3}. In Sweden Lindberg et al. (1998) determined gradients of -0.091 to 0.064 ng m^{-3} over forest soils. The gradients between -0.26 and 0.37 ng m^{-3} measured at our grassland site correspond well with these values.

3.5.5 GEM fluxes

Looking at the fluxes over the seasons GEM was deposited in minute amounts during the vegetation period. No exchange occurred during winter when the soil surface was

covered with snow (the slight emission rates determined for the snow covered period were not significantly different from zero). Comparison of the available day-time and night-time fluxes of the fair weather period revealed no significant differences – a slight deposition was recorded, independent of time. This is also demonstrated by the plots of and the GEM gradients, where high values of the friction velocity are associated with low GEM gradients and vice versa. The mean fluxes of 4.3 ng m^{-2} h^{-1} (aerodynamic) and 1.7 ng m^{-2} h^{-1} (MBR) determined for our site during the snow free season agree well with previous studies of uncontaminated background sites, where fluxes are generally extremely small. For example, Meyers et al. (1996) and Kim et al. (1995) measured GEM fluxes of 6.8 ng m^{-2} h^{-1} and -2.2 to 7.5 ng m^{-2} h^{-1} above background forest soils. Cobos et al. (2002) determined average GEM fluxes of 9.7 ng m^{-2} h^{-1} over an agricultural soil with the advanced relaxed eddy accumulation method. In Canada Schroeder et al. (2005) measured exchange rates of -0.4 to 2.25 ng m^{-2} h^{-1} over forest soils and of 1.1 to 2.95 ng m^{-2} h^{-1} over agricultural fields. Poissant & Casimir (1998) used a flux chamber and measured 8.3 ng m^{-2} h^{-1} over a grassy site. Flux chambers were also used by Ericksen et al. (2006) who determined a mean emission rate of 0.9 $\pm$0.2 ng m^{-2} h^{-1} from background sites across the USA. Based on the review of previous studies, Gustin et al. (2006) suggests that GEM exchange rates from low mercury containing soils are in the range of -1 to 3 ng m^{-2} h^{-1}. For comparison, GEM fluxes of 10 to 200 ng m^{-2} h^{-1} were measured over a soil contaminated with 60 g g^{-1} of mercury (Lindberg et al., 1995).

Several meteorological variables were measured at our site and the data were checked for correlations with the GEM fluxes. However, no significant correlations could be detected. We also screened our flux data for any response to abrupt changes in environmental conditions, e.g. intense showers, rain after longer dry periods and snow melt. None of these events had a visible effect on the GEM flux. Even grass cuts which would imply some GEM emission due to increases in surface temperature and irradiation had no effect. However, enhanced GEM emission caused by high soil water content or elevated temperatures (as described by Edwards et al., 2001) have been shown in lab experiments with soils from our study site (Fritsche et al., 2008b). In these experiments we used bare soil samples and flux chambers that generated rather little turbulence. It therefore seems that the GEM flux is strongly influenced by vegetation and atmospheric turbulence.

In section 3.4.2 we referred to a period in May 2006 with steadily increasing GEM deposition rates (see Fig. 3.1). This increase was more pronounced with the aerodynamic method and might be attributed to the fast growing vegetation that removes GEM from the atmosphere. Mercury accumulation in grass has been reported by e.g. Millhollen et al. (2006b).

Summarising our results, uncontaminated grasslands of the temperate sub-alpine climate belt seem to act as a small net sink for atmospheric mercury. This is confirmed by the study of Obrist et al. (2006) who estimated mean GEM deposition rates of 0.2 ng m^{-2} h^{-1} at another sub-alpine grassland site in central Switzerland. Net deposition also goes along with the general decrease of air mercury concentrations

over Europe since the early 1990's (Lindberg et al., 2007a).

Besides dry deposition of GEM, the mercury input with precipitation is another important pathway of atmospheric mercury to terrestrial surfaces. We were only able to quantify this input during a few rain events, but the obtained results are in accordance with other studies on wet deposition of atmospheric mercury. The summary of Fitzgerald & Lamborg (2004) for example reports Hg_{tot} concentrations in precipitation between 3 and 23 ng l^{-1}.

If precipitation and dry deposition data are projected to corresponding time scales the ratio of dry to wet deposition and their respective significance could be estimated. Based on our measurements, i.e. a mean Hg_{tot} concentration in precipitation of 7.0 ng l^{-1} and a mean deposition flux of 2 ng m^{-2} h^{-1} (average of both methods over entire period), the annual dry deposition would account for two third and wet deposition for one third of a total annual input of 0.26 g ha^{-1}. Thus dry deposition would exceed wet deposition by a factor of 2 and would therefore constitute the major deposition pathway.

3.6 Acknowledgements

We thank the Swiss National Science Foundation (project numbers: 200020-113327/1 to D. Obrist and C. Alewell; 200021-105949 to W. Eugster and R. A. Werner) for financing this project and would like to express our appreciation to H. Hürlimann, M. Caroni and H. Strohm for their assistance in soil and water analyses, H. Biester for the mercury analysis of our soil samples and R. Vogt as well as C. Ammann for their valuable help in micrometeorological issues.

Chapter 4

Summertime Hg^0 exchange of three temperate grassland sites

This chapter has been submitted to Atmospheric Chemistry and Physics as:
Fritsche, J., Wohlfahrt, G., Ammann, C., Zeeman, M., Hammerle, A., Obrist, D. and Alewell, C., 2007: Summertime elemental mercury exchange of temperate grasslands on an ecosystem-scale. Atmospheric Chemistry and Physics Discussions 8, 1951-1979, 2008.

4.1 Abstract

In order to estimate the air-surface mercury exchange of grasslands in temperate climate regions, fluxes of gaseous elemental mercury (GEM) were measured at two sites in Switzerland and one in Austria during summer 2006. Two classic micrometeorological methods (aerodynamic and modified Bowen ratio) have been applied to estimate net GEM exchange rates and to determine the response of the GEM flux to changes in environmental conditions (e.g. heavy rain, summer ozone) on an ecosystem-scale. Both methods proved to be appropriate to estimate fluxes on time scales of a few hours and longer. Average dry deposition rates up to 4.3 ng m^{-2} h^{-1} and mean deposition velocities up to 0.10 cm s^{-1} were measured, which indicates that during the active vegetation period temperate grasslands are a small net sink for atmospheric mercury. With increasing ozone concentrations depletion of GEM was observed, but could not be quantified from the flux signal. Night-time deposition fluxes of GEM were measured and seem to be the result of mercury co-deposition with condensing water. Effects of rain and of grass cuts could also be observed, but were of minor magnitude.

4.2 Introduction

The continued use of mercury in a wide range of products and processes and its release into the environment lead to exposition of mercury in ecosystems yet unspoiled. Its long atmospheric lifetime of about 1 to 2 years (Lin & Pehkonen, 1999)

enables elemental mercury (Hg^0) to migrate to remote areas far away from its emission source, and once deposited to terrestrial or aquatic surfaces it is exposed to the formation of even more toxic methylmercury (IOMC, 2002). A suite of factors determines the ultimate fate of elemental mercury and its eventual immobilisation at the Earth's surface. Depending on atmospheric chemistry, meteorological conditions and physicochemical properties of the soils mercury may be cycled fairly rapidly between terrestrial surfaces and the atmosphere (Gustin & Lindberg, 2005). However, it remains unclear whether deposited mercury is retained in background soils or whether terrestrial surfaces are even a net source of mercury (Pirrone & Mahaffey, 2005). Once deposited, mercury may be sequestered (e.g. adsorbed to soil organic matter and clay minerals), removed from the soil by leaching and erosion or re-emitted (Gustin & Lindberg, 2005). Mercury sequestered by terrestrial ecosystems might eventually be disconnected temporarily from the atmosphere-biosphere cycle, which would lead to a decrease in the pool of atmospheric mercury.

The function of vegetation in the mercury exchange with the atmosphere remains unclear. Mercury may be taken up by leaves or transferred from the soil through the plant to the atmosphere (Gustin & Lindberg, 2005; Millhollen et al., 2006a). Foliar uptake has been suggested to be an important pathway for atmospheric mercury to enter terrestrial ecosystems and may represent a significant, but poorly quantified sink within the biogeochemical cycle, possibly accounting for over 1'000 tons of mercury per year (Obrist, 2007). Du & Fang (1982) measured Hg^0 uptake of several C3 and C4 plant species and demonstrated that stomatal and biochemical processes control the uptake. Atmospheric mercury concentration was found to be the dominant factor associated with foliar mercury concentrations in different forb species (Fay & Gustin, 2007), and the successful application of different grass species in biomonitoring studies (De Temmerman et al., 2007) suggest that mercury uptake by plants is indeed of significance.

With innovations in sensitive measurement techniques in the last decade it is now possible to measure atmospheric mercury background concentrations currently ranging from 1.32 to 1.83 ng m^{-3} (Valente et al., 2007). Such instruments also allow the estimation of air-surface exchange fluxes of gaseous elemental mercury (GEM) by applying micrometeorological methods. They are based on vertical concentration profiles and permit spatially averaged measurements without disturbing ambient conditions – an essential element of long-term studies.

During our previous work on GEM exchange of a montane grassland in Switzerland we determined mean deposition rates of 5.6 ng m^{-2} h^{-1} during the vegetation period (Fritsche et al., 2008a). In the current study that work is extended to another montane and one lowland grassland site along the Alps with the aim to determine whether all temperate grasslands are net sinks for atmospheric mercury or whether GEM exchange is site specific. Two classical micrometeorological methods are applied to estimate the GEM fluxes: the aerodynamic method and the modified Bowen ratio (MBR) method. By performing these measurements during the vegetation period, we also attempt to capture changes in the GEM flux caused by alteration of environ-

mental conditions, e.g. grass cuts, heavy precipitation, and elevated summer ozone concentrations.

4.3 Experimental

4.3.1 Site description

For our GEM flux measurements we selected three grassland sites in Switzerland and Austria with existing micrometeorological towers. The first site, Fruebuel, is located on an undulating plateau 1'000 m a.s.l. in central Switzerland. It is intensively used for cattle grazing and is bordered by forest, wetlands and other grasslands. The second location, Neustift, is an intensively managed, flat grassland in the Austrian Stubai Valley at an elevation of 970 m a.s.l. This previously alluvial land lies between the Ruetz river and pastures and is primarily used for hay production. The third site is situated in Oensingen on the Swiss central plateau (Mittelland) at 450 m a.s.l. between the Jura and the western Alps. It serves as an experimental farmland with extensive management and neighbours agricultural land that borders on a motorway in the north-west.

All three sites are equipped with eddy covariance (EC) flux towers. The stations in Neustift and Oensingen are affiliated with the CarboEurope CO_2 flux network and are operated by the Institute of Ecology, University of Innsbruck, Austria and the Federal Research Station Agroscope ART, Switzerland, respectively. At Fruebuel the EC flux tower is operated by the Institute of Plant Science, ETH Zurich to investigate greenhouse gas fluxes from agricultural land in the context of a changing climate.

Details about the meteorological and pedological conditions of all three sites are listed in Tab. 4.1. The predominant wind direction at Fruebuel is SW to SSW, showing a distinct channelled flow as a result of the local, undulating, sub-alpine topography. The largest contributions to the footprint are within approximately 60 m of the eddy covariance tower. Neustift on the other hand represents a site with the characteristic wind regime of an Alpine valley – the wind blowing into the valley from NE during the day and blowing out of the valley from SW during the night. Vegetation is uniform for around 300 and 900 m in the directions of the day- and night-time winds, respectively, with the footprint maximum lying within these boundaries for more than 90% of all cases. In Oensingen the fetch length is about 70 m along the dominant wind sectors (SW and NE) and 26 m in the perpendicular axis. The fraction of the field contributing to the measured EC CO_2 flux is >70% during most of the daytime, whereas during night-times, this fraction is generally lower and highly variable due to very stable conditions.

The gleyic cambisols at Fruebuel and the stagnic cambisols at Oensingen are rather deep (>1 m), while the gleyic fluvisol in Neustift is very shallow (<30 cm). Total mercury concentrations at all sites are representative of uncontaminated background soils (see Tab. 4.1), although the Hg_{tot} concentration at Fruebuel lies at the threshold value of 100 ng g^{-1}. We performed our measurements between June and September

2006 for two weeks at each site.

4.3.2 Micrometeorological methods

A variety of micrometeorological techniques to estimate atmosphere-surface exchange fluxes of trace gases have been developed (Dabberdt et al., 1993; Lenschow, 1995; Baldocchi, 2006; Foken, 2006). Of these, the eddy covariance approach would be most straightforward, but is currently not feasible for GEM as no fast-response sensor is yet available (Dabberdt et al., 1993; Lindberg et al., 1995). We therefore resorted to two more empirical methods. The first, the aerodynamic technique, is an application of Fick's law of diffusion to the turbulent atmosphere (Baldocchi, 2006). Translated to an atmospheric trace gas the general relationship for the flux is

$$F_x = -K_x \frac{\partial c_x}{\partial z} \tag{4.1}$$

where F_x is the vertical trace gas flux, K_x the eddy diffusivity and $\partial c_x/\partial z$ the concentration gradient of an arbitrary, non reactive trace gas x (Dabberdt et al., 1993; Lenschow, 1995; Baldocchi, 2006). Corresponding equations have been formulated for the momentum flux (Q_M) as well as the fluxes of sensible (Q_H) and latent heat (Q_E). It is assumed that the sources and sinks of these scalars are equal and thus similarity between the eddy diffusivities ($K_x = K_H = K_E$) are implied.

The eddy diffusivity K_x is expressed by the aerodynamic method as

$$K_x = \frac{k \cdot u_* \cdot z}{\Phi_h(z/L)} \tag{4.2}$$

where k denotes the von Karman constant (0.4), u_* the friction velocity, z the measurement height, $\Phi_h(z/L)$ the universal temperature profile and L the Monin-Obukhov length. Generally the eddy covariance technique is used to determine the friction velocity and L is calculated from u_*, air temperature, air density and the sensible heat flux. By combination of Eq. (1) and (2) and subsequent integration we obtain

$$F_{GEM} = -\frac{k \cdot u_* \cdot (c_{GEMz_2} - c_{GEMz_1})}{\log(z_2/z_1) + \psi_{z_2} - \psi_{z_1}} \tag{4.3}$$

where ψ_{z_1} and ψ_{z_2} are the integrated similarity functions for heat at the measured heights. A more detailed description of this method is given in Edwards et al. (2005).

The second method employed is the modified Bowen ratio method, which is a slightly more direct technique to estimate the GEM flux. This method uses directly measured fluxes of a surrogate scalar (i.e. sensible heat or a second trace gas) and the vertical gradient of this scalar. In our studies we measured the fluxes of CO_2 with eddy covariance and its vertical gradient concurrently with the GEM gradients. The GEM flux is then calculated as

$$F_{GEM} = F_{CO_2} \cdot \frac{\Delta c_{GEM}}{\Delta c_{CO_2}} \tag{4.4}$$

Further details and previous applications of this method are described by e.g. Meyers et al. (1996) and Lindberg & Meyers (2001).

4.3.3 Instrumentation

Air concentrations of GEM were measured in 5-minute intervals with a dual cartridge mercury vapour analyser (Tekran 2536A, Tekran, Toronto, Canada). With this instrument mercury is preconcentrated by amalgamation and detected via cold vapour atomic fluorescence spectrometry; further details of its operation principals are described in e.g. Lindberg et al. (2000). The instrument was calibrated automatically every 24 hours by means of an internal mercury permeation source. Additional, manual calibrations were performed prior to each measurement campaign by injecting mercury vapour with standard gas tight syringes from a mercury vapour generation unit (Model 2505, Tekran, Toronto, Canada).

In order to compute GEM fluxes by the MBR method CO_2 concentrations were measured with a closed path infrared gas analyser (LI-6262, LI-COR Inc., Lincoln, Nebraska, USA) at a frequency of 1 Hz. Before each campaign the gas analyser was calibrated with argon as zero gas and pressurised air with 451 ppm CO_2 as span gas. The zero-offset of argon relative to a N_2/O_2 gas mixture was 0.4 ppm.

Meteorological data (air temperature, net radiation, PAR, humidity, wind speed, wind direction) were recorded by the micrometeorological instrumentation of the towers at the study sites. Carbon dioxide and water vapour fluxes were determined by eddy covariance using three-dimensional sonic anemometers and open path infrared gas analysers (Solent R2 and R3 [Gill Ltd., Lymington, UK] and LI-7500 [LI-COR Inc., Lincoln, Nebraska, USA]).

4.3.4 Measurement setup

Vertical concentration gradients were determined by measuring GEM and CO_2 at 5 heights above ground (0.2, 0.3, 1.0, 1.6 and 1.7 m). The same setup was installed at all three sites, although the lowest sampling heights had to be adjusted to the local height of the vegetation (10 – 60 cm at Fruebuel and Neustift, and 10 – 20 cm at Oensingen). The sampling lines consisting of 1/4"-tubing were mounted to a mast in the vicinity of the micrometeorological towers and connected to a 5 port solenoid switching unit. Depending on space and the setup of the micrometeorological equipment at each site, the sampling lines were between 7 and 15 m long (all lines at each site had equal length). Downstream of the switch unit, the Tekran instrument and the CO_2 analyser were connected in series. Filter cartridges with 0.2 μm Teflon® filters were mounted to the inlets of the sampling lines to prevent contamination of the analytical system. Tubing and fittings made of Teflon® were used and cleaned with HNO_3 and deionised water according to an internal standard operating procedure (adapted from Keeler & Landis (1994). The system was checked for contamination by measuring mercury-free air generated by a zero air generator (Model 1100, Tekran, Toronto, Canada).

Additionally, by constricting the sampling lines temporarily it was tested if the setup had any leaks.

Air was sampled at a flow rate of 1.5 l min^{-1} by the internal pump of the Tekran instrument. To maintain continuous flushing of all sampling tubes an auxiliary pump with a flow rate of 6.0 l min^{-1} was connected to the four lines that were currently not sampled. The sampled air was not dried, which required correction of the calculated fluxes for density effects (see below).

Air sampling was switched from a line at a lower height to one at an upper height every 10 minutes (i.e. the sequence with the heights mentioned above was 0.2 – 1.6 – 0.3 – 1.7 – 1.0 m). In this way a vertical concentration profile with five measurement points could be determined every 50 minutes. Higher frequencies were not feasible as the low ambient GEM concentrations require pre-concentration by the gold cartridges of the Tekran intrument for accurate analysis.

4.3.5 Flux calculations

Upon completion of the measurement campaigns, GEM and CO_2 fluxes were computed with a self-programmed Matlab® algorithm. Carbon dioxide fluxes were calculated to evaluate the quality of the GEM fluxes. By comparing the CO_2 fluxes determined by the aerodynamic method with the CO_2 fluxes obtained by eddy covariance we could assess the reliability of the aerodynamic method, i.e. matching CO_2 fluxes lend credibility to the calculated GEM fluxes (assuming the CO_2 fluxes determined by EC to be accurate).

After correction of the GEM and CO_2 concentrations with respect to the measured standards the atmospheric concentration trend was subtracted from the data by interpolating the concentration measured at the top sampling line to the measurements of the other lines. This step was considered essential as atmospheric concentrations changed during the course of a measurement cycle of 50 minutes (i.e. 20 minutes for one height pair) and overlaid the measured gradients. Next, GEM and CO_2 fluxes were calculated according to Eq. 4.3 and 4.4 for four successive height pairs per measurement cycle. The raw fluxes were then obtained by computing the median of these four values, thus reducing uncertainty substantially.

As the sampled air was not dried the raw fluxes were corrected for density effects of water vapour according to Webb et al. (1980). A correction for sensible heat was not considered necessary, because the sample air of all lines was brought to a common temperature before reaching the analysers and because the Tekran instrument monitors the GEM concentration relative to the sampled air mass with a mass flow controller. Finally, the GEM and CO_2 flux data were screened for outliers and values outside the range of the mean ± 3 standard deviations of the whole period were rejected.

4.4 Results

4.4.1 Data coverage

We performed our measurements at the three sites under fair weather conditions. However, due to power outages and showers during thunderstorms as well as instrument failures, not all variables required to calculate the GEM and CO_2 fluxes could be measured continuously. As shown in Tab. 4.1 GEM fluxes could be computed for up to 85% of the measurement periods. In Neustift and Oensingen the data coverage of the GEM fluxes calculated by the MBR method was considerably reduced due to failure of the eddy covariance systems.

As the resolution of gradient measurements is limited we determined the minimum resolvable gradient (MRG) in a similar way as described by Edwards et al. (2005). This was done at Fruebuel by mounting all five sampling lines at 1 m above ground, measuring the GEM and CO_2 concentrations for three days and computing the concentration differences between the line pairs used for the flux calculations. By defining the MRG as the mean of the concentration differences plus one standard deviation we obtained MRG's of 0.02 ng m^{-3} for GEM and 2.5 ppm for CO_2. This translates to minimum GEM fluxes determinable with the aerodynamic method of -2.8 to -4.6 ng m^{-2} h^{-1} for typical daytime and -0.5 to -1.9 ng m^{-2} h^{-1} for typical night-time turbulence regimes (for daytime u_*=0.17 to 0.27 m s^{-1} and z/L=-0.49 to -0.16; for night-time u_*=0.032 to 0.11 m s^{-1} and z/L=2.2 to 0.15 [data from the Fruebuel site]). Excluding outliers and flux values with gradients below the MRG, the overall data coverage for the GEM fluxes at the three sites was between 27 and 58% (see Tab. 4.1 for details). However, exchange rates calculated with smaller gradients than the MRG were included in the results reported below, as average fluxes would otherwise be overestimated.

4.4.2 Meteorological conditions

Meteorological conditions at the three sites were mainly sunny and stationary most of the time (see Fig. 4.1 to 4.3 and Tab. 4.1). The measurement campaign in Oensingen was scheduled for September 2006 when air temperature and irradiation were somewhat lower than at the other sites. However, conditions in Oensingen were unstable and very humid with evening and night-time thunderstorms. Atmospheric turbulence at Fruebuel and Neustift was very similar with average values of 0.17 m s^{-1}. The value for Oensingen was lower with 0.12 m s^{-1}. At the national air monitoring stations nearest to Fruebuel and Oensingen average O_3 concentrations of 123 and 25 μg m^{-3}, respectively, were measured during the study periods.

4.4.3 Atmospheric GEM concentrations

Average atmospheric GEM concentrations measured 1.7 m above ground were 1.2 $\pm$0.2 ng m^{-3} at both, the Fruebuel and Neustift sites, and 1.7 $\pm$0.5 ng m^{-3} at the site

Variable	Unit	Fruebuel	Neustift	Oensingen
Site				
Location	[-]	47°6′47″ N 8°32′16″ E	47° 07' 00" N 11° 19' 07" E	47° 17' 8.3" N 7° 43' 55.7" E
Measurement period	[-]	06.07.06 – 20.07.06	14.06.06 – 29.06.2006	14.09.06 – 26.09.06
Elevation	[m]	1000	970	450
Mean annual temperature	[°C]	7.0	6.3	9.5
Mean annual precipitation	[mm]	1200	850	1100
Soil specifications				
Type	[-]	gleyic cambisol	gleyic fluvisol	stagnic cambisol
Bulk density (A-horizon)	[g cm^{-3}]	1.50	1.03	1.2
C_{org} (A-horizon)	[mg g^{-1}]	18	28	28
pH (A-horizon)	[-]	4.5	6.1	5.3
Hg_{tot} concentration	[ng g^{-1}]	100.8	43.9	71.2
Micrometeorological conditions during measurements				
Air temperature, mean	[°C]	18.5	20.7	15.8
PAR, mean	[µmol $m^{-2}s^{-1}$]	560	550	310
Relative humidity, mean	%	75.9	69.7	95.6
u_*, mean	[m s^{-1}]	0.17	0.17	0.12
Water vapour flux, mean	[mmol $m^{-2}s^{-1}$]	2.7	2.0	1.7
Precipitation, total	[mm]	26	0	90
Soil water content, mean	[m^3 m^{-3}]	0.32	0.22	0.44
Data coverage of GEM fluxes determined by aerodaynmic / MBR methods				
Measurement coverage	%	84 / 84	85 / 73	68 / 40
Flux data coverage[f]	%	58 / 58	44 / 44	49 / 27
Atmospheric GEM				
GEM concentration, mean	[ng m^{-3}]	1.20 (0.76 to 1.61)[c]	1.22 (0.48 to 1.70)[c]	1.66 (0.94 to 4.71)[c]
GEM gradient[a], day, mean	[ng m^{-4}]	0.02 (−0.04 to 0.13)[c]	<0.02 (−0.06 to 0.07)[c]	<0.02 (−0.32 to 0.16)[c]
GEM gradient[a], night, mean	[ng m^{-4}]	0.06 (−0.03 to 0.27)[c]	0.02 (−0.06 to 0.17)[c]	−0.04 (−0.40 to 0.11)[c]
GEM flux, MBR, mean	[ng $m^{-2}h^{-1}$]	−1.6 (−14 to 14)[c]	−0.5[b] (−76 to 37)[c]	0.3[b] (−18 to 30)[c]
GEM flux, aerodynamic, mean	[ng $m^{-2}h^{-1}$]	−4.3 (−27 to 14)[c]	−2.1 (−41 to 26)[c]	0.5[b] (−33 to 33)[c]
Deposition velocity, mean ± std	[cm s^{-1}]	0.10 ±0.16	0.05 ±0.16	-
Number of determinations	[-]	327	355	235
Atmospheric CO_2				
CO_2 gradient[a], day, mean	[ppm m^{-1}]	9.3 (−1.4 to 19)[c]	3.4 (−7.6 to 9.6)[c]	7.8 (−6.1 to 18)[c]
CO_2 gradient[a], night, mean	[ppm m^{-1}]	−28 (−70 to 2.0)[c]	−43 (−170 to 12)[c]	−36 (−220 to 0.1)[c]
CO_2 flux, EC[e], mean	[µmol $m^{-2}s^{-1}$]	−6.4 (−44 to 58)[c]	3.6 (−40 to 33)[c]	−5.3 (−23 to 18)[c]
CO_2 flux, aerodynamic, mean	[µmol $m^{-2}s^{-1}$]	−5.4 (−64 to 61)[c]	17.9 (−50 to 95)[c]	−1.7 (−27 to 106)[c]

[a] calculated as described in section 4.3.5
[b] not significantly different from zero
[c] range
[d] standard error
[e] determined by eddy covariance
[f] minimum resolvable gradient as mean +1 std

Table 4.1: Summary of site specifications, environmental conditions as well as atmospheric GEM and CO_2 data.

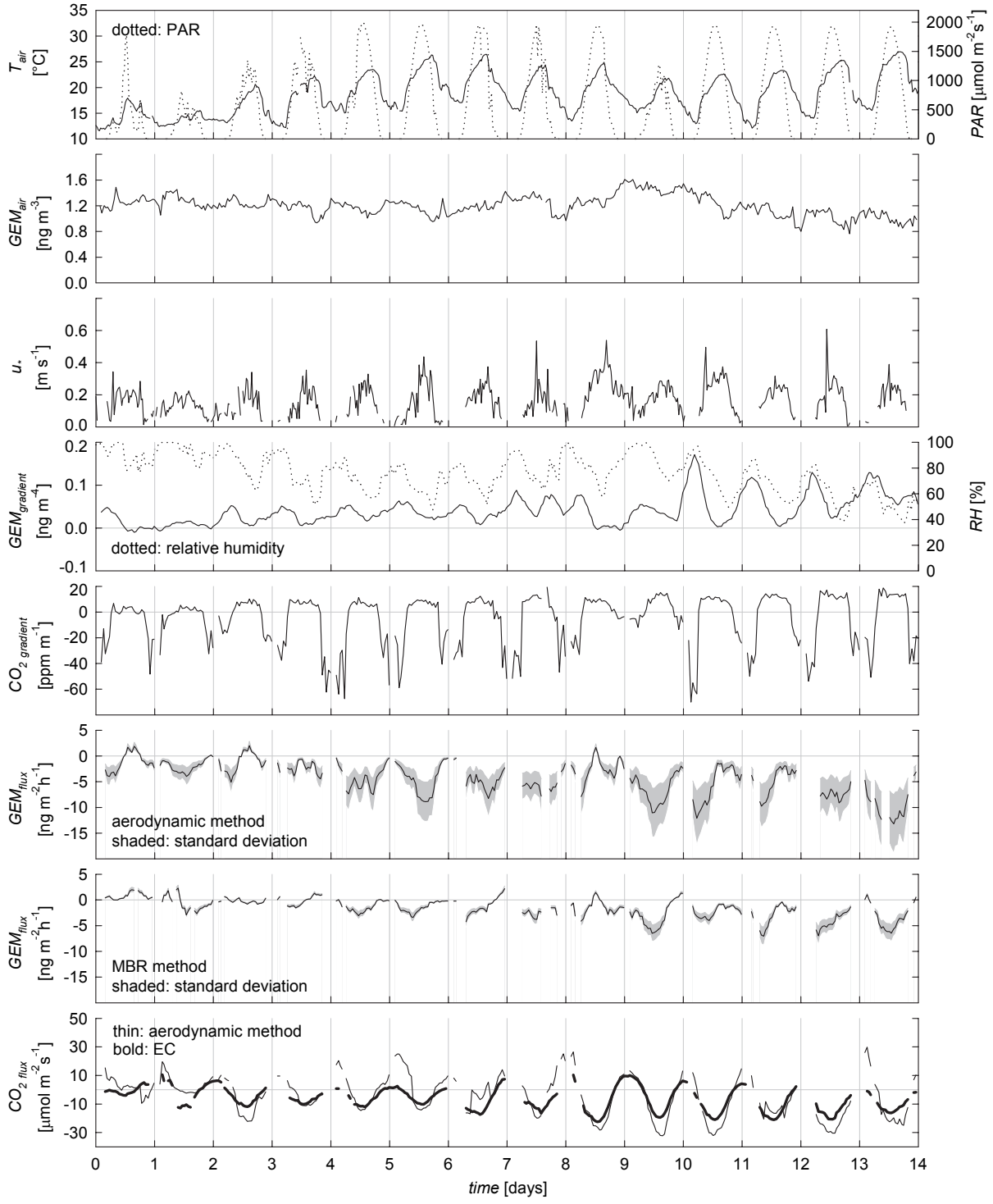

Figure 4.1: Time series of measurements at Fruebuel. From top to bottom: air temperature (T_{air}), photosynthetically active radiation (PAR), atmospheric GEM concentration at 1.7 m above ground (GEM_{air}), friction velocity (u_*·), GEM gradients and relative humidity, CO_2 gradients, turbulent fluxes of GEM (determined by the aerodynamic and MBR methods) and CO_2 (determined by the aerodynamic method and the eddy covariance technique). Flux data and GEM gradients were filtered by a 9-point moving average. Positive fluxes indicate emission, negative deposition.

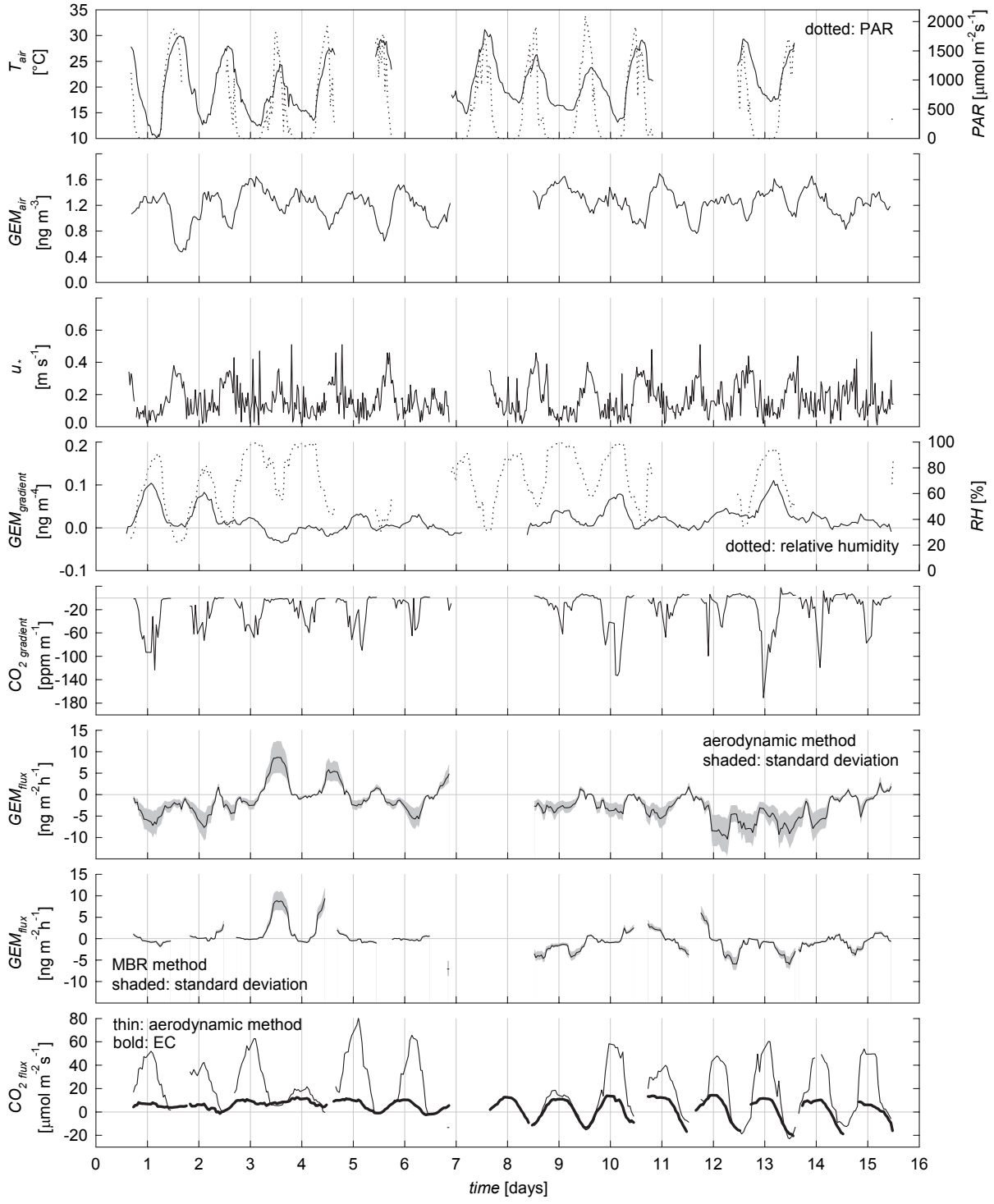

Figure 4.2: Same as 4.1, but for study site Neustift.

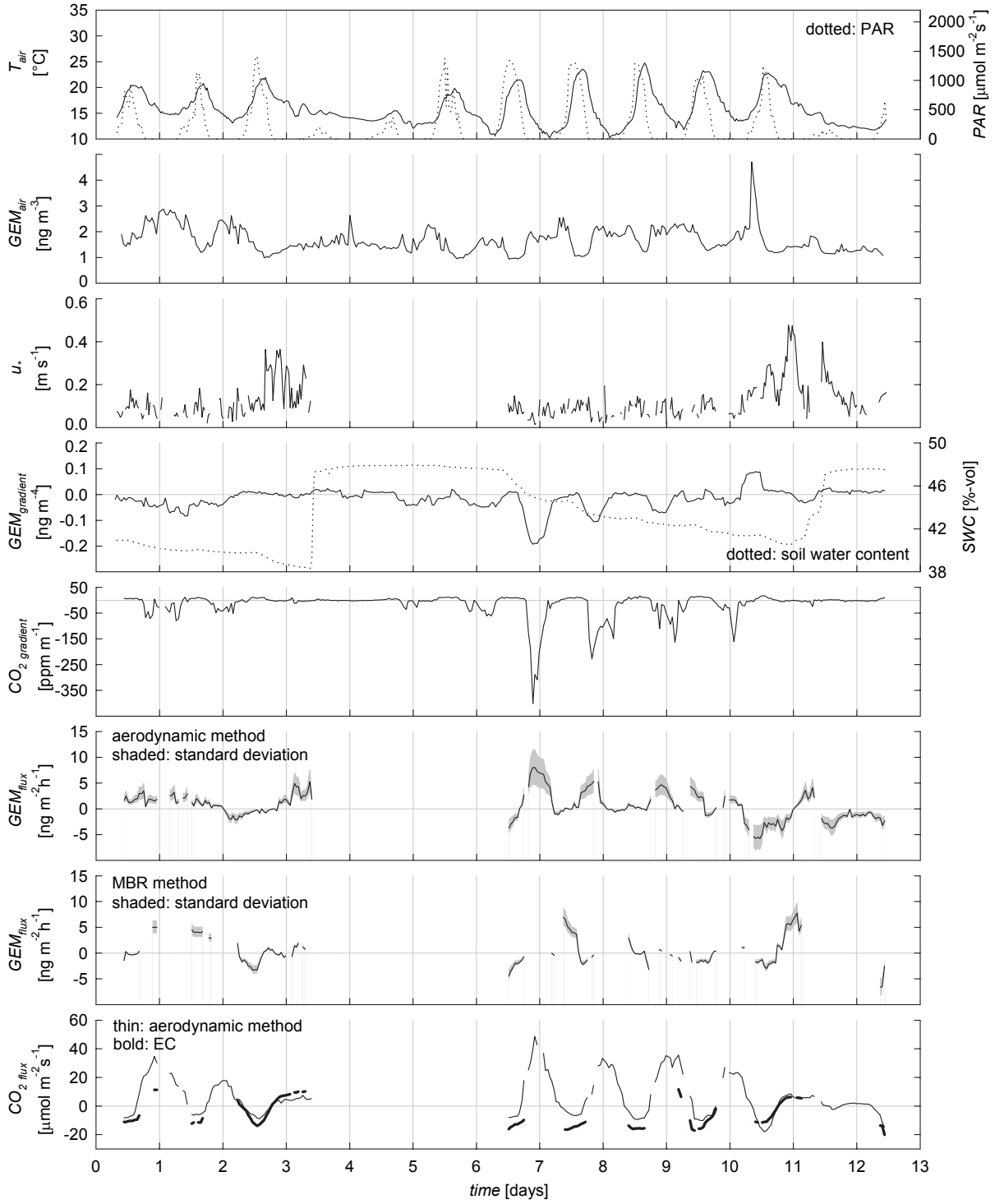

Figure 4.3: Same as 4.1, but study site Oensingen. Soil water content is shown instead of relative humidity in panel five.

in Oensingen (see Tab. 4.1). The highest concentration was measured in Oensingen during daytime with 4.7 ng m^{-3}, the lowest in Neustift with 0.5 ng m^{-3} during the night (see Fig. 4.1 to 4.3). As can be seen in Fig. 4.4 the concentrations in Neustift and Oensingen followed a distinct diurnal pattern with lowest GEM concentrations in the afternoon between 14 and 15 hours. This pattern was particularly pronounced in Neustift with an average diurnal amplitude of 0.32 ng m^{-3}. In contrast, a diurnal signal at Fruebuel was absent and concentrations nearly constant.

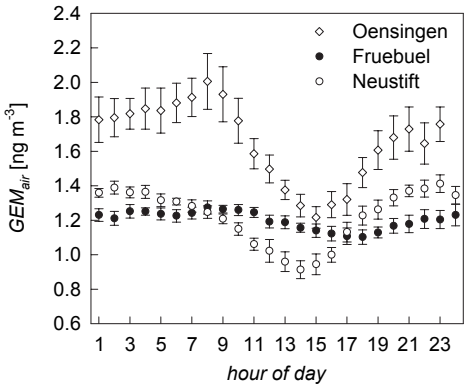

Figure 4.4: Diurnal trend of atmospheric GEM concentrations at the three study sites. Shown are hourly mean and standard errors of all measurement days (Fruebuel 14 days, Neustift 16 days, Oensingen 11 days).

Calculation of the correlation coefficients between ambient GEM concentration and meteorological variables revealed moderate linear relationships with relative humidity and atmospheric O_3 at Fruebuel and Oensingen (see Tab. 4.2). More pronounced correlations of GEM concentration were detected in Neusitft for most variables, notably air temperature and PAR, but no O_3 record was available for this site.

4.4.4 CO_2 and GEM fluxes

In Tab. 4.1 a summary of the average GEM and CO_2 gradients and fluxes is given for the investigated sites; the corresponding time series are shown in Fig. 4.1 to 4.3. Due to large spread, fluxes and GEM gradients were smoothed with a 9-point moving average (which corresponds to an interval of $\sim$8 hours). As expected, the vertical concentration gradients and fluxes of CO_2 varied substantially between day and night. While the highest average day-time gradient (9 – 15 hours) was recorded at Fruebuel with 9.3 ppm m^{-1}, the highest average night-time gradient (23 – 5 hours) was measured in Neustift with -43 ppm m^{-1}. The largest gradient of -220 ppm m^{-1} was measured at Oensingen during one night.

As mentioned in the experimental section CO_2 fluxes were determined two-fold, with eddy covariance and the aerodynamic method. The former yielded on average a net uptake or deposition of 6.4 μmol m^{-2} s^{-1} and 5.3 μmol m^{-2} s^{-1} at Fruebuel and Oensingen, respectively, and a mean net CO_2 emission of 3.6 μmol m^{-2} s^{-1} in

Variable	Fruebuel[b]		Neustift[c]		Oensingen[d]	
	r	p	r	p	r	p
Air temperature	−0.39	< 0.05	−0.77	< 0.05	−0.30	< 0.05
Soil temperature	−0.28	< 0.05	−0.64	< 0.05	−0.26	< 0.05
PAR	−0.17	< 0.05	−0.56	< 0.05	−0.27	< 0.05
Soil water content	0.44	< 0.05	0.31	< 0.05	−0.30	< 0.05
Absolute humidity	0.44	< 0.05	0.65	< 0.05	−0.08	0.14
Relative humidity	0.66	< 0.05	0.82	< 0.05	0.47	< 0.05
CO_2 concentration (LI-6262)	0.11	< 0.05	0.31	< 0.05	0.66	< 0.05
CO_2 flux (eddy covariance)	0.21	< 0.05	0.09	0.15	−0.03	0.81
H_2O flux (eddy covariance)	−0.16	< 0.05	−0.61	< 0.05	−0.52	< 0.05
O_3 concentration[a]	−0.43	< 0.05	-	-	−0.54	< 0.05
Wind speed	0.05	0.35	−0.52	< 0.05	−0.33	< 0.05

[a]data from nearest national monitoring station; [b]N=255 – 390; [c]N=194 – 375; [d]N=31 – 337

Table 4.2: Correlation of GEM concentration with meteorological variables.

Neustift. With the aerodynamic method average deposition of 5.4 μmol m^{-2} s^{-1} and 1.7 μmol m^{-2} s^{-1} were estimated for Fruebuel and Oensingen, and mean emissions of 17.9 μmol m^{-2} s^{-1} for Neustift (only data overlapping with the EC data were considered). Over the two-week period at Fruebuel CO_2 fluxes showed a linear trend towards higher deposition rates.

At all three sites GEM gradients showed a diurnal pattern, which was more pronounced at Fruebuel than at Neustift and Oensingen. Gradients were extremely small with a maximum value of 0.40 ng m^{-3} m^{-1} at Oensingen. Average day-time gradients reached 20.0 ng m^{-3} m^{-1} at Fruebuel and were below the minimum resolvable gradient at Neustift and Oensingen. With 0.06 ng m^{-3} m^{-1} the mean night-time gradient was highest at Fruebuel; for Neustift and Oensingen mean values of 0.02 and -0.04 ng m^{-3} m^{-1} were calculated. At Neustift and Fruebuel night-time gradients were highest in the early morning around 5 a.m. In contrast, night-time gradients at Oensingen were negative between measurement days 6 and 10, and peaked before midnight. Figure 4.1 also shows, that the amplitude of the GEM gradient at Fruebuel increased over time.

Computation of the fluxes yielded on average a small deposition of GEM at Fruebuel and Neustift and slight emission in Oensingen. Both micrometeorological methods were consistent regarding the sign of the average fluxes, but differed in their estimation of the exchange rates. At Fruebuel, the average GEM fluxes determined by the MBR method and the aerodynamic method were -1.6 and -4.3 ng m^{-2} h^{-1}, respectively. The corresponding exchange rates in Neustift were -0.5 and -2.1 ng m^{-2} h^{-1} and in Oensingen 0.3 and 0.5 ng m^{-2} h^{-1}. The latter two values as well as the exchange rate determined by MBR at Neustift were not significantly different from zero. The highest variability of the fluxes was recorded for Neustift with a range of -76 to 37 ng m^{-2} h^{-1}, determined with the aerodynamic method. At Fruebuel fluctuations

were smallest with a range of -14 to 14 ng m^{-2} h^{-1}, again determined with the aerodynamic method. Average deposition velocities ($v_d = -F_{GEM}/c_{GEM}$) for Fruebuel and Neustift were calculated to be 0.04 and 0.01 cm s^{-1} for the MBR method as well as 0.10 and 0.05 cm s^{-1} for the aerodynamic method. A linear trend of the GEM flux overlaid by a diurnal pattern with increasing amplitude was observed at Fruebuel. No such trend existed at Neustift and Oensingen and diurnal fluctuations were only visible during some periods and were more pronounced by the aerodynamic method.

4.5 Discussion

4.5.1 Evaluation of micrometeorological methods

As every micrometeorological method, flux-gradient techniques have certain limitations. One constraint is the footprint that depends on the prevailing atmospheric conditions, site heterogeneity and measurement height. When measuring gradients, the fetch of an upper sampling height is greater than the one at a lower sampling height and therefore generates some uncertainty. A further error is introduced by measuring in the so-called roughness sublayer, the region adjacent to the vegetation, that is directly affected by the influence of the local plants. In this zone common flux-gradient relationships become progressively less reliable as the gradient measurements approach the vegetated surface (Raupach & Legg, 1984; Baldocchi, 2006). For some periods this uncertainty had to be accepted in our study, as the measurements ran autonomously and the sampling lines could not be adjusted to the growing vegetation. Overall, errors associated with the aerodynamic method range between 10 and 30% and are greatest during periods with little turbulence (Baldocchi et al., 1988). Additionally, the MBR methods assumes that the transport processes are identical for both species, i.e. GEM and CO_2 (Lenschow, 1995). In the roughness sublayer this assumption is not guaranteed and might be another source of uncertainty.

In general, the MBR method yielded smaller average fluxes than the aerodynamic technique and on shorter time scales fluxes often differed considerably. The discrepancies of the averaged fluxes are likely to be of methodological nature as the methods differ in the way how they use the gradients to obtain the fluxes. While the aerodynamic method uses universal, empirical relationships to correct for atmospheric stability, the MBR approach relies on the accurate flux determination of the surrogate scalar by an independent method. The short-term fluctuations on the other hand are primarily the result of non-synchronous concentration measurements at the various heights as well as the rather low instrumental resolution of one flux value per 50 minutes and the small GEM gradients, which were around the minimum resolvable gradient of 0.02 ng m^{-3}. During several phases the two methods yielded different signs of the GEM flux (e.g. day 11 in Fig. 4.2). Closer analysis of the data revealed that this was caused by the smoothing process.

To evaluate the quality of the GEM fluxes, CO_2 exchange rates were also estimated with the aerodynamic method and compared to the EC CO_2 fluxes. Figures 4.1 and

4.2 illustrate that during some periods the aerodynamic technique strongly overestimated night-time fluxes relative to the EC method. In the stable nocturnal boundary layer, when u_* is small (<0.1 m s^{-1}), turbulent exchange is inhibited and vertical concentration gradients increase. Moreover, the aerodynamic method is based on the momentum flux equation as well as the wind speed/gradient relationship and requires some empirical formulae to describe atmospheric stability (Baldocchi et al., 1988). Uncertainties in these stability functions result in erroneous flux estimates for conditions of low turbulence (this limitation also applies to the GEM fluxes).

At Fruebuel we also obtained enhanced CO_2 fluxes by the aerodynamic gradient method during the day. This overestimation relative to the EC method might indicate that the gradient was measured too close to the vegetation cover when the grass grew closer to the lower sampling lines. Within and adjacent to the plant cover the universal flux-gradient relationships are no longer valid. Two additional problems may contribute to the observed discrepancy of the measured fluxes: I) When measuring gradients too close to the canopy, sources and sinks of CO_2 may not be identical any more and II), the footprints that are covered by the sampling lines at different heights are not identical. These considerations would lend more credibility to the GEM fluxes determined by MBR, as this method uses the ratio of the GEM and CO_2 gradients and is thus more robust. However, more accurate results by the MBR method can only be expected if sources and sinks of GEM and CO_2 are equal and if the special variability of the GEM and CO_2 fluxes are similar. Both assumptions are generally not met.

4.5.2 Atmospheric GEM concentrations

The mean global GEM concentration is reported to be around 1.7 ng m^{-3} (Valente et al., 2007). In Europe Munthe & Wängberg (2001) measured concentrations of 1.34 ng m^{-3} at Pallas in Finnland and Kim et al. (2005) 1.55 ng m^{-3} at Mace Head in Ireland. The average concentrations of 1.20 to 1.66 ng m^{-3} that we measured at our sites are consistent with these observations.

Moderate correlations of GEM concentration with atmospheric O_3 and relative humidity were detected. These relationships and the diurnal patterns of GEM and O_3 support the notion that O_3 is an effective reactant to remove Hg^0 from the atmosphere. Ozone has been identified to oxidise Hg^0 to Hg^{2+} (Lin & Pehkonen, 1999; Lindberg et al., 2007a), and it has been shown that O_3 concentrations as low as 20 ppb produce measurable quantities of Hg^{2+} in the atmosphere, which increase manifold with higher concentrations and solar irradiation (Hall, 1995). This would also explain the good correlation of GEM concentration with PAR at the Neustift site. In contrast, no effect of relative humidity on the reaction rate has been reported by Hall (1995). However, hydroxyl radicals which are another oxidant of Hg^0 are formed by the reaction of water vapour with photolysed ozone. This may clarify our observed correlation with relative humidity, although there might not be a cause and effect relationship.

The plot for Oensingen in Fig. 4.5 illustrates the diurnal fluctuations of GEM and O_3 clearly. However, deposition of GEM resulting from O_3 oxidation was not visible in the flux data as the extremely small variations in the GEM gradients caused by

this reaction could not be resolved and the oxidised mercury might not have been deposited immediately. At Fruebuel the daily variations were less pronounced, which seems to be the result of the exposed location of this site. Fruebuel is located on a plateau and is likely to receive fresh air by advection also during the night, which attenuates the diurnal signal of GEM and O_3. Oensingen and Neustift on the other hand are situated in valleys where air exchange in the stable nocturnal boundary layer is restricted and O_3 formed during the day is decomposed at higher rates.

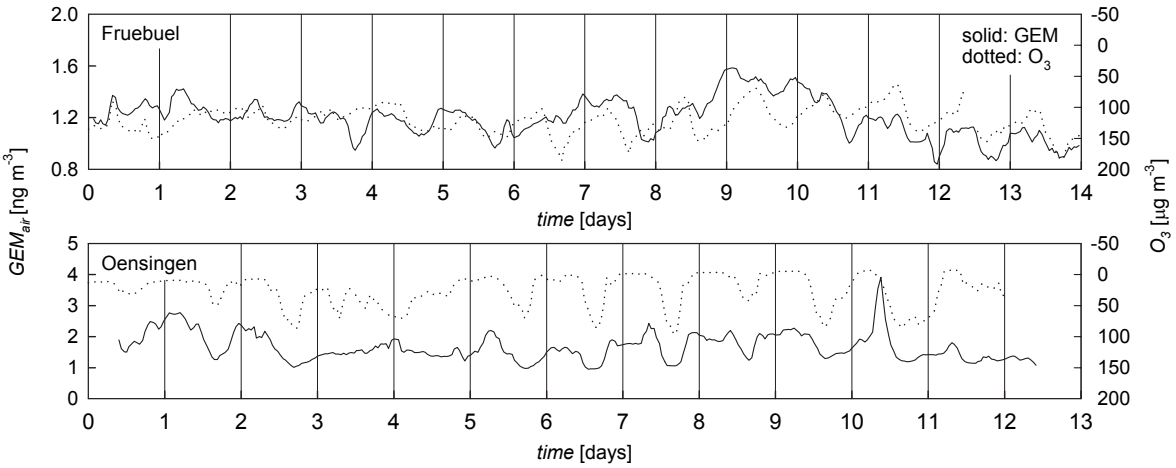

Figure 4.5: Time series of atmospheric GEM and ozone concentrations (O_3) at Fruebuel and Oensingen. GEM concentrations were filtered by a 3-point moving average. One μ g m^{-3} of O_3 corresponds to 0.5 ppb.

4.5.3 GEM exchange between atmosphere and grassland

With average GEM gradients between 0.02 and 0.06 ng m^{-3} m^{-1}, ranging from -0.40 to 0.27 ng m^{-3} m^{-1} our results are comparable to gradients measured in other ecosystems. For example, Lindberg & Meyers (2001) measured GEM gradients of 0.03 $\pm$0.03 ng m^{-3} m^{-1} over wetland vegetation, Kim et al. (1995) determined values of -0.16 to 0.32 ng m^{-3} (over 1.4 m) above forest soils in eastern Tennessee and Lindberg et al. (1998) measured gradients of -0.091 to 0.064 ng m^{-3} m^{-1} over forest soils in Sweden.

Although the GEM fluxes varied rather strongly, small but statistically significant net deposition rates could be observed at Fruebuel and Neustift. Similar exchange rates – but with inconsistent flux directions – have been estimated for various ecosystems. For example, Obrist et al. (2006) measured a mean deposition rate of 0.2 ng m^{-2} h^{-1} at another montane grassland site in Switzerland. In Canada Schroeder et al. (2005) observed fluxes between -0.4 to 2.2 ng m^{-2} h^{-1} over forest soils and 1.1 to 2.9 ng m^{-2} h^{-1} over agricultural fields. Values between -2.2 ng m^{-2} h^{-1} and 7.5 ng m^{-2} h^{-1} were also measured for forest soils by Kim et al. (1995), and Ericksen et al. (2006) determined a mean emission of 0.9 $\pm$0.2 ng m^{-2} h^{-1} from different background soils across the USA. Emissions of 8.3 ng m^{-2} h^{-1} from a grassy site

were measured by Poissant & Casimir (1998). In contrast, relatively high exchange rates in remote ecosystems are reported by Lindberg et al. (1992) who determined GEM emissions of 50 ng m^{-2} h^{-1} from forest soils and Cobos et al. (2002) who measured fluxes of -91.7 to 9.67 ng m^{-2} h^{-1} over an agricultural soil. Different methods were used in these studies and might explain some of the divergence between the findings. However, fluxes measured by our group at four different sites (Obrist et al. (2006);this study) indicate net deposition of GEM and imply that grasslands of the temperate montane climate belt are small net sinks for atmospheric mercury.

Other than at Fruebuel and Neustift our methods yielded no net flux in Oensingen. This discrepancy might be attributed to natural variability, as the observed background fluxes are already extremely low. However, during a period of four days, night-time GEM emission was observed (see Fig. 4.3). Heavy showers during thunderstorms between days 4 and 6 increased the soil water content by approx. 25%, which started to drop again during day six. It appears that the soil surface got waterlogged and as soon as the soil started to dry up again, gaseous mercury could evade from the soil (this process is also reflected in the concurrent CO_2 gradients and fluxes shown in Fig. 4.3). During the day no GEM emission was visible, which might be explained by the presence of O_3 that readily oxidises Hg^0.

At Fruebuel and Neustift night-time GEM gradients followed the pattern of relative humidity. Therefore, we suggest that during the night GEM was co-deposited with water condensing on the vegetation surfaces. Although incorporation of mercury into the plant material is conceivable, GEM was eventually re-emitted from the plant surface in the morning when temperature increased and water evaporated again. This re-emission might take place at a fast rate during a short interval that is not resolvable with our measurement technique.

A linear trend of the GEM flux could be observed at Fruebuel, resulting from the growing vegetation after a grass cut at the beginning of the campaign. In part this trend is artificial as the growing grass increases the atmospheric roughness sublayer, thereby reducing turbulence and enhancing the GEM gradients. However, with increasing plant surface area more GEM may be adsorbed by vegetation and adds to the positive gradients. The unbiased part of the trend is reflected in the CO_2 flux estimated by EC, the method that is independent of gradients measurements. In Neustift, where the grass was also cut at the start of the measurement campaign, no such trend was visible. The flux signal rather seems to have a component with a periodicity of 4 to 5 days that conceals any long-term trend. Further investigations would be required at this site to ascertain the processes resulting in this signal.

4.6 Conclusions

In order to estimate air-surface GEM fluxes of uncontaminated grasslands along the Swiss and Austrian Alps we applied two micrometeorological methods. Both, the aerodynamic and the MBR methods proved suitable to estimate net exchange rates on time scales of a few hours and longer. Due to the required pre-concentration technique

for the detection of GEM, fluxes could not be resolved sufficiently on shorter time scales.

With respect to gaseous exchange our results suggest that grasslands of the temperate montane climate are a net sink for atmospheric mercury. This sink is very small compared to emissions of contaminated and naturally enriched areas (these are in the order of 100 to >1000 ng m^{-2} h^{-1}). Nonetheless, mercury deposition to remote terrestrial ecosystems could add to significant amounts if these fluxes are confirmed in other systems. On the condition, that deposited mercury is stably bound in the pedosphere, this would also entail a long-term reduction in atmospheric mercury.

At two of our sites we observed day-time depletion of GEM, which is likely to be attributable to the oxidation of GEM by O_3 and other reactive trace gases. However, a net increase of the GEM deposition flux caused by O_3 oxidation could not be resolved with the applied methods. On the other hand, night-time deposition of GEM was measured frequently and seems to be the result of co-precipitation with condensing water. The effect of rain on the soil-atmosphere exchange of GEM is visible on the ecosystem level. Initially wet, drying surface soil seems to result in enhanced GEM emission that lasts for several days.

4.7 Acknowledgements

We thank the Swiss National Science Foundation (project numbers: 200020-113327/1 to D. Obrist and C. Alewell; 200021-105949 to W. Eugster and R. A. Werner) and the Austrian National Science Foundation (project number: P17560-B03 to Georg Wohlfahrt) for financing this project and would like to express our appreciation to F. Conen, W. Eugster and R. Vogt for their valuable help in experimental and micrometeorological issues.

Chapter 5

Hg^0 exchange of a snow covered grassland site

This chapter has been published in the Journal of Geophysical Research as:
Faïn, X., Grangeon, S., Bahlmann, E., Fritsche, J., Obrist, D., Dommergue, A., Ferrari, C.P., Cairns, W., Ebinghaus, R., Barbante, C., Cescon, P., Boutron, C., 2007: Diurnal production of gaseous mercury in the alpine snowpack before snowmelt, Journal of Geophysical Research, 112(D21311)

JOURNAL OF GEOPHYSICAL RESEARCH, VOL. 112, D21311, doi:10.1029/2007JD008520, 2007

Diurnal production of gaseous mercury in the alpine snowpack before snowmelt

Xavier Faïn,[1] Sylvain Grangeon,[1] Enno Bahlmann,[1] Johannes Fritsche,[2] Daniel Obrist,[3] Aurélien Dommergue,[1,4] Christophe P. Ferrari,[1,4,8] Warren Cairns,[5] Ralf Ebinghaus,[6] Carlo Barbante,[5] Paolo Cescon,[5] and Claude Boutron[1,7,8]

Received 7 February 2007; revised 5 July 2007; accepted 10 August 2007; published 13 November 2007.

[1] In March 2005, an extensive mercury study was performed just before snowmelt at Col de Porte, an alpine site close to Grenoble, France. Total mercury concentration in the snowpack ranged from 80 ± 08 to 160 ± 15 ng l^{-1}, while reactive mercury was below detection limit (0.2 ng l^{-1}). We observed simultaneously a production of gaseous elemental mercury (GEM) in the top layer of the snowpack and an emission flux from the snow surface to the atmosphere. Both phenomena were well correlated with solar irradiation, indicating photo-induced reactions in the snow interstitial air (SIA). The mean daily flux of GEM from the snowpack was estimated at ~9 ng m^{-2} d^{-1}. No depletion of GEM concentrations was observed in the SIA, suggesting no occurrence of oxidation processes. The presence of liquid water in the snowpack clearly enhanced GEM production in the SIA. Laboratory flux chamber measurements enabled us to confirm that GEM production from this alpine snowpack was first driven by solar radiation (especially UVA and UVB radiation), and then by liquid water in the snowpack. Finally, a large GEM emission from the snow surface occurred during snowmelt, and we report total mercury concentrations in meltwater of about 72 ng l^{-1}.

Citation: Faïn, X., et al. (2007), Diurnal production of gaseous mercury in the alpine snowpack before snowmelt, *J. Geophys. Res.*, *112*, D21311, doi:10.1029/2007JD008520.

1. Introduction

1.1. Mercury Cycle in the Environment

[2] Mercury (Hg) is present in the environment in various chemical forms and can be emitted by both natural [*Pyle and Mather*, 2003] and anthropogenic [*Pacyna et al.*, 2001] sources. In the atmosphere, gaseous elemental mercury (Hg°, GEM) is the predominant form with a northern hemispheric background of 1.5–2.0 ng m^{-3} [*Slemr et al.*, 2003] and a lifetime of about 6–24 months [*Lamborg et al.*, 2002]. Oxidized species of Hg such as particulate mercury (PM) and reactive gaseous mercury (RGM) are found at lower concentrations (pg m^{-3}) in the atmosphere, except near combustion sources and except under special conditions in the Arctic during spring [*Schroeder and Munthe*, 1998]. The major anthropogenic sources of Hg to the atmosphere include emissions from fossil fuel combustion, waste incineration, chlor-alkali plants and metal smelting and processing [*Pacyna and Keeler*, 1995].

1.2. The Role of Snow Surfaces in Polar Areas

[3] Polar studies have shown that snow surfaces in the Arctic play an important role in the mercury cycle. High latitude snowpacks could act as a sink for GEM [*Ferrari et al.*, 2004a], and halogens are likely involved in homogenous and heterogeneous processes leading to GEM oxidation in the air of snow. Moreover, Atmospheric Mercury Depletion Events (AMDEs), which occur after polar sunrise in the atmosphere both in the Arctic [*Schroeder and Munthe*, 1998] and in Antarctica [*Ebinghaus et al.*, 2002] can lead in some cases to a fast deposition of oxidized forms of onto snow surfaces [*Lindberg et al.*, 2002]. As a result, the arctic seasonal snowpack is suspected to contribute to the contamination of the aquatic reservoir during snowmelt. The polar snowpack can also act a source of GEM to the atmosphere. Photodissociation of Hg(II) complexes [*Lalonde et al.*, 2003] was proposed to explain GEM emissions from snow surfaces.

1.3. The Role of Snow Surfaces in Temperate Areas

[4] Although polar areas have been intensively investigated for several years, few studies have investigated the

[1]Laboratoire de Glaciologie et Géophysique de l'Environnement (UMR 5183 CNRS/Université Joseph Fourier), St Martin d'Heres cedex, France.
[2]Institute of Environmental Geosciences, University of Basel, Basel, Switzerland.
[3]Desert Research Institute, Division of Atmospheric Sciences, Reno, Nevada, USA.
[4]Polytech' Grenoble, Université Joseph Fourier, Grenoble cedex, France.
[5]Environmental Sciences Department, University of Venice, Venice, Italy.
[6]Institute for Coastal Research, GKSS Research Centre, Geesthacht, Germany.
[7]Unité de Formation et de Recherche de Physique, Université Joseph Fourier, Grenoble cedex, France.
[8]Also at Institut Universitaire de France.

0148-0227/07/2007JD008520$09.00

role of snow surfaces in the midlatitudes. A recent study by *Blais et al.* [2005] has reported a contamination of the ecosystems in these areas with fish mercury levels exceeding health consumption guidelines established by the WHO in several Pyrénées lakes (450 to 2500 m a.s.l., France). In the Alps, *Ferrari et al.* [2002] measured both total Hg (Hg_T) and reactive Hg (Hg_R) concentrations in the seasonal snow cover. However, to fully understand the cycle of Hg in midlatitude areas, we must also investigate the dynamics of GEM. Additionally, the fate of Hg during snowmelt and the possible contamination of ecosystems are major issues in alpine regions with a high population density. Therefore we carried out a full study of GEM, Hg_T and Hg_R in an alpine snowpack at Col de Porte Meteo France Center (1326 m a.s.l.), close to Grenoble, France. The specific goals were to evaluate Hg_T and Hg_R in alpine snow, to investigate GEM dynamics in the alpine snowpack for the first time and to document fluxes between the alpine snowpack and the atmospheric surface layer using both field measurements and laboratory data.

2. Experimental Section

2.1. Site Description

[5] We conducted GEM monitoring and snow sampling from 9 March to 24 March 2005 at the CEN (Centre d'Etude de la Neige), a Meteo France research center dedicated to snow studies. CEN is located on the north face of the Col de Porte pass, in the Chartreuse mountains, French Alps (45, 29°N, 5, 77°E, 1326 m a.s.l.). Col de Porte is located 10 km north of Grenoble, close to a recreation area where about 50 cars can park on Saturday or Sunday. Thus this area could not be considered as a pristine location, due to road traffic and the proximity of a city with half million inhabitants. Meteorological parameters as well as snowpack characteristics were continuously recorded by Meteo France. Surface snow temperature was measured using an infrared sensor Testoterm with an uncertainty of 1°C. Solar irradiation was recorded using a pyranometer Kipp & Zonen CM14. Snowpack temperatures at 20, 40, 60, 80, 100, and 120 cm depth were measured with highly sensitive and calibrated temperature probes (Pt 100, Honeywell Control System) inserted in the Teflon® head of GEM snow probes (see below). Temperature uncertainty of Pt 100 was estimated at about 0.5°C.

2.2. Reactive and Total Mercury in Snow and Meltwater

[6] On March 16, Snow samples were collected at CEN each 20 cm from the surface down to the depth of 80 cm. Snow samples were stored in the dark at −20°C until analysis in April, 2005. On 19 March, we also collected three water samples from runoff receiving the melting snow close to the snow sampling location. These runoffs are fed by snowmelt and disappear at the end of spring when the snowpack has disappeared. However, these flows could be sufficient to flush away sediments or organic materials in their wake. Water samples were not filtered; they were acidified and analyzed immediately after sampling. For both snow and water sampling, we used ultra clean Teflon® bottles and clean sampling procedures [*Boutron*, 1990; *Ferrari et al.*, 2000]. We analyzed for Hg_R and Hg_T in snow, and for Hg_T in water samples. Hg_R corresponds to the fraction of mercury involved in easily reducible complexes by $SnCl_2$ or $NaBH_4$ such as $HgCl_2$, $Hg(OH)_2$, HgC_2O_4 [*Lindqvist and Rodhe*, 1985]. Total Hg includes Hg_R and stable complexes such as HgS, Hg^{2+} bound to sulfurs in humic compounds and some organomercuric species [*Lindqvist and Rodhe*, 1985]. We performed triplicates analysis for all measurements.

[7] Hg_R was determined at the Department of Environmental Science of the University Ca'Foscari of Venice (Italy), using an Agilent 7500i ICP-QMS (Agilent Technologies, Yokogawa Analytical Systems, Tokyo, Japan). Snow samples were melted just prior to analysis. After reduction with a 0.1% (w/v) $NaBH_4$ solution stabilized with a pellet (∼0.1 g) of NaOH, GEM was swept from the solution to plasma by an adapted gas liquid separator from a Perkin Elmer FIAS. Instrument calibrations were carried out with Hg standards prepared from serial dilutions of a monoelemental Hg solution at 1000 $\mu g\ ml^{-1}$ (CPI International Santa Rosa, CA, USA). The detection limit of Hg was calculated as three times the standard deviation of the blank and was ∼0.2 ng l^{-1} for a 1 mL of sample.

[8] Total mercury measurements were carried out at LGIT (Grenoble, France) using an A.M.A. 254 (Advanced Mercury Analyser 254, Altec Ltd, Czech Republic). *Roos-Barraclough et al.* [2002] have described this apparatus and shown that the A.M.A. is fully compliant with E.P.A. standard method 7473 [*EPA*, 1998]. No digestion of the sample is required: the sample is heated (850°C) and combusted under a flow of oxygen. Even Hg trapped in mineral matrices is transferred to the gas phase. The mercury is then amalgamated on a gold trap, which is subsequently released in the elemental form and finally detected at 253.7 nm using atomic absorption spectrometry. A standard reference material (C.R.M. 7002, [Hg] = 0.090 ± 0.012 ppm) was used for the calibration of the apparatus and a recovery rate of ∼103% was achieved using six standard measurements. The detection limit, calculated as three times the standard deviation of the blank, was 0.04 ng of mercury.

2.3. GEM in the Air of Snow and in the Atmosphere

[9] Two gas phase mercury analysers (Model 2537A; Tekran Inc., Toronto, Canada) were used for the determination of GEM in ambient air, snow interstitial air (SIA) and for flux measurements using a dynamic chamber. The pre-filtered air stream (soda lime trap and 0.2 μm Teflon® particle filter) was collected on two gold cartridges A and B. GEM was thermally desorbed and detected by cold vapor atomic fluorescence spectrometry at 253.7 nm (Tekran, 1999). Dual gold cartridges allowed alternate sampling and desorption, resulting in continuous measurement of GEM on a predefined time base. The set-up, accuracy and precision of this instrument have been assessed during field intercomparisons at an urban/industrial site [*Schroeder et al.*, 1995] and at a remote marine background location. The Tekran analysers were operated with a 5-min sampling frequency and the air was sampled at a flow rate of 1.5 l min^{-1}. The analysers were calibrated every 25 h with an internal automatic permeation source injection. Additional manual injections were also carried out to ensure the reproducibility of the measurements. The detection limit for GEM in this operation mode is about

0.15 ng m^{-3}. From 10 to 14 March we sampled ambient air 150 cm above the snow surface. From 18 to 21 March, we used a 5-port Teflon® solenoid switch unit for measuring successively GEM concentration at 10 cm, 70 cm, 130 cm, 200 cm and 270 cm above the snow surface. This approach has been used to find out if a gradient of GEM concentrations could be detected indicating either deposition or emission processes above the surface as has been measured by *Obrist et al.* [2006] in a subalpine site. The concentration of GEM in SIA was intensively investigated from 9 to 10 March, March 15 to 17 from, and from 22 to 24 March. We used GAMAS probes (Gaseous Mercury in Interstitial Air in Snow) at several depths to measure GEM concentrations between 20 and 120 cm depth below the snow surface [*Dommergue et al.*, 2003a]. This system has been used successfully in different Arctic sites, for example, at Station Nord, Greenland [*Ferrari et al.*, 2004a], Kuujjuarapik, Canada [*Dommergue et al.*, 2003c] and Ny-Ålesund, Svalbard [*Ferrari et al.*, 2005]. Five GAMAS probes were connected to the Tekran analyser, using a 5-port Teflon® solenoid switch [*Fritsche et al.*, 2006]. This set-up allowed a cyclic sampling of each probe every 10 min. Measurements were performed in duplicates or triplicates. For triplicate sampling, mean uncertainty was ~0.94% independently of the depth investigated. Blanks of the probes were 0.05 ± 0.05 ng m^{-3}. Because liquid water entered the sampling lines when temperature in the snowpack rose about 0°C, we were not able to sample GEM in snow interstitial air during warm afternoons and nights.

2.4. Reliability of Interstitial Air Sampling

[10] Many compounds such as ozone [*Petersen et al.*, 2001], nitrogen oxides [*Honrath et al.*, 2002], formaldehyde [*Sumner and Shepson*, 1999], H_2O_2 [*Bales et al.*, 1995] and recently GEM [*Dommergue et al.*, 2002; *Steffen et al.*, 2002; *Ferrari et al.*, 2004a] have previously been measured in the air of snow. The transfer of chemicals in the air of snow and the exchanges with the atmosphere are driven mainly by two processes. First by diffusion which is a relatively slow transport process and the result of gradients in concentration and temperature, and second by ventilation which is caused by wind turbulence [*Albert and Shultz*, 2002]. Ventilation can significantly increase the rate of transfer of chemicals in the air of snow. Air pumping for analysis can generate a significant forced ventilation when the sampling flow rate is above 2 l min^{-1} [*Albert et al.*, 2002]. We were able to minimize this effect using a low flow rate at 1.5 l min^{-1}. Assuming that the 15 l of air sampled for each GEM measurement was originating from a sphere located at the vicinity of the probe, we estimated that the interstitial air was sampled in a radius of 10 cm around the probes. However, measurement at 20 cm depth could be confounded by cosampling of ambient air.

2.5. Flux Measurements

[11] GEM fluxes between the snowpack and the atmosphere were measured both in the field and laboratory using a flux chamber.

2.6. Field Measurements

[12] Snow-to-air fluxes were measured in 10 min intervals on the Col de Porte snowpack from March 18 to 25 using dynamic flux chambers similar to those used previously over soils [*Engle et al.*, 2001; *Obrist et al.*, 2005]. The flux chamber covered an area of 29 × 12 cm^2. The chamber was 10 cm high, and pushed 5 cm into the snow so that a headspace of 5 cm was above the snowpack. On one side, holes in the chamber wall enabled ambient air to enter the chamber (inlet) while on the other side we connected a Teflon® line for air pumping (outlet). A two-port switch unit (Tekran model 1110) connected to a Tekran 2537A analyzer controlled alternating sampling between two ¼" Teflon® lines. The first line was directly connected to the outlet of the chamber. The second line enabled sampling air at the inlet of the chamber. Particulate filters (0.2 μm) were mounted at the ends of both lines. The chamber was made of Polycast SOLACRYL™ SUVT, which is characterized by high transmissivity for UVB (~80% at a wavelength of 270 nm). Blanks were measured by sealing the bottom of the chamber with a Polycast SOLACRYL™ SUVT plastic plate and resulted in fluxes of 0.02 ± 0.11 ng m^{-2} h^{-1} for cartridge A and 0.03 ± 0.14 ng m^{-2} h^{-1} for cartridge B.

2.7. Laboratory Measurements

[13] We also conducted experiments using a laboratory flux chamber system and surface snow samples collected during the field campaign. We specifically assessed the influence of solar radiation, snow temperature and snowmelt on GEM emission processes. Snow samples were collected in the field using clean methods. Therefore the chemical composition at the time of collection should have been preserved. However, due to transportation, the cold storage of samples and the method used to introduce the snow into the laboratory flux chamber, the physical structure of the snow is partly lost. In this way surfaces that could play a role in the chemical reactivity of GEM may have been altered. A detailed description of the laboratory flux chamber is given by *Balhmann et al.* [2006]. This set-up can simulate snow-to-air exchange of gaseous compounds under controlled conditions of temperature and light radiation, and was used for preliminary studies by *Dommergue et al.* [2007]. Snow samples were placed in the Teflonized chamber, and ambient air which has been cleaned over active charcoal was pumped through the chamber at a predefined flow rate. Solar radiation was simulated by means of a short arc lamp (2000 W Xenon). The lamp was operated without any optical filter (wavelength below 280 nm), and with optical filters cut off at 295 nm and 340 nm. A cut off of 295 nm corresponds to the natural solar radiation under clear sky conditions. Total radiation intensity varied between 0 and 120 W m^{-2}. The flux chamber temperature was set to −4°C, except during the simulation of the snowmelt where we increased the temperature to +1°C.

2.8. Calculation

[14] GEM fluxes in the field and laboratory were calculated using the following equation:

$$F = \frac{C_O - C_I}{A} \times Q,$$

Table 1. Total Mercury Concentration in the Snowpack From the Surface to 80 cm Depth, Sampled at the End of the Field Campaign

Depth, cm	Hg_T, ng l^{-1}	Hg_R, ng l^{-1}
10	160 ± 15	<DL (0.2)
20	132 ± 13	<DL (0.2)
40	123 ± 13	<DL (0.2)
60	158 ± 16	<DL (0.2)
80	80 ± 08	<DL (0.2)

where F is the flux in ng m^{-2} h^{-1}, C_O and C_I are GEM concentrations in ng m^{-3} at the outlet and inlet ports respectively, A the surface area of the chamber in m^2 and Q the airflow rate in l min^{-1}. For the field flux chamber, A and Q were 348 cm^2 and 1.5 l min^{-1}. A and Q for the laboratory flux chamber were 0.2 m^2 and 5 l min^{-1} respectively.

3. Results

3.1. Snowpack Characteristics and Meteorological Conditions

[15] Heavy snowfall occurred on 6 March, and field measurements started on 7 March with a 130 cm thick snowpack. We had no more snow precipitation during the field campaign, and the thickness of the snowpack decreased progressively to 80 cm on 24 March. A pit was dug on 15 March for stratigraphy and density measurements. We observed a typical snowpack of isothermal metamorphism with melt events. Two icy layers (0.3–0.6 cm thick) were found at ~73 cm and ~81 cm depth. Warm days and clear nights led to the formation of a melt freeze crust on the top. Density increased progressively from ~0.2 g cm^{-3} at the snow surface to ~0.4 g cm^{-3} at the bottom of the snowpack. Four periods were identified to describe the variations of atmospheric and snow surface temperatures. From 7 to 10 March, snow surface and air temperatures stayed below zero, with no clear diurnal pattern. From 11 to 14 March, the snow surface was characterized by diel temperature pattern between −17°C and 0°C and atmospheric temperature stayed between −5°C and 2°C. From 15 to 21 March, the snow surface showed a daily variation pattern with a minimum around −4°C at night and a maximum at 0°C during the day. Atmospheric temperatures were above 0°C both at night and during the day with a maximum of about 15°C. Finally, on 22, 23, and 24 March during nights and days, surface snow temperatures were constant at 0°C, and atmospheric temperatures were always positive. During the whole field campaign, we observed low winds with a maximum speed of about 2 m s^{-1} on March 7. Irradiation showed a clear diel signal, but due to the location of CEN research center on the north face of the pass, and forest on its east side, direct solar radiation could not reach the snow surface before 9:30 in the morning.

3.2. Mercury Concentrations in Snow Pits and Meltwater

[16] Hg_R and Hg_T concentrations measured in the snowpack from the surface to 80 cm depth are reported in Table 1. Hg_R concentrations were always below the detection limit of the method (0.2 ng l^{-1}). Hg_T concentrations of 79 ± 1 ng l^{-1}, 63 ± 3 ng l^{-1} and 74 ± 2 ng l^{-1} were measured in the snowmelt runoff.

3.3. Variations of GEM Concentrations With Depth in the SIA

[17] Atmospheric GEM concentration during the field campaign was on average 1.8 ± 0.4 ng m^{-3} (n = 2300). From 18 to 22 March, no GEM gradient was observed between 10 and 200 cm above the surface. Figure 1 presents GEM profiles measured in the SIA on 15 March. We observed similar temporal variations of GEM concentration in the SIA during the whole field campaign. Figure 1 shows that all concentrations stayed permanently above atmospheric level from 6:30 to 14:00. Early in the morning, we measured relatively homogenous concentrations around 2.8 ng m^{-3} at all depths. From 6:00 (i.e., sunrise) to 13:00, we observed a strong increase in GEM concentration in the first centimeters of the snowpack. Before 10:00, highest concentrations were measured at 20 cm depth and we observed a decrease of GEM levels with depth. From 10:00 to 13:00, the highest concentrations were measured at 40 cm depth. Finally, maximum GEM concentrations of about 8 ng m^{-3} were measured at 40 cm depth around noon. Data obtained from the 20 cm depth probe have to be considered carefully because cosampling of atmospheric air is likely as mentioned before. Consequently, concentrations within the surface snowpack could be higher than the measured ones.

3.4. Variations of GEM Concentrations With Irradiation and Temperature in the SIA

[18] GEM concentrations measured during the entire field campaign in the snowpack at 20 and 80 cm depth are reported on Figure 2 with mean solar irradiation. GEM levels at 20 cm depth increased simultaneously with solar irradiation to reach concentrations as high as ~9 ng m^{-3}. Deeper in the snowpack, a delay was observed between increases of irradiation and GEM concentration. As shown in Figure 3, there was no clear trend in GEM variation with temperature below 0°C. However, as soon as temperature reached 0°C (i.e., snow was melting), we noticed a significant increase of GEM concentration in the SIA.

3.5. GEM Fluxes Between the Snowpack and the Atmosphere

[19] Figure 4 displays GEM exchange fluxes from the snowpack to the atmosphere from 18 to 20 March and from 22 to 24 March. GEM fluxes exhibited distinct diurnal patterns strongly correlated with solar irradiation. We observed peak emissions of GEM from the snowpack to the atmosphere during the day around 1.4 to 3.3 ng m^{-2} h^{-1} (see Table 2). Integration over the entire daytime period (from 6:00 to 21:00) resulted in daily GEM emissions of 3.9 to 12.2 ng m^{-2} d^{-1}. Over the entire measurement campaign of five days, this loss was estimated at ~50 ng m^{-2}. We measured mean incorporation fluxes of about ~0.15 ± 0.07 ng m^{-2} h^{-1}, from 21:00 to 6:00 during five days. Chamber blanks were determined at the beginning of the campaign and yielded a flux overestimation of 0.02 ± 0.11 ng m^{-2} h^{-1} (cartridge A) and 0.03 ± 0.14 ng m^{-2} h^{-1} (cartridge B). As deposition fluxes were close to the detection limit, we could not conclude that GEM incorpo-

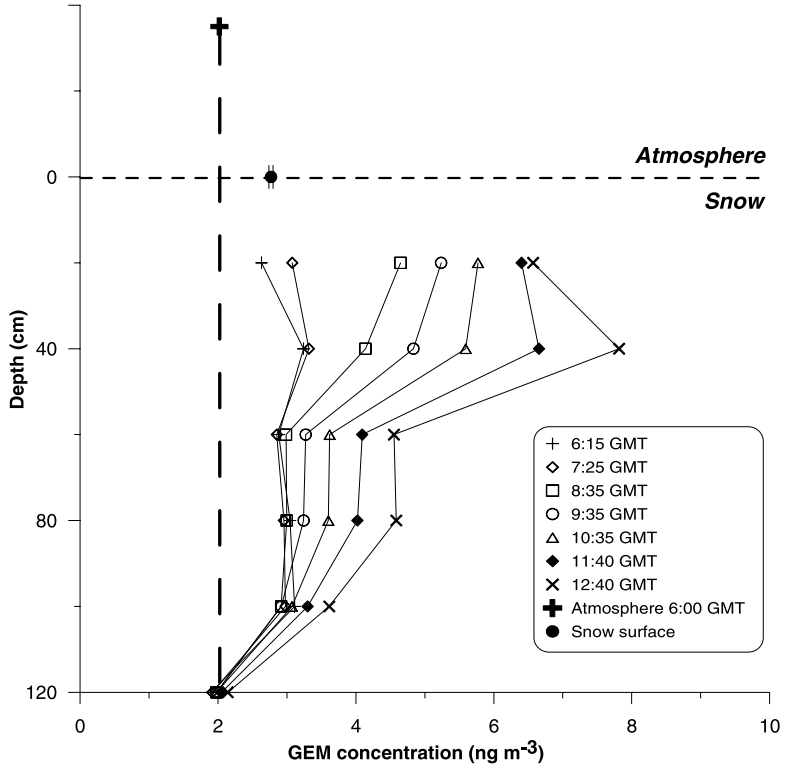

Figure 1. GEM profiles in interstitial snow air from the surface to 120 cm depth on March 15. Surface concentration reported here is an average of 20 measurements obtained the same day between 1:00 and 3:00 pm. The atmospheric level is the concentration determined at 6:00 am before sunrise. The error bar reported at the surface is one standard deviation of the mean values.

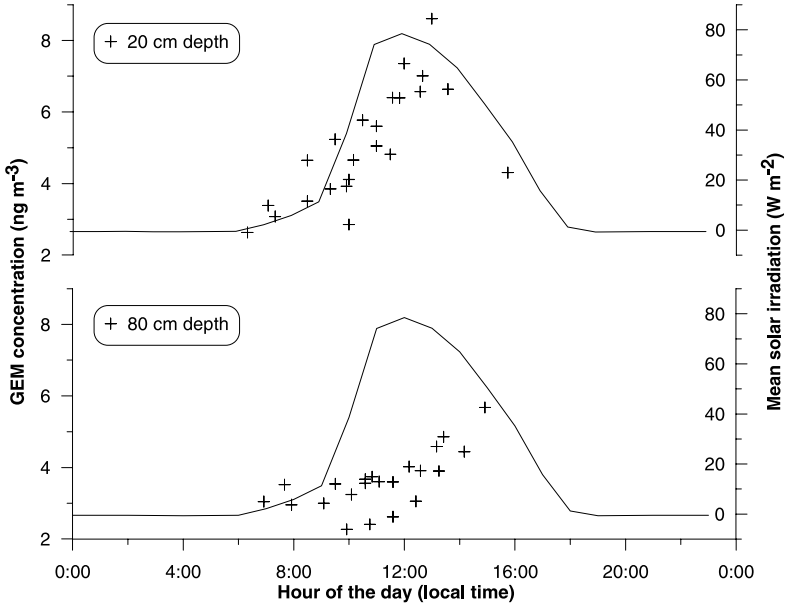

Figure 2. Variation of GEM concentrations in the snowpack (ng m^{-3}) at 20 and 80 cm depth with time. All data obtained during the field campaign are reported. Solar radiation is the mean calculated for the entire measurement period.

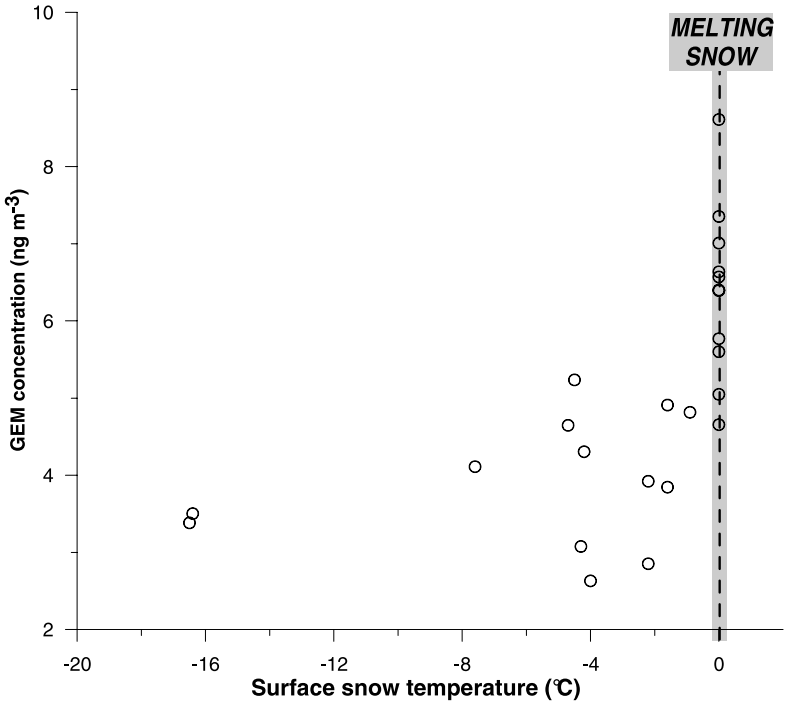

Figure 3. Increase of GEM concentration (ng m^{-3}) in the snow interstitial air at 20 cm depth with snow temperature from March 9 to 24.

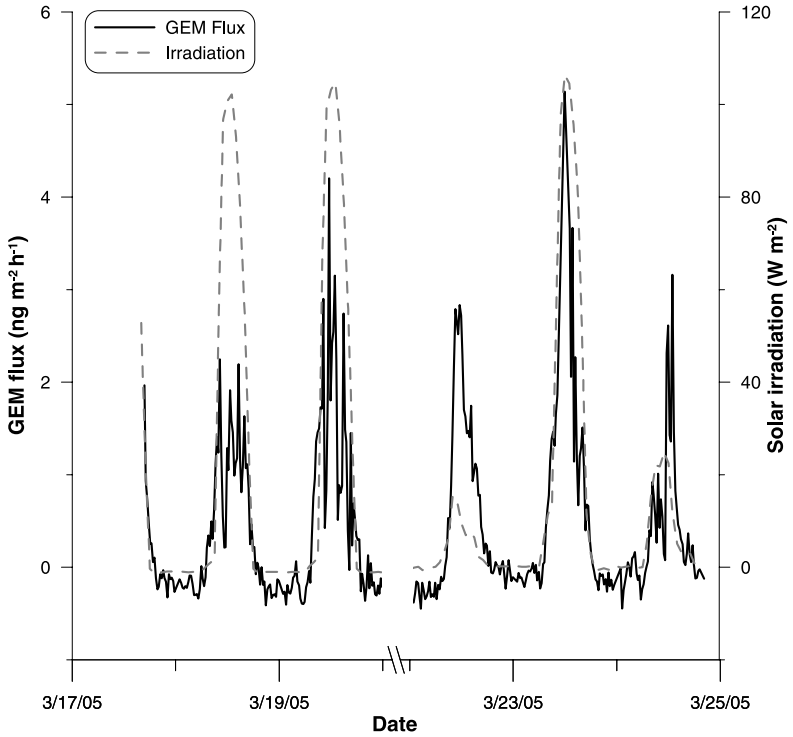

Figure 4. GEM fluxes (ng m^{-2} h^{-1}) from the snowpack to the atmosphere and solar irradiation (W m^{-2}) from March 17 to 24.

Table 2. GEM Fluxes (ng m^{-2} h^{-1}) From the Snowpack to the Atmosphere Measured During Daytime and Nighttime From 17 to 24 March

Time	Max Emission, ng m^{-2} h^{-1}	Integrated Emission, ng m^{-2} d^{-1}
18.03.2005[a]	1.4	7.84
19.03.2005[a]	3.08	12.09
20.03.2005[a]	2.28	10.22
23.03.2005[a]	3.34	12.2
24.03.2005[a]	1.63	5.64
Total[b]		49.99
Statistics[b]		
Mean	2.35	9.56
Std	0.86	2.83
P-value	5	5

[a]Day from 6:00 am to 9:00 pm.
[b]Values calculated from 5 days.

ration actually took place. We had no data from GEM in SIA at night as our probes could not be applied at night, but GEM concentrations at sunrise were always above atmospheric levels (see Figure 2).

3.6. Laboratory Flux Chamber Measurements

3.6.1. Irradiation Investigations

[20] In the laboratory, we first measured the evolution of GEM exchange fluxes with radiation intensity from 0 to 120 W m^{-2} [see *Balhmann et al.*, 2006 for details]. Such measurements were done using different filters. The snow was kept at −4°C. GEM fluxes exhibited linear relations with irradiation as reported in Table 3. At a constant radiation power of about 120 W m^{-2}, the maximum fluxes were 15.4 ng m^{-2} h^{-1}, 6.5 ng m^{-2} h^{-1} and 1.9 ng m^{-2} h^{-1} without a filter, with a 295 nm filter and with a 340 nm filter respectively. In the darkness and using the 295 nm filter, Table 3 reports a positive emission flux of about ∼0.4 ng m^{-2} h^{-1} which is not consistent with measurements carried out in the field. Using data presented on Table 3, we quantified the role of UVA, UVB and visible radiation in the snowpack. We identified the part of GEM emission due to three wavelength intervals corresponding to the different filters used: below 295 nm, from 295 to 340 nm, and above 340 nm. These results are presented in Figure 5 and show that both UVA (320–400 nm) and UVB (280–320 nm) wavelengths play an active role in photochemical processes in the snowpack. However, UVB light could be the most efficient for inducing GEM production.

3.6.2. Temperature Investigations

[21] Temperature data and consequently the influence of liquid water in the snowpack are reported in Figure 6, which shows the mercury emission flux as a function of time. Radiation phases during the experiment are indicated by shaded areas: we applied a radiation intensity of 120 W m^{-2} and a Pyrex filter to cut off wavelength below 295 nm throughout the experiment. At the beginning of the experiment, from 0 to 420 min, the temperature was kept at −4°C. After 425 min, the temperature of the chamber was set to +1.5°C allowing the snow to melt. As one can see in Figure 6, the flux exhibited several distinct patterns which are denominated by characters *a* to *d*.

[22] *Phase a.* During the first 300 min, the snow was kept in the dark at −4°C. The mean flux was 0.42 ± 0.05 ng m^{-2} h^{-1}. The chamber outlet mean concentration used for the determination of the GEM flux was 0.17 ± 0.02 ng m^{-3}.

[23] *Phase b*. During the next phase of the experiment we turned on the light and determined the photo induced flux over this sample at −4°C. The flux increased from 0.4 ng m^{-2} h^{-1} to about 8.2 ng m^{-2} h^{-1} within 20 min, which roughly corresponds to the turnover time of the chamber. After this rapid initial increase the flux decreased exponentially: the dashed line shows the extrapolated flux to the end of the experiment.

[24] *Phase c*. After 425 min the chamber temperature was set to +1.5°C allowing the snow to melt. With the beginning of the snowmelt, the flux increased from 5.9 ng m^{-2} h^{-1} to about 7.7 ng m^{-2} h^{-1} and then seemed to stabilize to a lower level of 6.8 ng m^{-2} h^{-1}.

[25] *Phase d.* When most of the snow had melted the emission of GEM from the snow suddenly decreased and stayed constant at about 2.0 ng m^{-2} h^{-1}.

4. Discussion

4.1. GEM in the Lower Atmosphere

[26] GEM atmospheric concentrations of 1.8 ± 0.4 ng m^{-3} measured at Col de Porte are close to the mean GEM concentration of about 1.82 ± 0.34 ng m^{-3} reported for the Wank station (47°31 N, 11°09 E, 1780 m a.s.l., Germany) in 1996 [*Slemr and Scheel*, 1998]. More recently, a subalpine site in Switzerland showed GEM concentrations of ∼1.6 ng m^{-3} during a summer measurement campaign [*Obrist et al.*, 2006]. No GEM gradient was observed between 10 and 200 cm above the snow surface at Col de Porte. This is in agreement with observations made in Barrow in the spring 2004. Indeed, *Aspmo* and coworkers observed a significant increase of GEM concentrations in a height of centimeters above the snow but they could not detect any significant concentration variations from 10 cm to 200 cm above the snowpack (*Aspmo*, personal communication). *Steffen et al.* [2002] reported homogenous GEM concentrations in the Arctic atmosphere within several meters above the snow surface during periods without any depletion event.

4.2. Mercury Balance in the Snowpack

[27] GEM in the SIA reached concentrations between 1.7 and 9 ng m^{-3}. As mentioned before, GEM data collected at 20 cm depth could be influenced by cosampling with ambient air, and by diffusion processes. A part of GEM formed in the snowpack close to the surface could diffuse immediately to the atmosphere. These considerations could explain that, after 10:00, the highest concentrations are not

Table 3. Linear Relations Between GEM Emission Fluxes and Radiation (R) Measured With a Cut Off of 340 nm, Cut Off of 295 nm and Without any Filter[a]

	$F_{GEM}(R)$	r^2	P-value
No Filter	0.107 × R + 0.564	0.99	11
Cut off 295 nm	0.048 × R + 0.348	0.98	10
Cut off 340 nm	0.010 × R + 0.744	0.88	11

[a]Radiation is in W m^{-2}, and GEM Flux in ng m^{-2} h^{-1}.

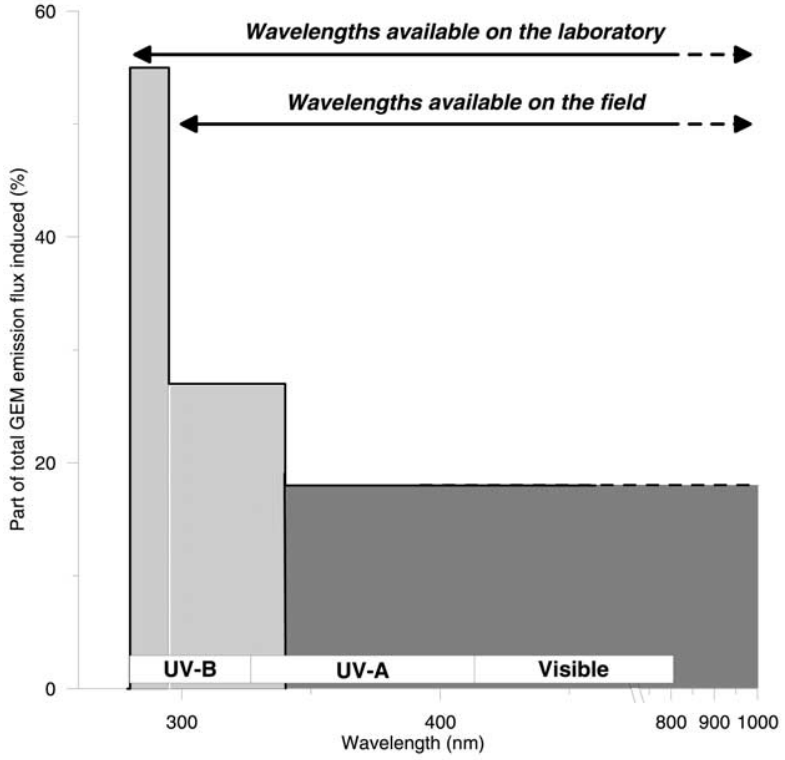

Figure 5. Schematic representation of the proportion of GEM emission induced by three wavelength intervals: below 295 nm, from 295 to 340 nm, and above 340 nm. Total GEM flux represents 100%. UVB (280–320 nm), UVA (320–400 nm) and visible (400–800 nm) intervals are represented. Arrows indicate the wavelengths available in the field and in the laboratory respectively.

measured anymore at 20 cm, but at 40 cm depth. GEM represented at Col de Porte approximately 0.1% of the mercury content in the snowpack. This value is comparable to the mercury balance in the Arctic snowpack estimated at Ny Ålesund (Svalbard) [*Ferrari et al.*, 2005] where GEM represented less than 1% of mercury. Total mercury exhibited a concentration range from 80 ± 08 ng l^{-1} to 160 ± 15 ng l^{-1} in the Col de Porte snowpack (see Table 1). This result is in good agreement with data reported by *Ferrari et al.* [2002] who measured Hg_T in different alpine snowpacks, including the Col de Porte snowpack. They obtained Hg_T concentrations as high as 130 ng l^{-1}. Such high concentrations of total mercury could be linked to anthropogenic influences and the proximity of a large urban area. Reactive mercury remained below the detection limit (0.2 ng l^{-1}) at all depths in the Col de Porte snowpack. *Ferrari et al.* [2002] measured Hg_R at the same location and also reported concentrations below their detection limit (which was about 0.8 ng l^{-1}). *Lalonde et al.* [2003] quantified Hg_R concentrations on a remote and temperate area in north-western Ontario (Canada) by gas-phase atomic fluorescence spectrometry with a detection limit of about 0.04 ng l^{-1}. They showed that 40% of Hg_R deposited during snow fall events were lost within 24 h due to reduction processes, with concentrations decreasing from ∼1.4 ± 0.5 ng l^{-1} to ∼0.8 ± 0.3 ng l^{-1}. Furthermore, measuring Hg_R in old snow layers, they obtained concentrations as low as 0.2 ± 0.1 ng l^{-1}. The concentrations we measured at Col de Porte are consistent with these data. Because the snow collected for Hg_R analysis was 10 days old, we assume that Hg_R previously deposited during wet events was completely lost. *Lalonde et al.* [2003] report that UVB-initiated Hg(II) reduction could lead to a net snow-to-air transfer of mercury. Our field and lab flux measurement support the hypothesis that Hg_R could be transformed after deposition. Production of GEM in the SIA was observed every day during our field work, and results obtained using our laboratory flux chamber suggest that UV radiation plays a key role in GEM emission from the snowpack (for more details see Section 4.4). Another option is that wet deposition could have been largely depleted in reactive mercury. Past studies on mercury speciation in clouds carried out at the site of Puy de Dome, 300 km from the area investigated, gave concentrations of about 10 to 50 ng l^{-1} for Hg_T and about 0.8 to 3.5 ng l^{-1} for Hg_R [*Gauchard et al.*, 2003]. Some recent research works also suggest that bacteria and microorganisms could interact with Hg_R in the snowpack [*Amato et al.*, 2007]. Possibly, the low measured Hg_R concentrations may be a combination of both minor wet deposition during snow fall episodes and destruction of reactive mercury complexes in the snowpack partially due to active photoreduction mechanisms that are discussed in Section 4.3.

4.3. The Alpine Snowpack, a Source of GEM

4.3.1. Irradiation and GEM Production

[28] Both destruction and production of GEM were observed in the SIA in polar areas [*Dommergue et al.*,

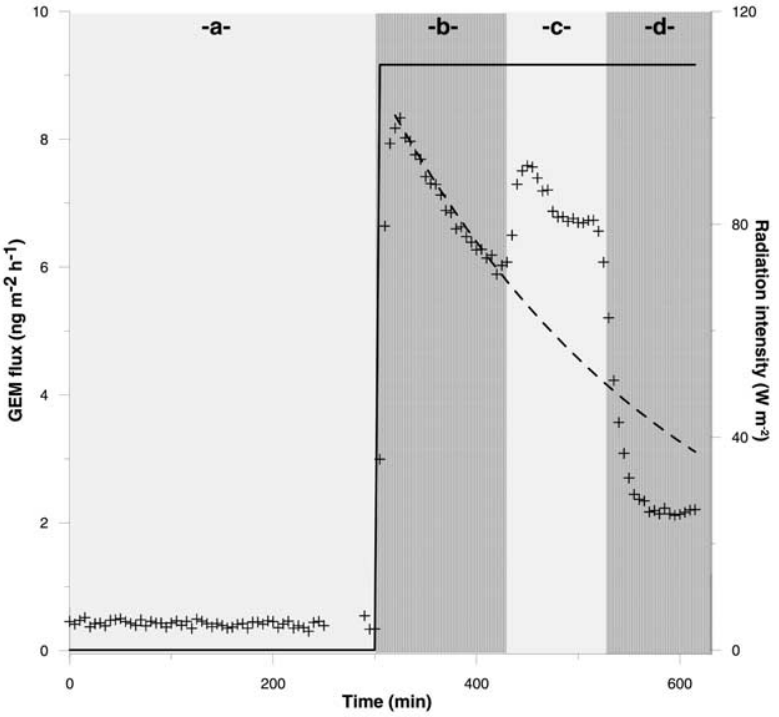

Figure 6. Variation of GEM flux (ng m^{-2} h^{-1}) with time measured in the laboratory flux chamber. Phase a reports dark flux at −4°C. During phase b, c and d, total irradiation was 120 W m^{-2} with wavelengths above 295 nm. Temperature in the chamber was kept at −4°C during phase b, and then increased to +1.5°C during phase c and d.

2003c; *Ferrari et al.*, 2004b]. In the arctic snowpack, GEM oxidation probably competes with Hg(II) reduction, and the SIA can exhibit GEM concentrations lower or higher than atmospheric levels. At Col de Porte, all the data collected during March 2005 from the surface to the bottom of the snowpack were above the atmospheric background (1.8 ng m^{-3}). Our results showed GEM production, but did not indicate the occurrence of GEM oxidation. GEM concentrations in the SIA and GEM emission from the snow surface at Col de Porte showed a diurnal pattern well correlated with solar irradiation as reported in Figures 3 and 5. These observations suggested that GEM production is driven by photolytic mechanisms. Previous studies have pointed out the role of irradiation in GEM production in the SIA [*Xiao et al.*, 1994; *Lalonde et al.*, 2002; *Dommergue et al.*, 2003c], and we observed at Col de Porte simultaneous increases of irradiation and GEM concentration at 20 cm depth (see Figure 2). A recent study showed that warmer, wetter and midlatitude snowpack are more transparent to UV radiation than dry and cold snowpacks from the high Arctic [*Fisher et al.*, 2005]. They also suggest that most of the photochemical reactions (85%) occur in the top 15–60 cm of the snowpack. Our alpine snowpack is warm around −2°C. We thus expect that photochemical reactions will occur from the surface to 40 cm depth. Deeper in the snowpack, as reported at 80 cm depth in Figure 2, a delay appears between the increase of GEM concentration and solar irradiation. Diffusion of GEM from the upper layer is therefore assumed to explain daily GEM variations in the bottom layers of the snowpack. The production of GEM at the surface of the snowpack could be the result of direct photodissociation of Hg(II) complexes, e.g., hydroxo or chlorocomplexes. *Ferrari et al.* [2002] showed that these complexes represent the predominant mercury species in the alpine snowpack. These reduction mechanisms were observed in water solutions [*Xiao et al.*, 1994] and suggested to occur in snow [*Lalonde et al.*, 2002, 2003]. However, GEM could also be produced by the reduction of Hg(II) complexes by photochemically produced compounds: hydroperoxyl radical (HO_2) was proposed as a potential reductant of Hg(II) in the snow [*Lin and Pehkonen*, 1999]. However, this hypothesis has to be considered carefully, since a recent study based on thermodynamical considerations showed that reduction of Hg(II) to GEM by HO_2 radicals should be of minor importance [*Gardfeldt and Jonsson*, 2003]. Moreover, even if we were not able to measure GEM in the SIA during the night, we noticed higher concentrations than atmospheric ones in the whole snowpack and especially in the surface layers (see Figure 2 with 2.6 ng m^{-3} at 20 cm depth and 3.4 ng m^{-3} at 40 cm depth before 6:30 am) at sunrise. It suggests that the reduction of Hg(II) could also be possible in the dark. This production of GEM in the dark has also been reported in snow samples collected in a midlatitude snowpack [*Lalonde et al.*, 2003] and inside an arctic snowpack [*Ferrari et al.*, 2004b].

4.3.2. Influence of Liquid Water in the Snowpack

[29] An increase of the snow temperature can affect GEM production in the alpine snowpack. We observed a significant increase of GEM concentrations in the snowpack

when the snow was melting as displayed in Figure 3. The link between snow temperature and GEM production has been reported for an arctic snowpack in Ny Ålesund, Svalbard [*Ferrari et al.*, 2005]. *Dommergue et al.* [2003b] measured peak GEM emission fluxes around 25 ng m^{-2} h^{-1} at Kuujjuarapik (Quebec, Canada) during the first day of snowmelt. *Lalonde et al.* [2003] observed significant photoreduction of Hg(II) complexes during snowmelt at temperate latitudes. Liquid water in the snowpack could enhance GEM production. The increase of snow temperature leads to an increase of the thickness of the water films around snow grains. This liquid layer is an active chemical reactor around snow grains [*Takenaka et al.*, 1992]. *Bales et al.* [1990] showed that ionic species accumulated during snow precipitation and finally concentrated in snow grains could be released in the earliest fraction of meltwater. This ionic pulse could also affect Hg(II) complexes. Reduction reactions could take place in the aqueous phase with enhanced reaction rates [*Xiao et al.*, 1994]. They showed that mercury complexes are efficiently photodissociated in aqueous solutions. Such photodissociation reactions may occur in snow [*Lalonde et al.*, 2002, 2003] and could be enhanced during snowmelt by the presence of liquid water in the snowpack.

4.3.3. GEM Fluxes From the Snowpack to the Atmosphere

[30] GEM emission fluxes measured at Col de Porte are quite close to fluxes reported for arctic and sub-arctic snowpacks if we do not consider large emissions measured immediately after AMDEs [*Dommergue et al.*, 2003c; *Schroeder et al.*, 2003; *Ferrari et al.*, 2005; *Brooks et al.*, 2006]. GEM fluxes from the snowpack to the atmosphere exhibited a diel pattern correlated with solar radiation for the whole period of the study (see Figure 4). These results confirm that GEM production in the snowpack is mainly due to photochemical mechanisms. Some measurements of GEM concentrations in the SIA before sunrise suggested dark production of GEM at night. Such dark production did not induce any detectable emission flux from the snow surface.

4.4. Modeling of Field Observations Using Laboratory Measurements

[31] Temperature in the snowpack and solar radiation were identified in the field to be the main environmental parameters driving GEM production in the SIA. Laboratory investigations with a flux chamber confirmed these observations, and enable a better simulation of GEM production processes.

4.4.1. Effect of Irradiation

[32] As reported in Table 3, there is a linear relationship between the GEM flux and the radiation intensity over different spectral ranges. These results support the hypothesis that the reemission of GEM from snowpacks is mostly driven by solar radiation. We calculated GEM emission ratios from our irradiation experiments with UVA, UVB and visible light. All ratios were independent of the radiation intensity. It is therefore concluded that UVA (320–400 nm) could induce GEM production, whereas UVB (280–320 nm) is the most efficient spectral band for GEM production. When the snow was exposed to light with unfiltered light (providing some UV wavelengths which are not available at the Earth's surface), the fluxes measured were twice as high as those measured with a spectrum available at the Earth's surface. However, one must notice that the use of a filter reduced the intensity of irradiation of about 10% over the entire spectrum. As we used GEM-free air at the inlet of the chamber, we were not representative of the atmospheric GEM background of ~1.8 ng m^{-3}. We artificially created high gradients between the SIA and the air above the snow surface in the laboratory. The GEM concentration at which no exchange occurs between the snow surface and the chamber is termed the compensation point [*Hanson et al.*, 1995]. This compensation point increased with radiation considering snow samples from Col de Porte. We obtained surprisingly a good agreement between field and laboratory flux data for high radiation values. For radiation of ~80 W m^{-2}, laboratory measurements gave a flux of ~4 ng m^{-2} h^{-1} using a cut-off of 295 nm (this filter enable to reproduce natural light radiation under clear sky conditions). This value is close to the fluxes measured in the field at midday (see Figure 4). However, considering low radiation values, the light induced fluxes measured in the laboratory were significantly higher than these obtained in the field. We assumed that the compensation point was high compared to 1.8 ng m^{-3} at ~80 W m^{-2}, but between 0 and 1.8 ng m^{-3} in dark conditions. Finally, the GEM flux observed in the darkness had no relevance to natural conditions. The laboratory measurements did not allow us to explain GEM chemistry in the Col de Porte snowpack at night.

4.4.2. Kinetic Considerations

[33] With constant radiation and temperature (phase b, Figure 6), the GEM flux decreased exponentially indicating a pseudo first order reaction. Without any filter the decay of the flux was given by:

$$F = 15.4 \times \exp(-0.185 \times t), \left(r^2 = 0.97, n = 41\right), \text{ in ng } m^{-2}h^{-1}$$

[34] The dashed line on Figure 6 indicates the expected decay of the flux with a cut off of 295 nm. This decay could be described by the following equation:

$$y = 6.5 \times \exp(-0.238 \times t), \left(r^2 = 0.98, n = 16\right)$$

[35] These data imply that 95% of the Hg(II) available for photoreduction was reduced within 16.2 h (filter 295 nm) and 12.6 h (no filter) respectively. It is noteworthy that the flux decreased with different time constants for the different spectral ranges. With a cut off of 295 nm, the kinetic constant was ~0.238 h^{-1}. The corresponding lifetime was ~4 h. This value could be compared to previous studies. It was lower than the photolysis rate constant of $Hg(OH)_2$ in aqueous phase given by *Xiao et al.* [1994], who found a value of ~0.432 h^{-1}. For freshwaters exposed to light, *Zhang and Lindberg* [2001] determined rate constants between ~0.1 and 0.3 h^{-1} for GEM production.

[36] As the penetration of UVB radiation into snowpacks is limited to the top layers of the snow [*Fisher et al.*, 2005], we also assessed the effect of mechanical disturbance of the top snow stratification on the light induced emission of mercury. A snow sample was exposed to light (cut off of 295 nm) for 3 h. Then the radiation was stopped and the

surface of the snow (~1 cm) was mechanically disturbed with a stainless steel spatula and afterward the radiation was continued for one additional hour. At the beginning of the experiment, we observed a flux of 6.1 ng m^{-2} h^{-1} which decreased to 3.5 ng m^{-2} h^{-1} after 3 h and recovered to 4.9 ng m^{-2} h^{-1}. Even if the flux did not completely recover, this data clearly show that mechanical or physical disturbance at the snow surface, e.g., due to melting, may recharge the mercury pool at the snow surface available for photoreduction.

4.4.3. The Role of Temperature and Liquid Water

[37] Phase c in Figure 6 shows the influence of the temperature in the snowpack on GEM production. When liquid water appeared in the snowpack, GEM emission flux rapidly increased to 7.7 ng.m^{-2}.h^{-1}, and then stabilized at ~7 ng m^{-2} h^{-1}. As discussed before, we assume that liquid layers around snow grains could act as a chemical reactor, concentrating ionic species. A large exchange area between water and the SIA, and higher kinetic rates in the aqueous phase could explain the higher fluxes. This hypothesis is further supported by the rapid decrease reported in phase d. When the snow has melted almost entirely, the exchange surface between water and air suddenly decreased, and all the ionic species, which were previously concentrated in a thin water film, were now diluted in a large volume of water. These preliminary results show that the fate of mercury during snowmelt could be a rapid reduction of Hg_R complexes in the snowpack followed by an emission of GEM to the atmosphere. However, Hg_R complexes could also be transferred to the meltwater where exchange with the atmosphere is much more limited. Hence mercury could become available for accumulation in ecosystems.

4.5. Fate of Mercury Species During Snowmelt

[38] *Dommergue et al.* [2003b] reported total mercury concentrations of about ~22.5 ng l^{-1} in surface snow and ~10.0 ng l^{-1} in meltwater samples at Kuujjuarapik (Quebec, Canada). At Col de Porte we measured concentrations almost one order of magnitude higher, with ~160 ng l^{-1} in surface snow and 79 ± 1, 63 ± 3 and 74 ± 2 ng l^{-1} in three meltwater samples. We obtained the same ratio between surface snow and meltwater concentrations at Col de Porte than at Kuujjuarapik, Quebec [2003c]. These preliminary results are of prime importance as they suggest that an important release of mercury could occur at springtime during snowmelt. Mercury levels in alpine meltwater are considerably higher than concentrations of ~1–7 ng l^{-1} reported for non-polluted river water [*Poissant*, 2002]. Further studies addressing the vulnerability and contamination of alpine ecosystems are needed, even if this release of mercury could occur in a limited period of the year.

5. Conclusion

[39] The present study reported GEM production and the exchange fluxes between the snowpack and the atmosphere in an alpine snowpack during snowmelt in spring 2005. Concentration of Hg_R was below detection limit and GEM in interstitial air represented less than 1% of the mercury in snowpack layers. The exchanges of GEM between the snowpack and the atmosphere were mostly driven by Hg(II) reduction during daytime, with mean integrated emissions from 5.64 to 12.20 ng m^{-2} d^{-1}. We demonstrated that liquid water in the snowpack enhanced GEM production. Irradiation and snow temperature played a key role in internal photoproduction of GEM, most likely by increasing the liquid layers at the surface of snow grains. These results were validated by laboratory flux chamber measurements: we were able to quantify the role of irradiation on GEM production.

[40] Rapid depletion of GEM has been observed in arctic snowpacks [*Dommergue et al.*, 2003c; *Ferrari et al.*, 2004b]. Halogen compounds such as bromine radicals were proposed to explain the involved oxidation processes [*Ariya et al.*, 2004; *Goodsite and Plane*, 2004]. Our results in the French Alps are in good agreement with this hypothesis: the alpine atmosphere, and thus the alpine snowpack, are poor in halogen compounds and no important GEM depletion could be observed neither in the atmosphere nor in the SIA.

[41] Preliminary studies of meltwater indicated higher levels of Hg as compared to non-polluted waters. Further studies are needed to better assess the fate of mercury during snowmelt in temperate areas as it could negatively affect drinking water quality.

[42] **Acknowledgments.** This research was funded by A.D.E.M.E. (Agence de l'Environnement et de la Maitrise de l'Energie, Programs 0162020 and 0462C0108) and the French PNCA program "Echanges Neige Polaire". We would like to thank the French Ministry of Research for its financial support of young scientists (so called A.C.I. JC 3012). Claude Boutron and Christophe Ferrari thank the Institut Universitaire de France (I.U.F.) for its financial help for this study. We thank Meteo-France and CEN staff for giving us the opportunity to work at the Col de Porte station, and for providing us meteorological data. We thank Florent Dominé for measuring the physical properties of the snowpack, and for his helpful comments concerning the snow characteristics.

References

Albert, M. R., and E. F. Shultz (2002), Snow and firn properties and air-snow transport processes at Summit, Greenland, *Atmos. Environ.*, *36*(15–16), 2789–2797.

Albert, M. R., A. M. Grannas, J. Bottenheim, P. B. Shepson, and F. E. Perron Jr. (2002), Processes and properties of snow-air transfer in the high arctic with application to interstitial ozone at Alert, Canada, *Atmos. Environ.*, *36*, 2779–2787.

Amato, P., R. Hennebelle, O. Magand, M. Sancelme, A. M. Delort, C. Barbante, C. Boutron, and C. Ferrari (2007), Bacterial characterization of the snowcover at Spitzberg, Svalbard, *FEMS Microbiol. Ecol.*, *59*(2), 242–254.

Ariya, P. A., et al. (2004), The Artic, a sink for mercury, *Tellus*, *56B*, 397–403.

Bales, R. C., R. Sommerfel, and D. Kebler (1990), Ionic tracer movement through a Wyoming snowpack, *Atmos. Environ.*, *24*, 2749–2758.

Bales, R. C., M. V. Losleben, J. R. McConnell, K. Fuhrer, and A. Neftet (1995), H_2O_2 in snow, air and open pore space in firn at Summit, Greenland, *Geophys. Res. Lett.*, *22*(10), 1261–1264.

Balhmann, E., R. Ebinghaus, and W. Ruck (2006), Development and application of a laboratory flux measurement system (LFMS) for the investigation of the kinetics of mercury emissions from soils, *J. Environ. Monit.*, *81*, 114–125.

Blais, J. M., S. Charpentié, F. Pick, L. E. Kimpe, A. St Amand, and C. Regnault-Roger (2005), Mercury, polybrominated diphenyl ether, organochlorine pesticide, and polychlorinated biphenyl concentrations in fish from lakes along an elevation transect in the French Pyrénées, *Ecotoxicol. Environ. Saf.*, *63*(1), 91–99.

Boutron, C. F. (1990), A clean laboratory for ultra-low concentration heavy metal analysis, *J. Anal. Chem.*, *337*, 482–491.

Brooks, S., A. Saiz-Lopez, H. Skov, S. Lindberg, J. M. C. Plane, and M. Goodsite (2006), The mass balance of mercury in the springtime arctic environment, *Geophys. Res. Lett.*, *33*, L13812, doi:10.1029/2005GL025525.

Dommergue, A., C. P. Ferrari, F. Planchon, and C. F. Boutron (2002), Influence of anthropogenic sources on total gaseous mercury variability in Grenoble suburban air (France), *Sci. Total Environ.*, *297*, 203–213.

Dommergue, A., C. P. Ferrari, and C. F. Boutron (2003a), First investigation of an original device dedicated to the determination of gaseous mercury in interstitial air in snow, *Anal. Bioanal. Chem.*, *375*, 106–111.

Dommergue, A., C. P. Ferrari, P.-A. Gauchard, C. F. Boutron, L. Poissant, M. Pilote, F. Adams, and P. Jitaru (2003b), The fate of mercury species in a sub-arctic snowpack during the snowmelt, *Geophys. Res. Lett.*, *30*(12), 1621, doi:10.1029/2003GL017308.

Dommergue, A., C. P. Ferrari, L. Poissant, P.-A. Gauchard, and C. F. Boutron (2003c), Diurnal cycles of gaseous mercury within the snowpack at Kuujjuarapik/Whapmagoostui, Québec, Canada, *Environ. Sci. Technol.*, *37*(15), 3289–3297.

Dommergue, A., E. Balhmann, R. Ebinghaus, C. Ferrari, and C. Boutron (2007), Laboratory simulation of Hg° emissions from a snowpack, *Anal. Bioanal. Chem.*, doi:10.1007/s00216-007-1186-2.

Ebinghaus, R., H. H. Kock, C. Temme, J. W. Einax, A. G. Löwe, A. Richter, J. P. Burrows, and W. H. Schroeder (2002), Antarctic springtime depletion of atmospheric mercury, *Environ. Sci. Technol.*, *36*(6), 1238–1244.

Engle, M. A., M. S. Gustin, and H. Zhang (2001), Quantifying natural source mercury emissions from Ivanhoe Mining Destrict, north-central Nevada, USA, *Atmos. Environ.*, *35*, 3987–3997.

EPA (1998), Method 7473: Mercury in solids and solutions by thermal decomposition, amalgamation, and atomic absorption spectrophotometry, pp. 36.

Ferrari, C. P., A. L. Moreau, and C. F. Boutron (2000), Clean conditions for the determination of ultra-low levels of mercury in ice and snow samples, *J. Anal. Chem.*, *366*, 433–437.

Ferrari, C. P., A. Dommergue, A. Veysseyre, F. A. M. Planchon, and C. F. Boutron (2002), Mercury speciation in the French seasonal snow cover, *Sci. Total Environ.*, *287*(1–2), 61–69.

Ferrari, C. P., A. Dommergue, and C. F. Boutron (2004a), Profiles of Mercury in the snow pack at Station Nord, Greenland shortly after polar sunrise, *Geophys. Res. Lett.*, *31*, L03401, doi:10.1029/2003GL018961.

Ferrari, C. P., A. Dommergue, H. Skov, M. Goodsite, and C. F. Boutron (2004b), Nighttime production of elemental gaseous mercury in interstitial air of snow at Station Nord, Greenland, *Atmos. Environ.*, *38*, 2727–2735.

Ferrari, C., et al. (2005), Snow-to-air exchanges of mercury in an Arctic seasonal snow pack in Ny-Alesund, Svalbard, *Atmos. Environ.*, *39*, 7633–7645.

Fisher, F. N., M. D. King, and J. Lee-Taylor (2005), Extinction of UV-visible radiation in wet midlatitude (maritime) snow: Implications for increased NOx emission, *J. Geophys. Res.*, *110*, D21301, doi:10.1029/2005JD005963.

Fritsche, J., D. Obrist, and C. Alewell (2006), Evidence of microbial control of Hg^0 emissions from uncontaminated terrestrial soils, *submitted to J. Plant Nutr. Soil Sci.*

Gardfeldt, K., and M. Jonsson (2003), Is bimolecular reduction of Hg(II) complexes possible in aqueous systems of environmental importance, *J. Phys. Chem.*, *107*, 4478–4482.

Gauchard, P.-A., A. Dommergue, C. P. Ferrari, L. Poissant, and C. Boutron (2003), Mercury speciation into tropospheric clouds, in *VIIth International Conference on Mercury as a Global Pollutant*, pp. 1577, RMZ-Materials and Geoenvironment, Ljubljana, Slovenia.

Goodsite, M. E., and J. M. C. Plane (2004), A Theoretical study of the oxidation of Hg° to $HgBr_2$ in the Troposphere, *Environ. Sci. Technol.*, *38*, 1772–1776.

Hanson, P. J., S. Lindberg, T. Tabberer, J. Owens, and K.-H. Kim (1995), Foliar exchange of mercury vapor: Evidence for a compensation point, *Water, Air, Soil Pollut.*, *80*, 373–382.

Honrath, R. E., Y. Lu, M. C. Peterson, J. E. Dibb, M. A. Arsenault, N. J. Cullen, and K. Steffen (2002), Vertical fuxes of NO_x; HONO, and HNO_3 above the snowpack at Summit, Greenland, *Atmos. Environ.*, *36*, 2629–2640.

Lalonde, J. D., A. J. Poulain, and M. Amyot (2002), The role of mercury redox reactions in snow on snow-to-air mercury transfer, *Environ. Sci. Technol.*, *36*(2), 174–178.

Lalonde, J. D., M. Amyot, M.-R. Doyon, and J.-C. Auclair (2003), Photo-induced Hg(II) reduction in snow from the remote and temperate Experimental Lake Area (Ontario, Canada), *J. Geophys. Res.*, *108*(D6), 4200, doi:10.1029/2001JD001534.

Lamborg, C. H., W. F. Fitzgerald, J. O'Donnell, and T. Torgersen (2002), A nonsteady-state compartmental model of global-scale mercury biogeochemistry with interhemispheric atmospheric gradients, *Geochim. Cosmochim. Acta*, *66*, 1105–1118.

Lin, C.-J., and S. O. Pehkonen (1999), The chemistry of atmospheric mercury: A review, *Atmos. Environ.*, *33*, 2067–2079.

Lindberg, S. E., S. Brooks, C.-J. Lin, K. J. Scott, M. S. Landis, R. K. Stevens, M. Goodsite, and A. Richter (2002), Dynamic oxidation of gaseous mercury in the Arctic troposphere at polar sunrise, *Environ. Sci. Technol.*, *36*(6), 1245–1256.

Lindqvist, O., and H. Rodhe (1985), Atmospheric mercury - A review, *Tellus*, *37B*, 136–159.

Obrist, D., M. S. Gustin, J. A. Arnone, D. W. Johnson, D. E. Schorran, and P. S. J. Verburg (2005), Measurements of gaseous elemental mercury fluxes over intact tallgrass prairie monoliths during one full year, *Atmos. Environ.*, *39*, 957–965.

Obrist, D., F. Conen, R. Vogt, R. Siegwolf, and C. Alewell (2006), Estimation of Hg° exchange between ecosystems and the atmosphere using 222Rn and Hg° concentration changes in the stable nocturnal boundary layer, *Atmos. Environ.*, *40*, 856–866.

Pacyna, J. M., and G. J. Keeler (1995), Sources of mercury in the Arctic, *Water, Air, Soil Pollut.*, *80*, 621–632.

Pacyna, E. G., J. M. Pacyna, and N. Pirrone (2001), European emissions of atmospheric mercury from anthropogenic sources in 1995, *Atmos. Environ.*, *35*(17), 2987–2996.

Petersen, G., R. Bloxam, S. Wong, J. Munthe, O. Krüger, S. R. Schmolke, and A. Vinod Kumar (2001), A comprehensive Eulerian modelling framework for airborne mercury species: model development and applications in Europe, *Atmos. Environ.*, *35*(17), 3063–3074.

Poissant, L. (2002), Mercury surface-atmosphere gas exchange in Lake Ontario/St. Lawrence river ecosystem, *Revue des Sciences de l'Eau*, *15*, 229–239.

Pyle, D. M., and T. A. Mather (2003), The importance of volcanic emissions for the global atmospheric mercury cycle, *Atmos. Environ.*, *37*, 5115–5124.

Roos-Barraclough, F., N. Givelet, A. Martinez-Cortizas, M. E. Goodsite, H. Biester, and W. Shotyk (2002), An analytical protocol for the determination of total mercury concentrations in solid peat samples, *Sci. Total Environ.*, *292*, 129–139.

Schroeder, W. H., and J. Munthe (1998), Atmospheric mercury - An overview, *Atmos. Environ.*, *32*(5), 809–822.

Schroeder, W. H., G. Keeler, H. Kock, P. Roussel, D. Schneeberger, and F. Schaedlich (1995), International field intercomparison of atmospheric mercury measurement methods, *Water, Air, Soil Pollut.*, *80*, 611–620.

Schroeder, W. H., A. Steffen, K. Scott, T. Bender, E. Prestbo, R. Ebinghaus, J. Y. Lu, and S. E. Lindberg (2003), Summary report: First international Arctic atmospheric mercury research workshop, *Atmos. Environ.*, *37*(18), 2551–2555.

Slemr, F., and H. E. Scheel (1998), Trends in atmospheric mercury concentrations at the summit of the Wank mountain, southern Germany, *Atmos. Environ.*, *32*(5), 845–853.

Slemr, F., E. G. Brunke, R. Ebinghaus, C. Temme, J. Munthe, I. Wangberg, B. Schroeder, A. Steffen, and T. Berg (2003), Worldwide trend of atmospheric mercury since 1977, *Geophys. Res. Lett.*, *30*(10), 1516, doi:10.1029/2003GL016954.

Steffen, A., W. H. Schroeder, J. Bottenheim, J. Narayana, and J. D. Fuentes (2002), Atmospheric mercury concentrations: Measurements and profiles near snow and ice surfaces in the Canadian Arctic during Alert 2000, *Atmos. Environ.*, *36*(15–16), 2653–2661.

Sumner, A. L., and P. B. Shepson (1999), Snowpack production of formaldehyde and its effect on the Arctic troposphere, *Nature*, *398*, 230–233.

Takenaka, N., A. Ueda, and Y. Maeda (1992), Acceleration of the rate of nitrite oxidation by freezing in aqueous solution, *Nature*, *358*, 736–738.

Xiao, Z. F., J. Munthe, D. Strömberg, and O. Lindqvist (1994), Photocemical behavior of inorganic mercury compounds in aqueous solution, in *Mercury as a Global Pollutant - Integration and Synthesis*, edited by C. J. Watras and J. W. Huckabee, pp. 581–592, Lewis Publishers, Boca Raton.

Zhang, H., and S. E. Lindberg (2001), Sunlight and Iron(III)-induced photochemical production of dissolved gaseous mercury in freshwater, *Environ. Sci. Technol.*, *35*, 928–935.

E. Bahlmann, C. Boutron, A. Dommergue, X. Faïn, C. P. Ferrari, and S. Grangeon, Laboratoire de Glaciologie et Géophysique de l'Environnement (UMR 5183 CNRS/Université Joseph Fourier), 54, rue Molière, B.P. 96, 38402 St Martin d'Heres cedex, France. (fain@lgge.obs.ujf-grenoble.fr)

C. Barbante, W. Cairns, and P. Cescon, Environmental Sciences Department, University of Venice, Calle Larga S. Marta, 2137, I-30123 Venice, Italy.

R. Ebinghaus, Institute for Coastal Research, GKSS Research Centre, Max-Planck-Street 1, D-21502 Geesthacht, Germany.

J. Fritsche, Institute of Environmental Geosciences, University of Basel, Bernoullistrasse 30, 4056 Basel, Switzerland.

D. Obrist, Desert Research Institute, Division of Atmospheric Sciences, 2215 Raggio Parkway, Reno, NV 89512, USA.

Chapter 6

Effect of grass cover on Hg^0 exchange – some preliminary results

6.1 Objective

Our estimations of the GEM (gaseous elemental mercury) flux of alpine grasslands described in Chapters 2 to 4 have revealed some ambiguous results. With our flux measurements in the field we came to the conclusion, that temperate grasslands are net sinks for atmospheric GEM. On the other hand, our laboratory incubation experiments with soils from the Fruebuel site yielded net emission of GEM (see Chapter 2). This ambiguity is in line with previous studies, which have confirmed that the GEM exchange in natural ecosystems is still unclear and controversial (Rasmussen, 1994; Fitzgerald et al., 1998; Gustin et al., 2003). For example, some earlier studies suggested that vegetation had the ability to "transpire" mercury by release through foliage (e.g. Siegel & Siegel, 1988). However, the reverse potential of plants to accumulate atmospheric GEM in foliage has also been documented by a number of researchers (e.g. Lindberg et al., 1979; Bacci et al., 2000). The first year-long study to continuously measure atmospheric GEM exchange in a vegetated prairie ecosystem indicated net mercury emissions during warm and active vegetation periods and net mercury uptake during colder seasons, but a clear net loss over the entire year (Obrist et al., 2005). Measurements over temperate forests (Lindberg et al., 1998) and a wetland ecosystem in the Everglades (Lindberg et al. 2002) also indicate substantial mercury emissions during warm seasons.

In order to investigate the role of microbiologically mediated mercury volatilisation, the incubation experiments described in Chapter 2 were performed with bare soil samples that had the uppermost soil layer removed. We hypothesise that the inconsistency between field measurements and laboratory incubations mentioned above is explained by the absence of a vegetation cover that interferes with the mercury exchange between soil and atmosphere. Plants might influence the GEM exchange through their respiration processes, their ability to intercept mercury from the atmosphere and their influence on chemical processes in the rizosphere. By comparing GEM emissions of vegetated with bare soils a missing link in the exchange processes

of terrestrial ecosystems might be explained.

6.2 Experimental

To investigate the effect of plants on the exchange of GEM, fluxes over vegetated and bare soil samples were measured with the same method as described in Chapter 2, but larger incubation chambers were used and the experiment was set up in a temperature controlled climate chamber that allowed the handling of bigger soil samples (see Fig. 6.1).

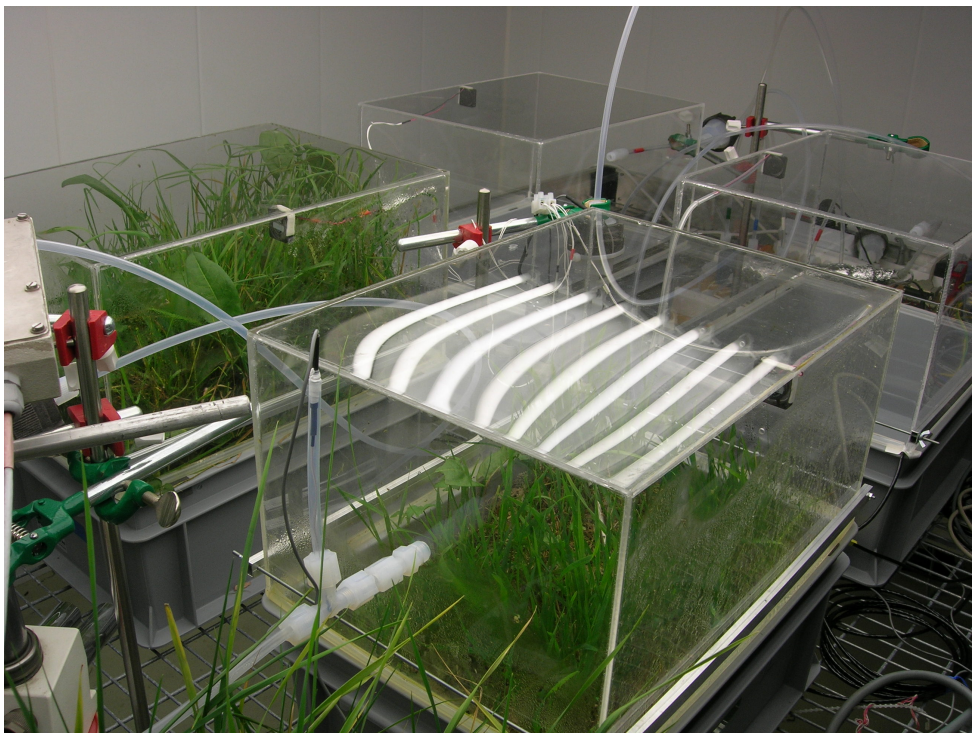

Figure 6.1: Experimental setup of incubation chambers in the temperature controlled climate chamber

Eight soil monoliths in the size of 26.5 × 67.5 × 15.0 cm were cut with their original vegetation cover from the Fruebuel site and directly transferred to the laboratory (details of the site see Chapter 3). Two samples were placed in polypropylene containers, covered with translucent lids made of polycarbonate (Plexiglas sunactive®, Radon GmbH, Laubach, Germany) and put on a sample tray together with an empty container as a blank and one filled with deionised water (Milli-Q®; "water-blank"). The latter was used to isolate any interactions of atmospheric mercury with the water saturated atmosphere.

The lids of all containers were equipped with fans (flowrate 32 l min^{-1}) to generate gentle turbulence within the chambers. A night-day cycle was simulated by using a set of 20 neon tubes (OSRAM FQ 80W/840 Lumilux plus Cool White) with a power of 80 W each, switching on and off every 12 hours. At the level of the sample surface

		Mean[a]	Standard deviation[a]
Soil			
Mass of soil samples	[g]	8256	687
Soil type	-	Cambisol	-
Soil texture	-	Loamy silt	-
pH	-	4.5	0.1
Soil water content	%	27.1	1.8
Hg_{tot} soil	[ng g^{-1}]	91.8	20.4
C_{org}	%	5.6	1.1
Clay fraction	%	23.3	2.7
Bulk density	[g cm^{-3}]	0.74	0.04
Fraction <2 mm	%	97.5	1.7
Effective cation exchange capacity	[μmol_c g^{-1}]	94.5	6.4
Total acidity	[μmol_c g^{-1}]	33.1	1.1
Base saturation	%	64.7	2.6
Available field capacity	%	25.6	1.8
Field capacity	%	41.8	2.1
Air capacity	%	11.0	0
Pore volume	%	53	2
Vegetation			
Mass of clipped green grass	[g]	100.3	12.8
Leaf area of clipped green grass	[cm^2]	3376	889
Hg_{tot} grass	[ng g^{-1}]	14.0	1.0

[a]N=8

Table 6.1: Properties of investigated soil samples

with the lids installed this generated an irradiation of 20 W m^{-2} in the longwave and 90 W m^{-2} in the shortwave spectrum (without the lids the respective values were 80 W m^{-2} and 90 W m^{-2}). The temperature in the climate chamber was kept at constant 15°C.

The same instrumental setup with a Tekran 2537A Mercury Vapour Analyzer (Tekran Inc., Toronto, Canada) and a LI-6262 infrared gas analyser (LI-COR Inc., Lincoln, USA) was applied as described in Section 2.3.2. Carbon dioxide fluxes were determined as a measure of plant photosynthesis and respiration. The instruments were supplemented with soil temperature probes in each incubation chamber as well as air temperature probes at the inlet line and within the headspace of one soil sample. Additionally, the humidity in the climate chamber was recorded with a psychrometer. The soil water content was kept constant at the level of the sampling date (∼27%) by watering every 5 to 7 days with a water mixture of similar chemical composition to rain water falling at the Fruebuel site (tap water diluted with Milli-Q® in a ratio of 1:29).

The experiments were operated with flow rates between 1.5 and 7.4 l min^{-2}. Air-sampling was switched intermittently between the four containers and ambient air (inlet) every 10 minutes. While one line was analysed, the others were flushed to

maintain a steady flow through all samples. During the whole study the sampling lines were swapped twice between the containers to eliminate any line bias. Each sampling line was equipped with a 0.2 μm particle filter and a water trap to reduce the high humidity of the air drawn from the incubation chambers. Quality control and assurance procedures were the same as documented in Section 2.3.2.

A total of eight incubation runs with four sets of samples were performed. Each set consisted of two soil samples, one blank and one "water-blank". Upon the start of each run the fluxes of GEM and CO_2 were measured with the two fresh samples for 7 to 10 days. Next, the grass of one sample was clipped and the incubation continued until the plants re-grew to the initial height again ($\sim$14 days). Now, the grass of the other sample was clipped and the fluxes measured for another 14 to 21 days. Having completed this sequence the next set of samples was measured. Prior and after each manipulation the containers with the samples were weighted to gain the sample and vegetation masses as well as the soil water content.

6.3 Preliminary results

The incubation experiments described here were conducted under controlled laboratory conditions. However, during the study we realised that some factors were not adequately taken into consideration. First, despite a relatively high flow rate of up to 7.4 l min^{-1}, the humidity within the chambers was often very high, resulting in mouldering on the soil surface after about two weeks of incubation. Additionally, due to the high humidity it could not be ruled out that mercury amalgamation in the Tekran instrument was impaired. Second, the GEM concentration of the ambient air used for the study varied considerably (0.7 to 31 ng m^{-3}) and was thus nonrepresentative of background conditions. As a consequence the experiments were stopped after eight runs and will eventually be continued after the setup has been improved. Nonetheless, some preliminary results are presented below.

The properties of the soil samples from the Fruebuel site are listed in Tab. 6.1. Except for the Hg_{tot} content, which ranged from 71 to 113 ng g^{-1}, the soil properties of the samples were nearly identical. With an average Hg_{tot} concentration of 14 ng g^{-1}, the plants were less enriched in mercury than the soil.

As described in the previous section, the effect of vegetation on the GEM exchange was investigated by measuring the fluxes over vegetated and bare soil samples. Figures 6.2 and 6.3 illustrate this effect. The plots in Fig. 6.2 show the synchronised measurements of the CO_2 and GEM fluxes of six individual incubation runs. In the upper panels the shift of the CO_2 flux after the grass cut is clearly visible and the plot in the third panel confirms that the CO_2 uptake of the vegetated sample exceeds that of the bare sample (the diurnal cycle of the fluxes has been filtered out, which renders the CO_2 fluxes of the first three days positive).

A similar effect of the grass cut on the GEM exchange was not immediately visible. During all incubation runs with bare and vegetated samples, net deposition of GEM was measured, and the deposition increased linearly with the inlet GEM concentration

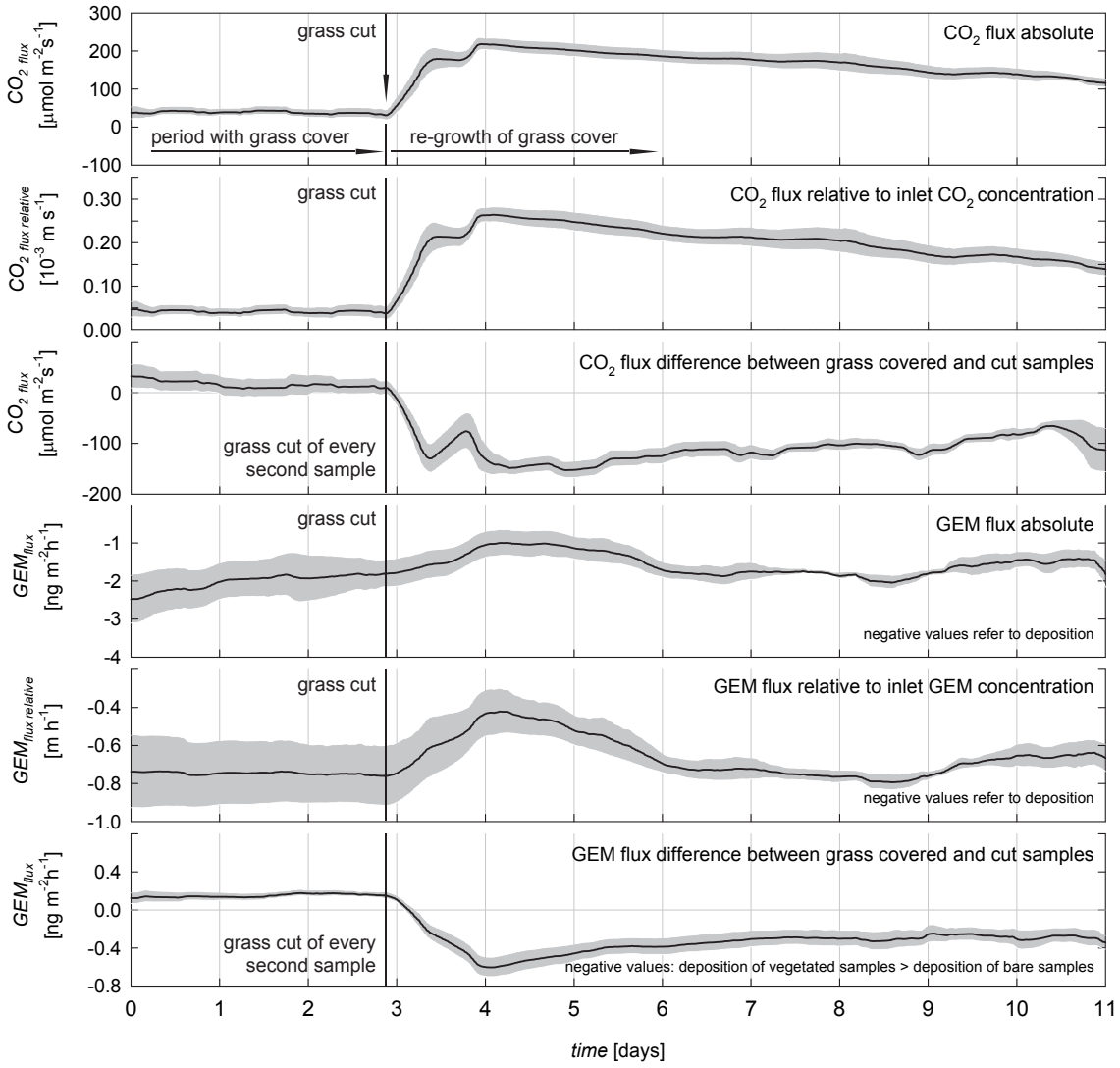

Figure 6.2: Fluxes of CO_2 and GEM measured during the incubation of bare and vegetated soil samples. Plots show the synchronised data of six incubation runs (the black line represents the mean, the shaded area the standard error). The diurnal signal has been removed with a 24 hour smoothing filter.

(see Fig. 6.3). Therefore, a change in GEM deposition was only visible when the flux data were computed relative to the inlet GEM concentration or as a difference between vegetated and bare soil samples as demonstrated in panel 5 and 6 of Fig. 6.2. The plots show that after the grass cut the GEM deposition was reduced within one day by 0.63 ng m^{-2} h^{-1} to 0.85 ng m^{-2} h^{-1} at an average inlet concentration of 1.98 ng m^{-3}. This reduction was reversed again within several days as vegetation sprouted and grew again.

Panel 6 in Fig. 6.2 shows, that the maximum difference in the GEM deposition rate between vegetated and bare samples was about 0.58 ng m^{-2} h^{-1}, with higher deposition rates recorded for the former. This value is also reflected in Fig. 6.3, where the

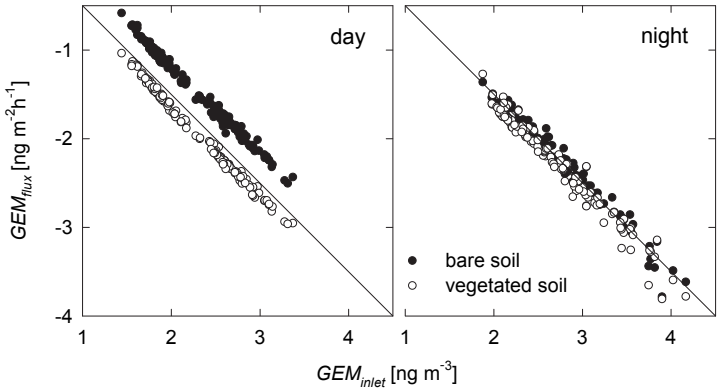

Figure 6.3: Comparison of GEM fluxes of a vegetated and a bare soil sample, separated by day and night. Data represent a 3-days period starting one day after grass cut. Negative values indicate deposition

fluxes of both samples are shown separately for dark and light conditions. The plots illustrate, that daytime fluxes are generally lower than night-time fluxes, as the points of the daytime plot are shifted to the upper left corner. This characteristic is likely to originate from the formation of a stable nocturnal boundary layer, which raises ambient GEM concentrations. The plots also show, that the GEM deposition flux of the vegetated sample was 0.33 ng m^{-2} h^{-1} higher during the day, but equalled the fluxes of the bare sample during the night. If follows, that the observed GEM deposition seems clearly linked to light irradiation. The temperature in the headspace of the samples was shifted by 6°C between day and night, but differed by less than 1°C between vegetated and bare samples. A temperature effect can therefore be excluded. We assume, that the smaller deposition to the bare sample during daytime is caused by photoreduction of Hg^{2+} species at the soil surface, which sets off some GEM deposition. However, it might also be plausible that deposition is reduced due to the lower humidity when plants are absent. This notion would support the results obtained in our field studies (Chapter 4), where GEM deposition seemed directly correlated to relative humidity. In conclusion, the vegetation cover seems to enhance GEM deposition and may therefore explain the discrepancy between our earlier soil incubation experiments and the field measurements. To address the involved processes in more detail, an improved experimental setup, that allows better control of the test parameters, will be required.

Final remarks and outlook

In this study various aspects of the Hg^0 exchange of uncontaminated grasslands have been addressed. With laboratory incubation experiments it was shown that soil microbiological activity plays a central role in the mercury exchange with the atmosphere (Chapter 2). Soils whose microbiological activity had been stimulated by temperature shifts, rewetting or previous, partial sterilisation exhibited pronounced Hg^0 emissions that lasted for several days. The processes responsible for this effect cannot be grasped yet, but seem to involve either direct reduction of Hg^{2+} by mercury tolerant communities or indirect transformation by microbially decomposed substances capable of Hg^{2+} reduction.

After these incubation studies Hg^0 fluxes were measured at two subalpine and one lowland grasslands in Switzerland and Austria (Chapters 3 and 4). It was demonstrated that during the vegetation period atmospheric Hg^0 is deposited at small rates, while fluxes during the snow covered season are insignificant. During the snow-free periods the deposition of Hg^0 to plant and soil surfaces seemed to occur primarily during the night by co-deposition with condensing water. It is suggested, that some Hg^0 is emitted again in the morning during sunrise, while the rest is sequestered by the soil or incorporated into plant tissue.

In Chapter 3 it was estimated that about two thirds of the total mercury input from the atmosphere could be attributed to dry deposition. While dry deposition seems to occur primarily in the form of Hg^0, the dominant species in wet deposition is dissolved and particulate Hg^{2+} (Lindberg et al., 2007a). Unlike Hg^0, deposited Hg^{2+} may be more stably bound to the soil matrix or to plant surfaces and be less likely re-emitted again. Hence, wet deposition might still be more effective in removing atmospheric mercury than dry deposition.

During the field campaigns of this study enhanced Hg^0 emissions were observed after rain events and gradually increasing Hg^0 uptake was recorded with growing grass. It could also be shown, that Hg^0 gradients often followed the diurnal pattern of meteorological variables and that atmospheric Hg^0 concentrations were strongly affected by elevated ozone levels. Net deposition of mercury resulting from oxidation by ozone could not be detected with the applied micrometeorological methods as Hg^0 oxidation seems to occur uniformly across the lower atmospheric surface layer and does not result in an elevated Hg^0 gradient.

Direct effects of forcing factors like temperature and soil water content, as they were observed in the incubation experiments, could not be detected in the field stud-

ies. This is likely to be the result of complex interactions of many processes that obscure the relationships between the Hg^0 fluxes and the forcing factors.

The Hg^0 exchange with the atmosphere during snow-covered conditions was investigated in more detail during a field study in the French Alps (Chapter 5). During snow melt in March pronounced daytime emission of Hg^0 from the snow surface was observed. It could be shown, that this emission is primarily driven by solar radiation (the UVB spectral band appears to be most efficient) and temperature, which generates a liquid phase with a high surface area that enhances Hg^{2+} reduction.

Finally, the studies were moved to the laboratory again to investigate the role of the vegetation cover in the Hg^0 exchange in more detail (Chapter 6). It could be shown, that vegetated soils take up mercury on higher rates than bare soils. The results indicate a balancing effect of irradiation, which promotes mercury volatilisation at the soil surface, when vegetation is absent.

Two micrometeorological methods were applied to estimate Hg^0 fluxes in the field, and both proved suitable to estimate net exchange rates. However, the results suffered strong variability due to the extremely low gradients encountered in the investigated background ecosystems. In general, when applied to mercury, micrometeorological methods must still be considered as experimental and validation of the measured fluxes is a major research need. More advanced methods, such as the relaxed eddy accumulation method, and ongoing developments in fast response sensors for mercury hold potential to improve flux estimations considerably.

Overall, it can be concluded that uncontaminated grasslands of temperate climate regions are a net sink for atmospheric mercury. Yet, it has to be confirmed that this sink is permanent and rapid changes in environmental conditions (e.g. springtime snow melt or heavy showers after dry periods) might offset the deposition by short and intensive emission boosts of Hg^0.

It remains to resolve whether mercury is currently increasing or decreasing in the active reservoirs of the Earth's surface. Continued research of agricultural fields, wetlands and forests is needed to accurately quantify their source/sink strength and their significance in the air-surface exchange of mercury. To clarify the ultimate fate of atmospheric mercury it will also be necessary to investigate the interaction of the environmental variables that alter the mobility and reactivity of mercury, to study the microbially mediated transformation processes in soils and to examine the potential of plants to assimilate, translocate and emit mercury. Amongst others this will require continued monitoring of the mercury fluxes with methods that permit high temporal resolution.

Acknowledgements

This dissertation has been a challenging piece of work and thanks to many people I have progressed to the state where I can draw the final conclusions. The last three years have been somewhat rugged, with ups and downs and the occasional doubt of the chosen endeavour. Yet, the encouragement of friends and the support of colleagues have carried me to the finish line.

I especially want to thank Christine Alewell for providing the platform to build my dissertation, for her help on questions related to my research and her support on issues that gave me the chance to look over the edge of the scientific world. My appreciation is also owed to Franz Conen who was always willing to offer his help to resolve an urgent problem and to come up with new ideas to address ambiguous research topics. Furthermore, I thank Daniel Obrist for grinding his mind to establish the research on mercury in Basel and for procuring the financial resources.

My PhD-project involved quite a bit of practical work in the field as well as in the laboratory. For their help to get and keep all systems running I want to thank Lukas Zimmermann, Irene Lehner and Florian Storck. Special thanks also to Matthias Zeemann, Christof Ammann, Georg Wohlfahrt, Werner Eugster and Roland Vogt for the opportunity to get access to different field sites, for providing me with heaps of data and for their essential support regarding micrometeorology. Moreover, I thank Heidi Strohm and Marianne Caroni for their analytical work and the provision of the climate chamber. I would also like to express my appreciation to all members of the Institute of Environmental Geosciences not only for proof-reading of "those" scientific papers, but also for their assistance in technical issues when needed. In this regard my special thank to Dominik Bänniger who induced me to view the advantages of alternative word processing devices and who helped me to resolve apparently irresolvable programming aspects.

Last but not least a big "Thank you" to Katrin Oppel who has added enormously to the quality of my life here in Basel and who has cheered me up in times of low spirits.

Bibliography

Alberts, J. J., Schindler, J. E., & Miller, R. W. (1974). Elemental Mercury Evolution Mediated by Humic Acid. *Science*, **184**, 895–896.

Bacci, E., Gaggi, C., Lanzillotti, E., Ferrozzi, S., & Valli, L. (2000). Geothermal power plants at Mt. Amiata (Tuscany-Italy): mercury and hydrogen sulphide deposition revealed by vegetation. *Chemosphere*, **40**(8), 907–911.

Bahlmann, E. & Ebinghaus, R. (2003). Process studies on mercury fluxes over different soils with a Laboratory Flux Measurement System (LFMS). *Journal De Physique IV*, **107**, 99–102.

Bahlmann, E., Ebinghaus, R., & Ruck, W. (2006). Development and Application of a Laboratory Flux Measurement System (LFMS) for the Investigation of the Kinetics of Mercury Emissions from Soils. *Journal of Environmental Monitoring*, **81**(2), 114–125.

Baldocchi, D. (2006). Advanced topics in biometeorology and micrometeorology: Lecture on micrometeorological flux measurement methods. University of California, Berkeley, USA.

Baldocchi, D., Hicks, B. B., & Meyers, T. P. (1988). Measuring biosphere-atmosphere exchanges of biologically related gases with micrometeorological methods. *Ecology*, **69**(5), 1331–1340.

Bauer, D., Campuzano-Jost, P., & Hynes, A. J. (2002). Rapid, ultra-sensitive detection of gas phase elemental mercury under atmospheric conditions using sequential two-photon laser induced fluorescence. *Journal of Environmental Monitoring*, **4**(3), 339–343.

Carpi, A. & Lindberg, S. (1997). Sunlight-Mediated Emission of Elemental Mercury from Soil Amended with Municipal Sewage Sludge. *Environmental Science and Technology*, **31**(7), 2085–2091.

Charlet, L., Bosbach, D., & Peretyashko, T. (2002). Natural attenuation of TCE, As, Hg linked to the heterogeneous oxidation of Fe(II): an AFM study. *Chemical Geology*, **190**(1-4), 303–319.

Cobos, D. R., Baker, J. M., & Nater, E. A. (2002). Conditional sampling for measuring mercury vapor fluxes. *Atmospheric Environment*, **36**(27), 4309–4321.

Dabberdt, W. F., Lenschow, D. H., Horst, T. W., Zimmerman, P. R., Oncley, S. P., & Delany, A. C. (1993). Atmosphere-Surface Exchange Measurements. *Science*, **260**(5113), 1472–1481.

De Temmerman, L., Claeys, N., Roekens, E., & Guns, M. (2007). Biomonitoring of airborne mercury with perennial ryegrass cultures. *Environmental Pollution*, **146**(2), 458–462.

Dickens, H. E. & Anderson, J. M. (1999). Manipulation of soil microbial community structure in bog and forest soils using chloroform fumigation. *Soil Biology and Biochemistry*, **31**(14), 2049–2058.

Dipner-Gerber, M., Schibli, C., & Eggenberg, S. (2004). Trockenwiesen und -weiden der Schweiz, Vorgehen und Ergebnisse Kanton Zug. Technical report, BUWAL, Bern, Switzerland.

Dommergue, A. (2003). *Dynamique du mercure dans les neiges de hautes et moyennes latitude: Etudes in situ et en conditions simulees des mechanismes de reactivite et d'echanges*. Phd, Université Joseph Fourier.

Du, S. H. & Fang, S. C. (1982). Uptake of Elemental Mercury-Vapor by C3-Species and C4-Species. *Environmental and Experimental Botany*, **22**(4), 437–443.

Dyer, A. J. (1974). A review of flux-profile relationships. *Boundary-Layer Meteorology*, **7**(3), 363–372.

Edwards, G. C., Rasmussen, P. E., Schroeder, W. H., Kemp, R. J., Dias, G. M., Fitzgerald-Hubble, C. R., Wong, E. K., Halfpenny-Mitchell, L., & Gustin, M. S. (2001). Sources of variability in mercury flux measurements. *Journal of Geophysical Research-Atmospheres*, **106**(D6), 5421–5435.

Edwards, G. C., Rasmussen, P. E., Schroeder, W. H., Wallace, D. M., Halfpenny-Mitchell, L., Dias, G. M., Kemp, R. J., & Ausma, S. (2005). Development and evaluation of a sampling system to determine gaseous Mercury fluxes using an aerodynamic micrometeorological gradient method. *Journal of Geophysical Research-Atmospheres*, **110**(D10306).

Engle, M. A., Sexauer Gustin, M., Lindberg, S. E., Gertler, A. W., & Ariya, P. A. (2005). The influence of ozone on atmospheric emissions of gaseous elemental mercury and reactive gaseous mercury from substrates. *Atmospheric Environment*, **39**(39), 7506–7517.

Ericksen, J. A., Gustin, M. S., Xin, M., Weisberg, P. J., & Fernandez, G. C. J. (2006). Air-soil exchange of mercury from background soils in the United States. *Science of the Total Environment*, **366**(2-3), 851–863.

Eugster, W. & Zeeman, M. (2006). Micrometeorological techniques to measure ecosystem-scale greenhouse gas fluxes for model validation and improvement. In

C. R. Soliva, J. Takahashi, and M. Kreuzer, editors, *Greenhouse Gases and Animal Agriculture: An Update*, Int. Congr. Series No. 1293, pages 66–75. Elsevier, The Netherlands.

Fay, L. & Gustin, M. (2007). Assessing the influence of different atmospheric and soil mercury concentrations on foliar mercury concentrations in a controlled environment. *Water Air And Soil Pollution*, **181**(1-4), 373–384.

Ferrari, C., Dommergue, A., Veysseyre, A., Planchon, F., & Boutron, C. (2002). Mercury speciation in the French seasonal snow cover. *Science of the Total Environment*, **287**(1-2), 61–69.

Fitzgerald, W., Engstrom, D., Mason, R., & Nater, E. (1998). The case for atmospheric mercury contamination in remote areas. *Environmental Science and Technology*, **32**(1), 1–7.

Fitzgerald, W. F. (1995). Is Mercury Increasing in the Atmosphere - the Need for an Atmospheric Mercury Network (Amnet). *Water Air and Soil Pollution*, **80**(1-4), 245–254.

Fitzgerald, W. F. & Lamborg, C. H. (2004). Geochemistry of mercury in the environment. In H. D. Holland and K. K. Turekian, editors, *Treatise on Geochemistry*, volume 9, Environmental Geochemistry, pages 107–148. Elsevier-Pergamon, Oxford, 1st edition.

Foken, T. (2006). *Angewandte Meteorologie: mikrometeorologische Methoden*. Springer, Berlin.

Fritsche, J., Obrist, D., Zeeman, M., Conen, F., Eugster, W., & Alewell, C. (2008a). Elemental mercury fluxes over a sub-alpine grassland in Switzerland determined with two micrometeorological methods. *Atmospheric Environment*, **in press**.

Fritsche, J., Obrist, D., & Alewell, C. (2008b). Evidence of microbial control of Hg0 emissions from uncontaminated terrestrial soils. *Journal of Plant Nutrition and Soil Science*, **in press**.

Gabriel, M. C. & Williamson, D. G. (2004). Principal Biogeochemical Factors Affecting the Speciation And Transport of Mercury through the terrestrial environment. *Environmental Geochemistry and Health*, **26**(4), 421–434.

Graydon, J. A., St Louis, V. L., Lindberg, S. E., Hintelmann, H., & Krabbenhoft, D. P. (2006). Investigation of mercury exchange between forest canopy vegetation and the atmosphere using a new dynamic chamber. *Environmental Science and Technology*, **40**(15), 4680–4688.

Grigal, D. F. (2003). Mercury sequestration in forests and peatlands: A review. *Journal of Environmental Quality*, **32**(2), 393–405.

Gustin, M., Lindberg, S. E., Austin, K., Coolbaugh, M. F., Vette, A., & Zhang, H. (2000). Assessing the contribution of natural sources to regional atmospheric mercury budgets. *The Science of The Total Environment*, **259**(1-3), 61–71.

Gustin, M., Ericksen, J., Schorran, D., Johnson, D., Lindberg, S., & Coleman, J. (2004). Application of controlled mesocosms for understanding mercury air-soil-plant exchange. *Environmental Science and Technology*, **38**(22), 6044–6050.

Gustin, M. S. & Lindberg, S. E. (2005). Terrestrial mercury fluxes: is the net exchange up, down, or neither? In N. Pirrone and K. R. Mahaffey, editors, *Dynamics of mercury pollution on regional and global scales*, pages 241–259. Springer, New York.

Gustin, M. S., Biester, H., & Kim, C. S. (2002). Investigation of the light-enhanced emission of mercury from naturally enriched substrates. *Atmospheric Environment*, **36**(20), 3241–3254.

Gustin, M. S., Coolbaugh, M. F., Engle, M. A., Fitzgerald, B. C., Keislar, R. E., Lindberg, S. E., Nacht, D. M., Quashnick, J., Rytuba, J. J., Sladek, C., Zhang, H., & Zehner, R. E. (2003). Atmospheric mercury emissions from mine wastes and surrounding geologically enriched terrains. *Environmental Geology*, **43**(3), 339–351.

Gustin, M. S., Engle, M., Ericksen, J., Lyman, S., Stamenkovic, J., & Xin, M. (2006). Mercury exchange between the atmosphere and low mercury containing substrates. *Applied Geochemistry*, **21**(11), 1913–1923.

Hall, B. (1995). The Gas-Phase Oxidation of Elemental Mercury by Ozone. *Water Air and Soil Pollution*, **80**(1-4), 301–315.

Horwath, W. R. & Paul, E. A. (1994). Microbial Biomass. In R. W. Weaver, editor, *Methods of Soil Analysis, Part 2, Microbiological and Biochemical Properties*, pages 753–773. Soil Science Society of America, Inc., Madison, USA.

IOMC (2002). Global Mercury Assessment. Technical report, UNEP Chemicals, Geneva.

Iverfeldt, A., Munthe, J., Brosset, C., & Pacyna, J. (1995). Long-Term Changes in Concentration and Deposition of Atmospheric Mercury over Scandinavia. *Water Air and Soil Pollution*, **80**(1-4), 227–233.

Johansson, K., Bergback, B., & Tyler, G. (2001). Impact of Atmospheric Long Range Transport of Lead, Mercury and Cadmium on the Swedish Forest Environment. *Water, Air and Soil Pollution: Focus*, **1**, 279–297.

Keeler, G. J. & Landis, M. S. (1994). Standard operating procedure for sampling vapor phase mercury. University of Michigan, USA.

Kim, K. H., Lindberg, S. E., & Meyers, T. P. (1995). Micrometeorological Measurements of Mercury-Vapor Fluxes over Background Forest Soils in Eastern Tennessee. *Atmospheric Environment*, **29**(2), 267–282.

Kim, K.-H., Ebinghaus, R., Schroeder, W. H., Blanchard, P., Kock, H. H., Steffen, A., Froude, F. A., Kim, M.-Y., Hong, S., & Kim, J.-H. (2005). Atmospheric Mercury Concentrations from Several Observatory Sites in the Northern Hemisphere. *Journal of Atmospheric Chemistry*, **50**(1), 1–24.

Lalonde, J., Poulain, A., & Amyot, M. (2002). The role of mercury redox reactions in snow on snow-to-air mercury transfer. *Environmental Science and Technology*, **36**(2), 174–178.

Landa, E. R. (1978). Microbial Aspects of Volatile Loss of Applied Mercury(II) from Soils. *Journal of Environmental Quality*, **7**(1), 84–86.

Landis, M. S., Lynam, M. M., & Stevens, R. K. (2005). The monitoring and modelling of mercury spcies in support of local, regional and global modelling. In N. Pirrone and K. R. Mahaffey, editors, *Dynamics of mercury pollution on regional and global scales*, pages 124–151. Springer, New York.

Lee, X. H. (2000). Water vapor density effect on measurements of trace gas mixing ratio and flux with a massflow controller. *Journal of Geophysical Research-Atmospheres*, **105**(D14), 17807–17810.

Lee, Y., Bishop, K., Munthe, J., Iverfeldt, A., Verta, M., Parkman, H., & Hultberg, H. (1998). An examination of current Hg deposition and export in Fenno-Scandian catchments. *Biogeochemistry*, **40**(2 - 3), 125–135.

Lenschow, D. (1995). Micrometeorological techniques for measuring biosphere-atmosphere trace gas exchange. In P. Matson and R. Harriss, editors, *Biogenic trace gases: measuring emissions from soil and water*, pages 126–163. Blackwell Science Ltd, Cambridge.

Lin, C. J. & Pehkonen, S. O. (1999). The chemistry of atmospheric mercury: a review. *Atmospheric Environment*, **33**(13), 2067–2079.

Lindberg, S. & Meyers, T. (2001). Development of an automated micrometeorological method for measuring the emission of mercury vapor from wetland vegetation. *Wetlands Ecology and Management*, **9**(4), 333–347.

Lindberg, S., Vette, A., Miles, C., & Schaedlich, F. (2000). Mercury speciation in natural waters: Measurement of dissolved gaseous mercury with a field analyzer. *Biogeochemistry*, **48**(2), 237–259.

Lindberg, S., Brooks, S., Lin, C., Scott, K., Landis, M., Stevens, R., Goodsite, M., & Richter, A. (2002). Dynamic oxidation of gaseous mercury in the Arctic troposphere at polar sunrise. *Environmental Science and Technology*, **36**(6), 1245–1256.

Lindberg, S. E., Jackson, D. R., Huckabee, J. W., Janzen, S. A., Levin, M. J., & Lund, J. R. (1979). Atmospheric emission and plant uptake of mercury from agricultural soils near the Almaden mercury mine. *Journal of Environmental Quality*, **8**(4), 572–578.

Lindberg, S. E., Meyers, T. P., Taylor, G. E., Turner, R., & Schroeder, W. (1992). Atmoshere-surface exchange of mercury in a forest: Results of modeling and gradient approaches. *Journal of Geophysical Research-Atmospheres*, **97**(D2), 2519–2528.

Lindberg, S. E., Kim, K. H., Meyers, T. P., & Owens, J. G. (1995). Micrometeorological Gradient Approach for Quantifying Air- Surface Exchange of Mercury-Vapor - Tests over Contaminated Soils. *Environmental Science and Technology*, **29**(1), 126–135.

Lindberg, S. E., Hanson, P. J., Meyers, T. P., & Kim, K. H. (1998). Air/surface exchange of mercury vapor over forests - The need for a reassessment of continental biogenic emissions. *Atmospheric Environment*, **32**(5), 895–908.

Lindberg, S. E., Ebinghaus, R., Engstrom, D., Feng, X., Fitzgerald, W. F., Pirrone, N., Prestbo, E., & Seigneur, C. (2007a). A Synthesis of Progress and Uncertainties in Attributing the Sources of Mercury in Deposition. *AMBIO*, **36**(1), 19–33.

Lindberg, S. E., Bullock, O. R., Ebinghaus, R., Engstrom, D., Feng, X., Fitzgerald, W. F., Pirrone, N., Prestbo, E., & Seigneur, C. (2007b). The Madison declaration on mercury pollution. *AMBIO*, **36**(1), 62–65.

Mason, R. P., Morel, F. M. M., & Hemond, H. F. (1995). The role of microorganisms in elemental mercury formation in natural waters. *Water, Air, and Soil Pollution*, **80**(1 - 4), 775–787.

Mergler, D., Anderson, H., Chan, L., Mahaffey, K., Murray, M., Sakamoto, M., & Stern, A. (2007). Methylmercury exposure and health effects in humans: A worldwide concern. *AMBIO*, **36**(1), 3–11.

Meyers, T. P., Hall, M. E., Lindberg, S. E., & Kim, K. (1996). Use of the modified Bowen-ratio technique to measure fluxes of trace gases. *Atmospheric Environment*, **30**(19), 3321–3329.

Millhollen, A., Obrist, D., & Gustin, M. (2006a). Mercury accumulation in grass and forb species as a function of atmospheric carbon dioxide concentrations and mercury exposures in air and soil. *Chemosphere*, **65**(5), 889–897.

Millhollen, A. G., Gustin, M. S., & Obrist, D. (2006b). Foliar mercury accumulation and exchange for three tree species. *Environmental Science and Technology*, **40**(19), 6001–6006.

Monin, A. S. & Obukhov, A. M. (1954). *Basic laws of turbulent mixing in the surface layer of the atmosphere (in Russian)*. Trudy Geofizicheskogo Instituta, Akademiya Nauk SSSR.

Morel, F. M. M., Kraepiel, A. M. L., & Amyot, M. (1998). The chemical cycle and bioaccumulation of mercury. *Annual Review of Ecology and Systematics*, **29**, 543–566.

Munthe, J. & Wängberg, I. (2001). Atmospheric Mercury in Sweden, Northern Finland and Northern Europe. Technical report, IVL Swedish Environmental Research Institute, Gothenburg.

Obrist, D. (2007). Atmospheric mercury pollution due to losses of terrestrial carbon pools? *Biogeochemistry*, **85**, 119–123.

Obrist, D., Gustin, M. S., Arnone III, J. A., Johnson, D. W., Schorran, D. E., & Verburg, P. S. (2005). Measurements of gaseous elemental mercury fluxes over intact tallgrass prairie monoliths during one full year. *Atmospheric Environment*, **39**(5), 957–965.

Obrist, D., Conen, F., Vogt, R., Siegwolf, R., & Alewell, C. (2006). Estimation of Hg^0 exchange between ecosystems and the atmosphere using ^{222}Rn and Hg^0 concentration changes in the stable nocturnal boundary layer. *Atmospheric Environment*, **40**(5), 856–866.

Pacyna, J., Munthe, J., Larjava, K., & Pacyna, E. G. (2005). Mercury emissions from anthropogenic sources: Estimates and measurements for Europe. In N. Pirrone and K. R. Mahaffey, editors, *Dynamics of mercury pollution on regional and global scales*, pages 52–64. Springer, New York.

Pirrone, N. (2001). Mercury research in Europe: towards the preparation of the EU air quality directive. *Atmospheric Environment*, **35**(17), 2979–2986.

Pirrone, N. & Mahaffey, K. R. (2005). Where we stand on mercury pollution and its health effects on regional and global scales. In N. Pirrone and K. R. Mahaffey, editors, *Dynamics of mercury pollution on regional and global scales*, pages 1–21. Springer, New York.

Pirrone, N., Munthe, J., Barregard, L., Ehrlich, H. C., Petersen, G., Fernandez, R., Hansen, J. C., Grandjean, P., Horvat, M., Steinnes, E., Ahrens, R., Pacyna, J., Borowiak, A., Boffetta, P., & Wichmann-Fiebig, M. (2001). EU Ambient air pollution by mercury (Hg) - Position paper.

Poissant, L. & Casimir, A. (1998). Water-air and soil-air exchange rate of total gaseous mercury measured at background sites. *Atmospheric Environment*, **32**(5), 883–893.

Rasmussen, P. E. (1994). Current Methods of Estimating Atmospheric Mercury Fluxes in Remote Areas. *Environmental Science and Technology*, **28**(13), 2233–2241.

Raupach, M. R. & Legg, B. J. (1984). The uses and limitations of flux-gradient relationships in micrometeorology. *Agricultural Water Management*, **8**(1-3), 119–131.

Ravichandran, M. (2004). Interactions between mercury and dissolved organic matter - a review. *Chemosphere*, **55**(3), 319–331.

Rogers, R. D. & Mc Farlane, J. C. (1979). Factors Influencing the Volatilization of Mercury from Soil. *Journal of Environmental Quality*, **8**(2), 255–260.

Roth, K. (2006). Bodenkartierung und GIS-basierte Kohlenstoffinventur von grasland-böden: Untersuchungen an den ETH-Forschungsstationen Chamau und Früebüel (ZG, Schweiz). Technical report, Department of Geography, University of Zurich, Zurich.

Salminen, R. (2006). Geochemical Atlas of Europe. Part 1 - Background Information, Methodology and Maps.

Schlueter, K. (2000). Review: evaporation of mercury from soils. An integration and synthesis of current knowledge. *Environmental Geology*, **39**(3-4), 249–271.

Schroeder, W., Anlauf, K., Barrie, L., Lu, J., Steffen, A., Schneeberger, D., & Berg, T. (1998). Arctic springtime depletion of mercury. *Nature*, **394**(6691), 331–332.

Schroeder, W. H. & Munthe, J. (1998). Atmospheric mercury - An overview. *Atmospheric Environment*, **32**(5), 809–822.

Schroeder, W. H., Beauchamp, S., Edwards, G., Poissant, L., Rasmussen, P., Tordon, R., Dias, G., Kemp, J., Heyst, B. V., & Banic, C. M. (2005). Gaseous mercury emissions from natural sources in Canadian landscapes. *Journal of Geophysical Research*, **110**(D18302).

Schuster, E. (1991). The behavior of mercury in the soil with special emphasis on complexation and adsorption processes - a review of the literature. *Water, Air, and Soil Pollution*, **56**, 667–680.

Schuster, P., Krabbenhoft, D., Naftz, D., Cecil, L., Olson, M., Dewild, J., Susong, D., Green, J., & Abbott, M. (2002). Atmospheric Mercury Deposition during the Last 270 Years: A Glacial Ice Core Record of Natural and Anthropogenic Sources. *Environmental Science and Technology*, **36**(11), 2303–2310.

Siciliano, S., O'Driscoll, N., & Lean, D. (2002). Microbial Reduction and Oxidation of Mercury in Freshwater Lakes. *Environmental Science and Technology*, **36**(14), 3064–3068.

Siegel, S. M. & Siegel, B. Z. (1988). Temperature determinants of plant-soil-air mercury relationships. *Water, Air and Soil Pollution*, **40**(3-4), 443–448.

Summers, A. O. & Silver, S. (1978). Microbial Tranformations of Metals. *Annual Review of Microbiology*, **32**, 637–672.

Toyota, K., Ritz, K., & Young, I. (1996). Survival of bacterial and fungal populations following chloroform-fumigation: Effects of soil matric potential and bulk density. *Soil Biology and Biochemistry*, **28**(10-11), 1545–1547.

Tsai, C.-S., Killham, K., & Cresser, M. S. (1997). Dynamic response of microbial biomass, respiration rate and ATP to glucose additions. *Soil Biology and Biochemistry*, **29**(8), 1249–1256.

Valente, R., Shea, C., Humes, K., & Tanner, R. (2007). Atmospheric mercury in the Great Smoky Mountains compared to regional and global levels. *Atmospheric Environment*, **41**(9), 1861–1873.

Van Faassen, H. (1973). Effects of mercury compounds on soil microbes. *Plant Soil*, **38**, 485–487.

Wallschlager, D., Herbert Kock, H., Schroeder, W. H., Lindberg, S. E., Ebinghaus, R., & Wilken, R.-D. (2000). Mechanism and significance of mercury volatilization from contaminated floodplains of the German river Elbe. *Atmospheric Environment*, **34**(22), 3745–3755.

Wangberg, I., Munthe, J., Berg, T., Ebinghaus, R., Kock, H. H., Temme, C., Bieder, E., Spain, T. G., & Stolk, A. (2007). Trends in air concentration and deposition of mercury in the coastal environment of the North Sea Area. *Atmospheric Environment*, **41**(12), 2612–2619.

Webb, E. K., Pearman, G. I., & Leuning, R. (1980). Correction of Flux Measurements for Density Effects Due to Heat and Water-Vapor Transfer. *Quarterly Journal of the Royal Meteorological Society*, **106**(447), 85–100.

Wolf, D. C. & Skipper, H. D. (1994). Soil Sterilization. In R. W. Weaver, editor, *Methods of Soil Analysis, Part 2, Microbiological and Biochemical Properties*, pages 41–51. Soil Science Society of America, Inc., Madison, USA.

Wolfe, M., Schwarzbach, S., & Sulaiman, R. (1998). Effects of mercury on wildlife: A comprehensive review. *Environmental Toxicology and Chemistry*, **17**(2), 146–160.

Wood, J. M. (1974). Biological Cycles of Toxic Elements in the Environment. *Science*, **183**, 1049–1052.

Zhang, H. & Lindberg, S. E. (1999). Processes influencing the emission of mercury from soils: A conceptual model. *Journal of Geophysical Research-Atmospheres*, **104**(D17), 21889–21896.

Curriculum Vitae

Johannes Fritsche

born on 30 October 1973 in Bludenz, Austria

Education

2004 – 2007	PhD at Institute of Environmental Geosciences, University of Basel, Switzerland **Doctoral Thesis:** Elemental mercury exchange between air and uncontaminated grasslands: Determination of fluxes with micrometeorological methods and identification of forcing factors
1997 – 2003	Master of Engineering in Industrial Environmental Protection at the University of Leoben, Austria **Thesis:** Determination of anthropogenic input of Ru, Rh, Pd, Re, Os, Ir and Pt in soils along Austrian motorways by isotope dilution ICP-MS
1993 – 1996	University entrance qualification course at Liechtensteinische Ingenieurschule, Liechtenstein
1989 – 1992	Apprenticeship as Material Tester at HILTI Corporation, Thüringen, Austria
1988 – 1989	Polytechnikum Thüringen, Austria
1984 – 1988	Hauptschule Nüziders, Austria
1980 – 1984	Volksschule Ludesch, Austria

Professional Experience

11/2006 – 6/2007	Energy Engineer, Weisskopf Partner GmbH, Zürich, Switzerland
12/2003 – 10/2004	Assistant, EAWAG, Dübendorf, Switzerland
1992 – 1996	Laboratory Technician, HILTI Corporation, Thüringen, Austria